THE EFFECTS OF SOLIDIFICATION RATE AND HEAT TREATMENT ON THE MICROSTRUCTURE AND MECHANICAL PROPERTIES OF CERAMIC SHELL INVESTMENT CAST CF3M

By

RACHAEL ESTHER COHEN

Bachelor of Science
University of Connecticut
Storrs, Connecticut
1976

Master of Science
University of Massachusetts
Amherst, Massachusetts
1982

Master of Science
University of Vermont
Burlington, Vermont
1986

Submitted to the Faculty of the
Graduate College of the
Oklahoma State University
in partial fulfillment of
the requirements for
the Degree of
DOCTOR OF PHILOSOPHY
December 1990

THE EFFECTS OF SOLIDIFICATION RATE AND HEAT TREATMENT

ON THE MICROSTRUCTURE AND MECHANICAL PROPERTIES

OF CERAMIC SHELL INVESTMENT CAST CF3M

Thesis Approved:

Delcie R Durham

Thesis Advisor

David G. Gilley

Richard L Lowery

C E Price

John W Negus

Norman N Thadhani

Dean of the Graduate College

ACKNOWLEDGMENTS

I would like to thank my major advisor, Dr. Delcie Durham, for her guidance and understanding. Her enthusiastic approach to any challange will always serve as an inspiration to me. I also want to thank Dr. C. Eric Price for his many hours spent with me at the Electron Microscopy Laboratory and the many additional hours of good humored intellectual discussion. I am grateful to the other committee members, Dr. Dick Lowery, Dr. David Lilley and Dr. John Nazemetz, for their thoughtful consideration and criticism of this work.

This work could not have been completed without the generous donation of time, equipment, supplies, and expertise from the following Oklahoma businesses: The Investment Division of American Foundry Group, Bixby Oklahoma; Metlab, Tulsa, Oklahoma; Mercury Marine Division of Brunswick, Stillwater, Oklahoma. This work was partially supported by NSF EPSCORE Grant No. EN-87-R-129, Fracture Toughness Enhancement of Cast Austenitic Stainless Steel By Process Parameter Control of Microstructure.

I appreciate the generous help of Maggy Piranian and Dr. David London at the University of Oklahoma Microprobe Laboratory for the use of the WDS system. Many thanks to Calvin Nichols who constructed the first wood pattern for our castings. I also want to thank Paul

Ratke for his hard work and good humor while we worked together on this project.

I greatly appreciate the special friends I have here in Stillwater, who have made me feel at home and encouraged me to succeed. And finally, to my family, especially my mother and in memory of my father, thank you for the love and support through the years of engineering school.

TABLE OF CONTENTS

LIST OF TABLES

LIST OF FIGURES

CHAPTER I

INTRODUCTION

Historically, production of sound investment castings has been a matter of experience and luck. Today, with the demand for higher quality castings for the chemical, aerospace, defense and medical fields, premium investment foundries are recognizing the need for improved technology and process control. These improvements will develop only if data become available to quantify the relationships among processing parameters, microstructure and final properties. This project will characterize the changes in the microstructure of ceramic shell investment cast CF3M with heat treatment in order to determine if a superior combination of impact and tensile strength can be achieved.

CF3M stainless steel is significantly different from 316L, its wrought equivalent, due to the presence of 5-25 % delta ferrite in the austenite matrix. As shown in Table 1, CF3M specifications allow slightly more chromium and silicon and slightly less nickel. As can be seem by the values in Table 1, the equivalence is based on corrosion resistance not microstructure or mechanical properties.

The amount and morphology of the delta ferrite significantly affects the properties of the CF3M casting. Tensile and yield strengths increase with ferrite content. Impact energy has shown

TABLE 1

COMPARISON OF CF3M AND 316L
(ASM 9:3, ASTM A167, A743)

wt%	CF3M	316L
Cr	17.0-21.0	16.0-18.0
Ni	9.0-13.0	10.0-14.0
Mo	2.0-3.0	2.0-3.0
C	0.03 max	0.03 max
Mn	1.5 max	2.0 max
Si	1.5 max	1.0 max
P	0.040 max	0.045 max
S	0.04 max	0.03 max
MIN TENSILE STRENGTH MPa (ksi)	485 (70)	485 (70)
MIN YIELD STRENGTH MPa (ksi)	205 (30)	170 (25)
MIN % ELONGATION in 50 mm (2 in)	30	40
TYPICAL CHARPY V-NOTCH J (ft-lbs)	163 (120)	135 (100)

both increases and decreases with ferrite content indicating that other influences, such as ferrite morphology or slight chemistry differences, may play a part.

Typically, the primary control for the amount of delta ferrite is the variation of composition within the ASTM specification, but the casting process and heat treatment also affect the amount and morphology of delta ferrite. These processing effects make the control of delta ferrite more complicated than simply checking the composition of the melt. The complex influences of alloying elements may have contributed to the conflicting results seen in the impact energy values in the literature making comparisons among studies questionable. This study eliminates the complicated chemistry variables by using one melt and varying the ferrite amount and morphology by heat treatment.

A sound, high quality CF3M investment casting is a result of a series of complex events; foundry melt processing, solidification and heat treatment. In the foundry, variables include composition, superheat, mold material, mold temperature, mold geometry, gating, risering, and the presence of chills, insulation or exothermics. The foundry variables control the heat transfer, producing thermal gradients which control solidification. In turn, the solidification controls the cast microstructure and its characteristics such as % delta ferrite, dendrite spacing, interdendritic material, segregation and porosity. Heat treatment, such as the solution anneal recommended for CF3M, will change the amount and morphology of the delta ferrite. Finally, the microstructure determines the final in-use performance by determining properties such as strength,

ductility, toughness, fatigue behavior, weldability, machinability, and corrosion resistance.

The problem of sorting out the influences on a final cast product is enormous. It is no wonder that many foundries rely only on intuition and experience. In the highly competitive and growing market for precision castings, this valuable experience and intuition must be combined with improved technology and controls. This project provides, not only basic scientific information on the behavior of CF3M, but also data for better control in the foundry.

The present study examines the effects of solidification and heat treatment on the microstructure and mechanical properties of a ceramic shell investment cast CF3M. Ceramic investment molds are unique because they involve slower heat transfer than other mold materials. The heat transfer characteristics in the investment mold can be changed by varying mold thickness and refractory type, although it is not practical for most foundries to run more than one or two mold shell systems. The solidification conditions in this study have been chosen to represent practical extremes encountered in the foundry; hot insulated molds and uninsulated molds. The heat treatments chosen take place at the highest temperature within the range of industrial applications using ASTM specifications and ASM recommendations, 1121°C (2050°F).

Mechanical testing takes place in the as-cast and heat-treated conditions. Room temperature tensile tests as well as Charpy impact tests over a temperature range have been chosen to provide mechanical property data.

The microstructure of the as-cast and heat treated test specimens is characterized by dendrite arm spacing, % delta ferrite, ferrite morphology and, in some cases, fracture surface.

This study relates the mechanical properties of CF3M to the solidification and microstructure. By omitting melt composition effects, the variation in as-cast microstructure available in the foundry can be determined. The effect of this variation on the mechanical properties is documented and the microstructural features which control the change in properties are determined. The information obtained provides a measure of the sensitivity of the mechanical properties to the microstructure on a fundamental basis and answers the need to quantify the amount of control available within one melt composition. This is a much needed step towards better technology transfer from the laboratory to industry.

CHAPTER II

LITERATURE REVIEW

Solidification of CF3M

CF3M freezes by dendritic solidification. Figure 1 shows a cross section sketch of a corner of an ingot with a chill zone along the mold, a columnar zone and a central equiaxed zone. The proportions of these zones depend on the nucleation conditions set up by the temperature gradients and alloy composition. Taking a closer look at the columnar dendrite, Figure 2 shows the three dimensional, tree-like structure which can be characterized by primary or secondary dendrite arm spacing.

The primary dendrite arms grow in the direction of heat flow and their spacing depends on the product, GR, where G is the thermal gradient in the region where liquid and solid coexist, the mushy region, and R is the growth velocity of the solid-liquid interface. Primary dendrite arm spacings can not be reliably measured in a mixed columnar and equiaxed structure but secondary arm spacings are easily measured and are also dependent on cooling rate making them a useful way of characterizing the microstructure (Flemings 1974).

Dendritic solidification of CF3M results in a duplex ferrite-austenite microstructure. Some of the most comprehensive work

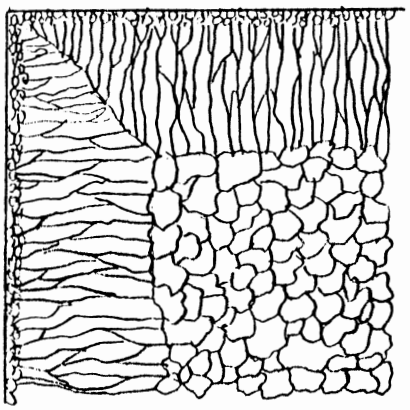

Figure 1. Typical Ingot Structure

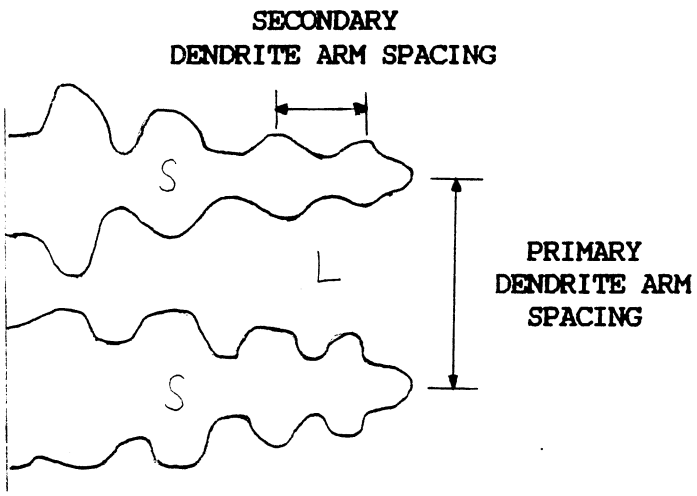

Figure 2. Columnar Dendrites

in the area concerns weld solidification. The main difference between welds and investment castings is the much slower solidification rate in the castings. Although caution must be used in directly applying the weld solidification models to investment castings, the weld models suggest possible mechanisms based on solidification theory which may be generally applicable (Ratke et al 1989).

Figure 3 shows a section through the Fe-Cr-Ni phase diagram at 68 wt% Fe (Leone and Kerr 1982). The composition of CF3M used in this study falls in the primary delta ferrite region. The sequence of solidification of CF3M under equilibrium conditions is: liquid -> liquid + delta ferrite -> liquid + delta ferrite + austenite -> delta ferrite + austenite. In reality, solidification is rarely slow enough to occur under equilibrium conditions. There is not enough time for complete diffusion and the liquid becomes richer in solute. As the solid front progresses it becomes richer in solute compared to the solid behind it. For CF3M this means that the first solid delta ferrite is enriched in chromium and depleted in nickel. According to Lippold and Savage, the rest of the dendrite solidifies as delta ferrite of near nominal composition and no austenite is formed from the liquid. The final duplex microstructure is a result of a massive diffusionless transformation of the delta ferrite to austenite leaving ferrite along the dendrite cores in the chromium rich areas (Lippold and Savage 1979). This theory makes sense for the very fast cooling rates in welding where diffusion rates may be insufficient to redistribute solute and allow diffusion controlled transformation.

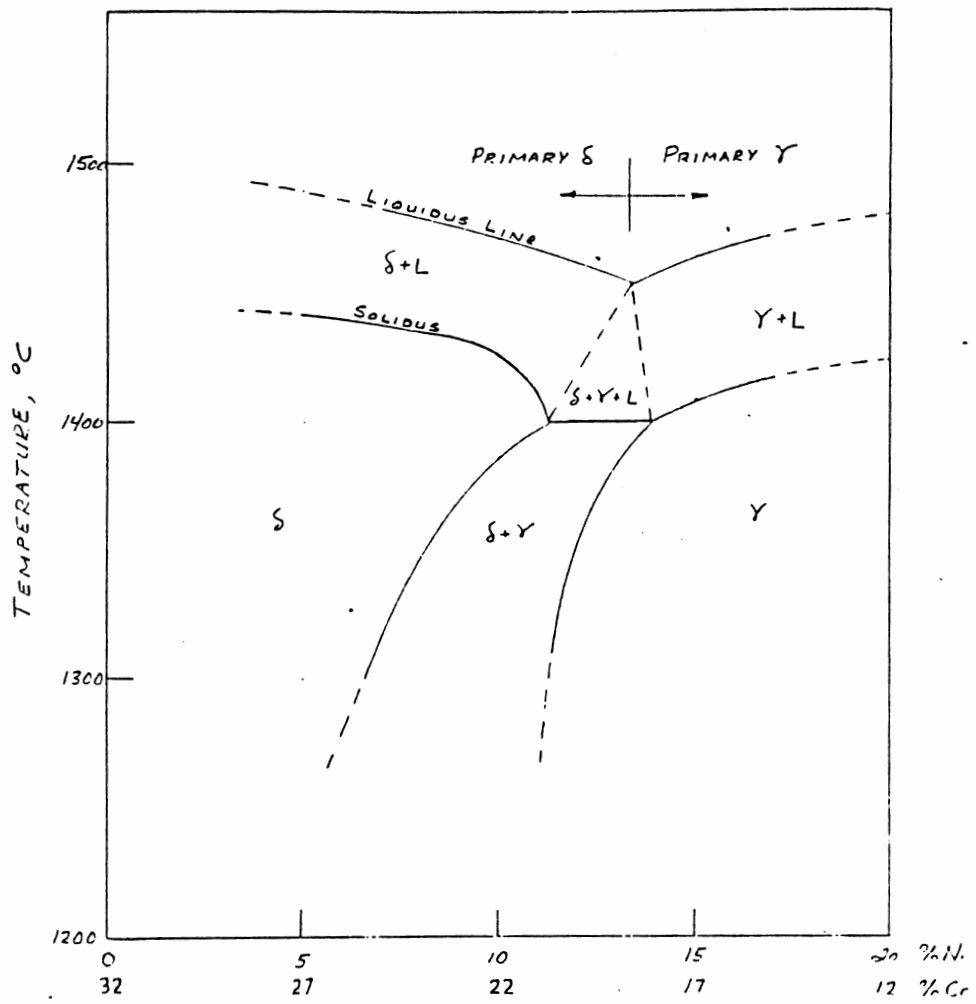

Figure 3. Section Through the Fe-Cr-Ni Phase Diagram at 68 wt% Fe (Leone and Kerr 1982).

Leone and Kerr proposed a mechanism more likely for the slower cooling rates of castings. It is more similar to the equilibrium solidification in that austenite does solidify from the liquid as a secondary phase around the delta ferrite dendrite core. As cooling progresses, the austenite grows into the melt as well as into the delta ferrite from the ferrite to austenite transformation (Leone and Kerr 1982). This mechanism also results in the duplex structure of delta ferrite along the cores of the dendrites within an austenite matrix.

As-cast Microstructure of CF3M

Figure 4 shows typical CF3M as-cast microstructures produced by investment casting in ceramic shells (Ratke et al 1989). Figure 4a is typical of material solidifying adjacent to the mold wall and the morphology in Figure 4b is representitive of a large portion of the central region of the castings. The dark areas are delta ferrite and the lighter matrix is austenite. Various ferrite morphologies have been described in the literature such as the vermicular and lacy structures in Figure 4 (David 1981). If the criteria of Takalo et al were used, both the microstructures in Figure 4 would be considered curved, soft forms and be termed vermicular (Takalo et al 1976). Care must be used when choosing terms to describe the ferrite morphology.

Some investigators maintain that the morphology differences are only due to the changes in the relative orientation of the dendrites arising from differences in cooling rates (Raghunathan 1979).

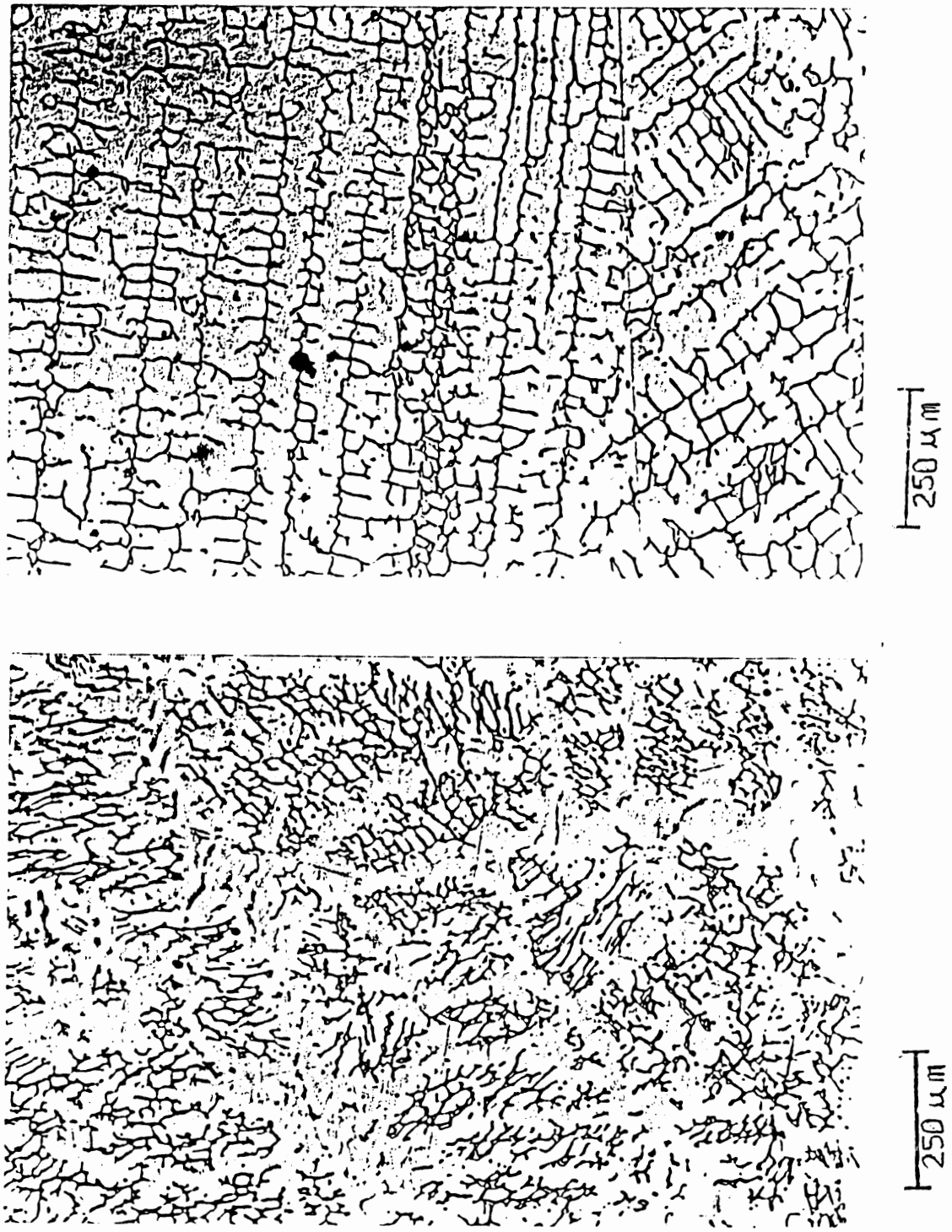

Figure 4. As-cast Microstructure Showing the Vermicular (top) and Lacy (bottom) Morphologies (Ratke 1988).

Because the mechanism of solidification is not fully understood, the ferrite morphology is presently useful only as a descriptive tool.

The amount of ferrite can be controlled by varying the amount of ferrite formers and austenite formers within the ASTM specified composition range. For CF3M, the major ferrite formers are chromium, silicon and molybdenum and the major austenite formers are nickel, carbon and manganese. Figure 5 shows the three widely used diagrams for predicting ferrite content from composition (Klemp and Sikkenga 1986). The Schaeffler and DeLong diagrams were specifically developed to predict the phases present in weldments. The Schoefer diagram is more applicable to castings. For the melt chemistry in this work, the Schoefer diagram predicts a ferrite content of 15.5% with a scatter band of 10.5-21.5%. These predictions require accurate chemistry measurements. They do not take into account the solidification rate or heat treatment, both of which affect the amount and morphology of delta ferrite. These important effects will be addressed in this project.

Solidification Rate and CF3M Microstructure

The rate of solidification is primarily determined by the temperature gradients set up in the mold and metal after pouring. Higher solidification rates produce a finer microstructure and a lower ferrite content. This effect has been suggested as a method of ferrite control in austenitic stainless steel weld metal and may have important implications to castings (David 1981). David goes on to say the variations in ferrite level with solidification rate are related to the kinetics of the primary ferrite -> austenite

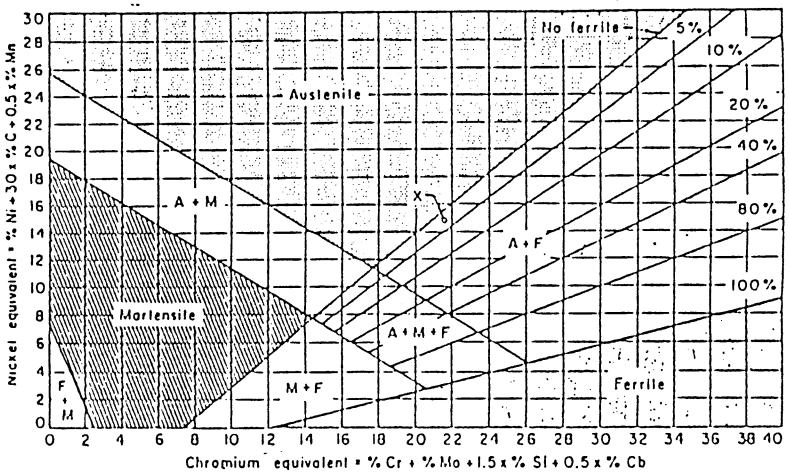

Schaeffler Diagram

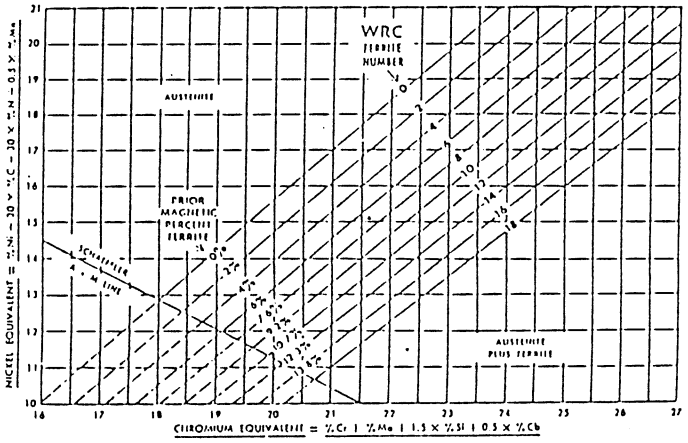

DeLong Diagram

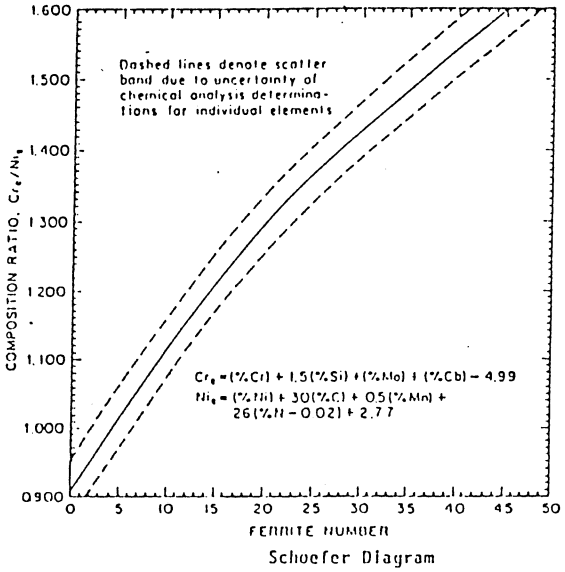

Schoefer Diagram

Figure 5. Diagrams Used to Predict Ferrite Content from Composition.

transformation. The kinetics depend on the diffusion distances which are determined by the dendrite arm spacing. It is well established that dendrite arm spacing decreases with increasing solidification rate resulting in a finer structure. The finer structure reduces diffusion distances and more of the primary delta ferrite can transform to austenite, resulting in a lower ferrite content in the final as-cast microstructure. Working against the finer spacing and shorter diffusion distances is the shorter time for diffusion at high temperature. The final ferrite content at high solidification rates is a result of these two opposing mechanisms.

At low solidification rates the above argument is reversed. The dendrite arm spacing is larger. The coarser structure increases diffusion distances and less primary delta ferrite transforms to austenite, leaving a higher ferrite content in the final as-cast microstructure.

Controlling the solidification rate may prove useful as a way to control the amount and morphology of ferrite in CF3M castings. To further complicate matters, in addition to the solidification rate, the post solidification heat treatment also changes the microstructure.

Heat Treatment and CF3M Microstructure

The solution anneal heat treatment for CF3M is said to be straightforward and well established. Handbooks recommend a minimum temperature of 1900°F (1040°C) and a maximum temperature of 2050°F (1120°C) (ASTM A743, ASM 1980). The specifications say heat to temperature, then quench in air, water or oil. This

maintains complete solution of carbides to maximize corrosion resistance. For investment castings, one hour at about 2000°F (1093°C) has been recommended (Garrow 1966).

The delta ferrite in CF3M has been considered to be stable over the temperature ranges encountered in service and during heat treatment. It has also been assumed there is no significant change in the amount of ferrite between the as-cast and heat treated conditions (Peckner and Bernstein 1977). Several investigators have proved this assumption wrong and even within the heat treatment specifications, dramatic effects can be observed on the amount and morphology of the delta ferrite in austenitic stainless steel castings.

One investigator, looking at 316L welds, reported reductions in ferrite of 5% or more as well as spheroidization of the remaining ferrite after a standard solution anneal at 1900°F (1038°C) (Delong 1974). David also observed a reduction in ferrite and a similar change in morphology with heat treatments as short as 10 min at 1922°F (1050°C) in 308 weld metal (David 1981). Raghunathan et al looked at 316 welds of 316L sheets and found similar changes in ferrite content and morphology (Raghunathan et al 1979).

The previous three studies examined weld metal but similar reductions and spheroidization of ferrite were obtained during the course of this research with CF3M castings (Ratke 1987). Ratke found reductions in ferrite which ranged from 2% after 2 min at 1900°F (1040°C) to 72% after one hour at 2050°F (1121°C). Note that all the temperatures in these investigations were within the heat treatment specification. The specification allows for variations in

time, temperature and cooling rate which have been shown to significantly change the amount and morphology of the ferrite. Clearly, the solution heat treatment of CF3M is not as straightforward as previously thought and may provide a useful means of ferrite control in CF3M castings.

CF3M Microstructure and Mechanical Properties

The importance of control of ferrite in CF3M becomes clear if we examine the effect of ferrite content on mechanical properties. Since CF3M cannot be strengthened by heat treatment or hot or cold working, incorporating ferrite into the austenite matrix is the only strengthening mechanism available. Both yield and tensile strengths increase with increasing ferrite content. The presence of ferrite also improves the weldability and maximizes corrosion resistance in some environments (Weiser 1980).

The relationship between ferrite content and mechanical properties in CF cast alloys was studied in detail by Beck et al. Their data show, at room temperature, higher ferrite content increases strength with only slight losses in ductility (Beck et al 1965). The goals of this study were to examine the feasibility of controlling the ferrite content in the foundry and to look at the effects of ferrite on the corrosion resistance and mechanical properties. Also included were effects of various aging times and temperatures.

The changes in ferrite contents in Beck's study were controlled by composition only, so all comparisons are between pours not within a pour. The specimens were given a 2 hour solution heat treatment at

2050°F (1121°C) with a water quench. All testing took place on the solution annealed and aged specimens. No as-cast measurements of microstructure or mechanical properties were reported.

The three CF3M pours included in Beck's study had ferrite contents of 0%, 20%, and 39% after the solution anneal. Table 2 summarizes their data for CF3M. As with the other CF alloys, tensile and yield strengths increase with increasing ferrite and ductility and Charpy impact values decrease.

In 1976, Beck was involved in another comprehensive study of the mechanical and corrosion properties of cast austenitic stainless steel (Wieser et al 1976). This study also concentrated on aging but contained some property data from two CF3M pours; one low ferrite, 9%, and one higher ferrite, 19%. As with the 1965 study, no as-cast properties were reported. The lower ferrite content CF3M pour contained high nitrogen. Table 3 summarizes their data for CF3M. Again, increases in strength and decreases in ductility are seen with increases in ferrite. An interesting difference between this 1976 study and the 1965 study is the conflict in Charpy data. The 1976 work shows higher Charpy impact values with higher ferrite while the 1965 study showed the reverse.

In a recent work by Shendye, room temperature Charpy values decreased with increased ferrite content (Shendye et al 1987). Shendye used a solution anneal of 1 hour at 2050°F (1121°C) with a water quench. Again, no as-cast values are reported.

Another recent study included CF3M pours but mechanical data is reported for CF8M only. Again, an increase in strength with increases in ferrite content is observed (Riihimaki 1987). The

TABLE 2

FERRITE CONTENT AND MECHANICAL PROPERTIES OF CF3M
(Beck et al 1965)

Ferrite volume %	0	20	39
Tensile Strength (ksi)	67.6	89.6	92.5
Yield Strength (ksi)	28.6	46.2	55.0
Elongation %	70	53	43
Reduction in area %	73	67	65
Charpy Impact (ft-lbs)	155	128	78

TABLE 3

FERRITE CONTENT AND
MECHANICAL PROPERTIES OF CF3M
(Wieser et al 1976)

Ferrite number	9	19
Tensile Strength (ksi)	78.2	81.0
Yield Strength (ksi)	38.3	40.5
Elongation %	54	42
Reduction in area %	65	73
Charpy Impact (ft-lbs)	137	152

relationship between ferrite content and impact strength was not as clear. No details were given on the testing technique or solution annealing method. It appears from their graph of impact data that there is no strong relationship between impact strength and ferrite content until after approximately 30 hours of aging at 752°F (400°C) when impact strength was lower with higher ferrite content.

Table 4 summarizes the data discussed above. Although the relationship between strength and delta ferrite appears to be well documented, the effect of ferrite on the impact strength of CF3M is not clear. Very little information is available on solution annealed CF3M mechanical properties and essentially no information is available on investment cast CF3M, either as-cast or after solution heat treatment. The as-cast properties must be examined in addition to the solution annealed condition to determine the range of control available for ferrite content and morphology. The effect of ferrite on the impact properties is especially important as the need for tough as well as strong and corrosion resistant castings grows.

TABLE 4

SUMMARY OF FERRITE CONTENT AND MECHANICAL PROPERTIES
(Beck et al 1965, Wieser et al 1976, Shendye et al 1987).

Ferrite Content*	0	7	FN9	FN19	20	20	39
Tensile Strength (ksi)	67.6	---	78.2	81.0	89.6	---	92.5
Yield Strength (ksi)	28.6	---	38.3	40.5	46.2	---	55.0
Elongation %	70	---	54	42	53	---	43
Reduction in area %	73	---	65	73	67	---	65
Charpy Impact (ft-lbs)	155	262	137	152	128	145	78

*FN - Ferrite Number, all other ferrite content values are volume %

CHAPTER III

EXPERIMENTAL RATIONALE

As discussed in the literature review, both the rate of solidification and the heat treatment have been shown to affect the amount and morphology of delta ferrite, yet very little work has been done toward taking advantage of these effects in the foundry. This study addresses this by examining the microstructures resulting from solidification rates typically encountered in an investment foundry. The mechanical properties are then examined in the as-cast and heat treated conditions. Although the solution anneal heat treatment is known to change the ferrite amount and morphology, this effect has not been examined in detail. Specifically, there is essentially no information available on as-cast vs. heat treated CF3M. The microstructures and the mechanical properties of these two conditions must be examined in detail within one pour chemistry to begin to sort out the influences of processing parameters on the properties of CF3M.

This study determines the relationships between processing parameters and final performance, with microstructure being the key link in the chain. These relationships for CF3M are useful for examining control limits for the whole class of cast austenitic stainless steel alloys. The results will be improved processing and improved control of processing by providing much needed data to

investment foundry control systems, whether they be computer or human. Current foundry processes can be optimized with the help of additional data, producing increased quality and competitiveness. New processes will be developed faster with improved cooperation between research and industry as in this project.

CHAPTER IV

EXPERIMENTAL PROCEDURES

Overview

The experiments were designed to determine if investment cast CF3M, heat treated to the maximum ferrite content, would exhibit a superior combination of impact and tensile strength when compared to the commonly accepted one hour solution anneal. After pouring of the CF3M at the foundry, the microstructural response to heat treatment needed to be determined for this specific alloy before going any further. After the heat treatment time-ferrite content relationship was established, the mechanical test specimens were heat treated and tested. Figure 6 shows an overview of the experimental work.

Casting and Specimen Preparation

Investment casting requires the production of an expendable wax pattern which is coated with a series of ceramic slurries containing binders. The primary slurry coats contain very fine particles which give an excellent surface finish. The subsequent secondary coats contain coarser refractory sands. The coatings are dried and fired and the wax is melted and burned out leaving the mold ready for pouring. Figure 7 shows an example of this process for one of the

1. Casting of material at foundry

2. Preparation of test specimens

3. As-cast Charpy tests

4. Microstructural characterization of as-cast material

5. Heat treatment Series 1

6. Microstructural characterization of Series 1

7. Heat treatment Series 2

8. Microstructural characterization of Series 2

9. Heat treatment of tensile and Charpy bars

10. As-cast and heat treated tensile tests

11. Heat treated Charpy tests

12. Fractography

Figure 6. Overview of Experimental Sequence.

large test slabs produced during the course of this work. First, a wood pattern was made in the shape of the final casting desired. Next, a polymer resin two part mold was made to use for casting the wax patterns. A wax pattern like the one shown was attached to a gating system to produce the ceramic mold resulting in the final casting on the right of Figure 7.

The test slabs for the Charpy specimens were produced in the Mechanical and Aerospace Engineering Research Laboratory by the ceramic shell investment casting method using supplies and procedures representing current technology in high quality investment casting. A plexiglass mold was used to cast the wax patterns which were then assembled with a pouring cup and sprue into trees. After the pattern trees were cleaned with solvent and pre-wet with Primcote colloidal silica binder, succesive layers of Primcote based slurry, zircon sand and fused silica stucco were applied. The tensile specimen trees were prepared in a similar manner at the foundry.

The molds were taken to American Foundry's Investment Division in Bixby, Oklahoma, for dewaxing, burn out, firing and pouring. After autoclave dewaxing, half of the molds were insulated with 1/2 inch of Fiberfax carborundum. The insulated molds were placed in a 1093°C (2000°F) furnace for burn out and firing. The uninsulated molds were burned out and fired at 982°C (1800°F). The insulated molds were poured within 30 seconds of removal from the furnace. The uninsulated set of molds were poured approximately five minutes after removal from the furnace. Pouring temperature was 1621°C (2950°F). Table 5 shows the chemistry of the melt as measured by spectrometry at the foundry compared with the ASTM specification.

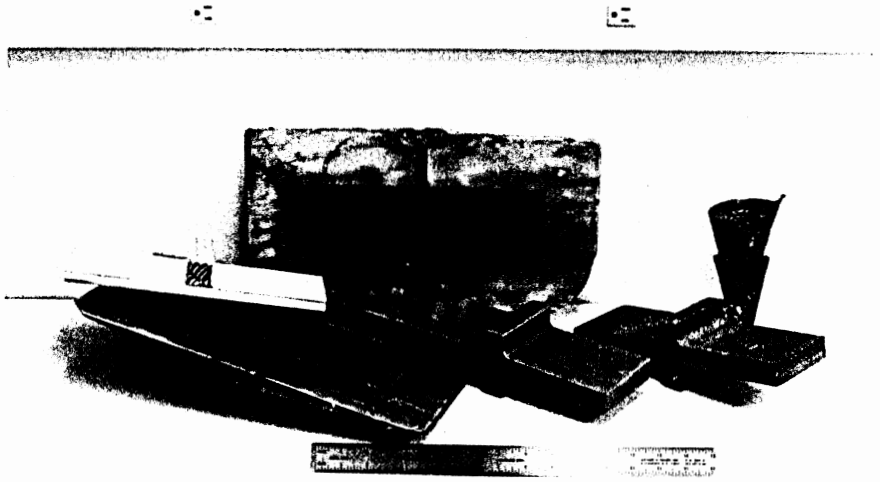

Figure 7. Steps in the Production of a Test Casting.

TABLE 5

MELT CHEMISTRY COMPARED WITH ASTM 743

	Cr	Ni	Mo	C	Mn	Si	P	S
wt%	18.66	9.79	2.29	0.03	1.33	1.13	0.018	0.018
				ASTM 743				
MAX	21.00	13.00	3.0	0.03	1.50	1.50	0.040	0.040
MIN	17.00	9.00	2.0					

The molds were allowed to cool in the sand pouring bed for approximately one hour and in insulated metal buckets for an additional two hours.

After the molds were broken off, the specimens were removed from the gating systems and the remaining ceramic was removed with a 204°C (400°F) NaOH caustic bath. Figure 8 shows the test slab trees, tensile trees and large test slabs after all but one of the molds have been removed. The pour yielded two large test slabs, two tensile specimen trees of six bars each and four trees of test slabs for Charpy specimens. Each Charpy test slab was machined into five Charpy specimens as shown in Figure 9, for a total of 40 specimens. After Charpy testing, the bars provided material for heat treatment tests and microstructural evaluation as shown in Figure 9. Half of the material was cast in uninsulated molds and the other half was cast in insulated molds.

Heat Treatment

Heat treatments were carried out in the MAE laboratory at the highest recommended solution anneal temperature for CF3M; 1121°C (2050°F), followed by a water quench. This is within the standard ASTM and ASM specifications, time at temperature being dependent on section size (ASTM A743, ASM 1980). A Lindberg 1700°C laboratory crucible furnace with a Eurotherm 810 controller provided resolution to 1°C.

The heat treatment specimens were 1cm x 1 cm x approximately 1 cm cut from used as-cast Charpy bars. Figure 9 showed the location and orientation of the specimens. All specimens were labelled to

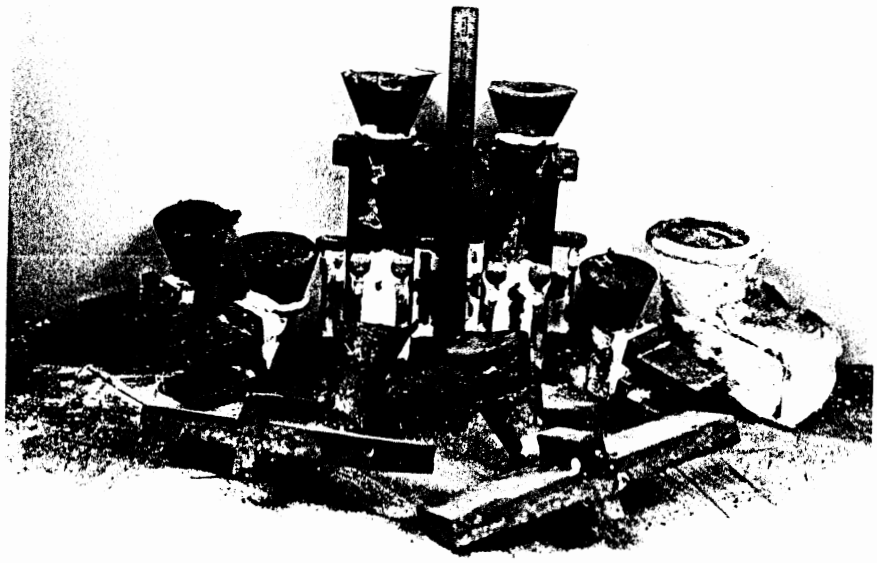

Figure 8. Castings Obtained from the Foundry Pour.

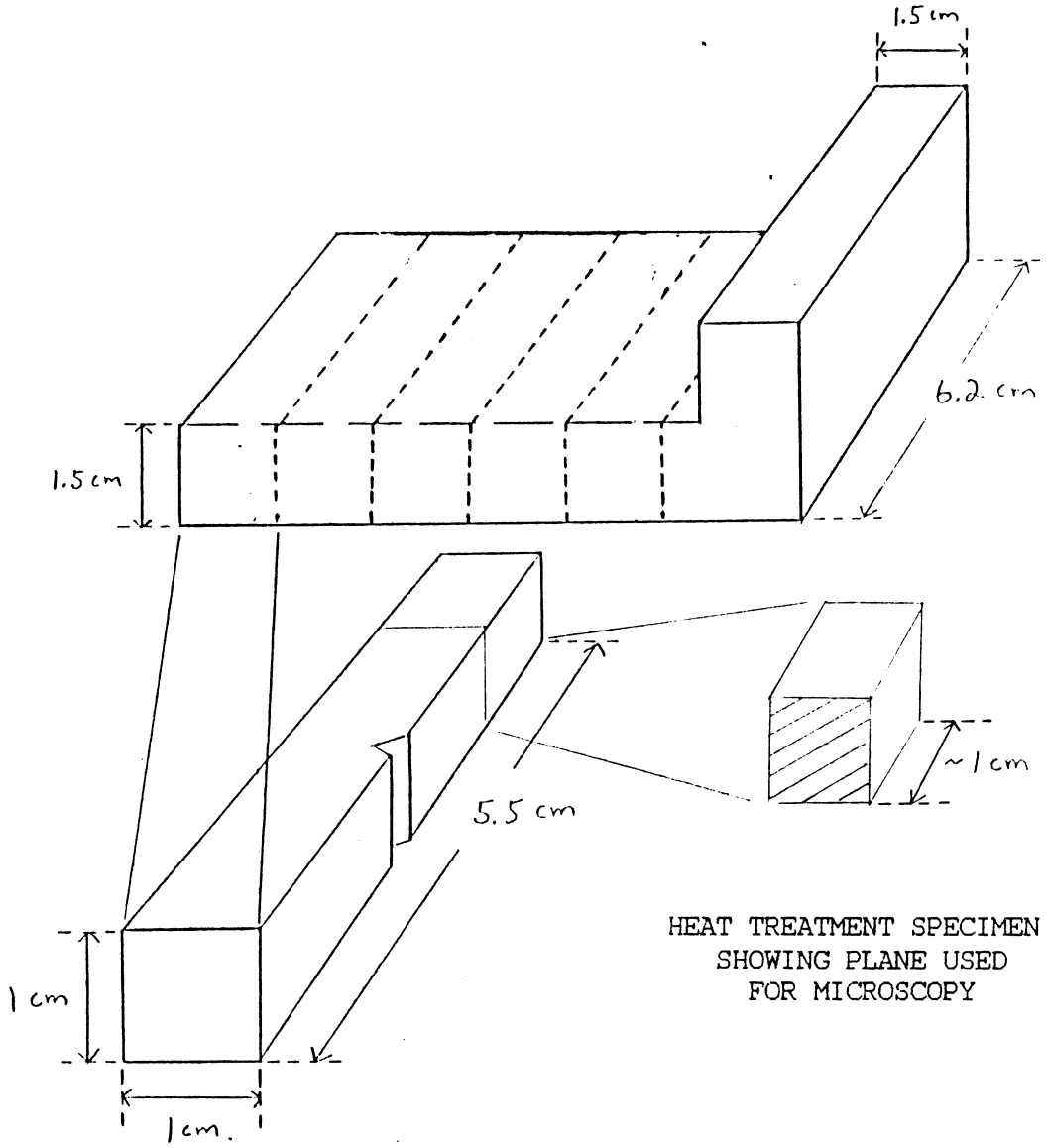

Figure 9. Sectioning of the Cast Test Slabs into Charpy Impact Bars and Heat Treatment Specimens.

identify their original location and orientation on the cast tree.

Timing of the heat treatments started after the furnace regained the temperature lost upon opening the furnace door; approximately 50 seconds. This recovery time included an overshoot of about 8°C approximately 10 seconds after the furnace door was closed with a return to the 1121°C test temperature within one minute. In the second heat treatment series, the furnace stabilized 5-10 seconds faster due to the placement of blocks of stainless steel in the furnace to aid in heat transfer. Heat transfer calculations conservatively estimate that the specimens reached 1120°C after 40 seconds of exposure to the furnace environment and therefore were at the test temperature when timing of the heat treatments began. Appendix A provides details of the heat transfer model calculations.

Three heat treatment series were done. The first, Series 1, was to measure the response of this particular chemistry and processing to heat treatment over a wide range of times; 2 to 480 minutes. The second, Series 2, was to examine in more detail the response during the first 30 minutes of heat treatment. Based on the information from the first two series, the mechanical test specimens were then heat treated. Table 6 summarizes the heat treatment regimens.

Mechanical Testing

Rockwell Hardness

Rockwell hardness measurements were made on a Leco R-600 digital Hardness Tester. The calibration of the machine was checked with commercial standards before each set of measurements.

TABLE 6

HEAT TREATMENT REGIMENS
UNINSULATED AND INSULATED MOLD SPECIMENS

TIME (min)	SERIES 1	SERIES 2	MECHANICAL TEST SPECIMENS
2	X	X	
4	X	X	
5			X
8	X	X	
12		X	
15	X		X
16		X	
20		X	
24		X	
28		X	
30	X		X
32		X	
60	X	X	X
90	X		
240	X		
480	X		

Tensile Testing

Tensile testing was conducted to examine the effect of microstructure on the tensile strength and % elongation. The two trees of tensile specimens provided six specimens per mold condition. For the uninsulated and insulated mold specimens, testing was done in the as-cast and heat treated 5 min, 15 min, 30 min and 60 min conditions.

The tensile specimen dimensions were: nominal diameter, 6.25 mm (0.25 in) and gage length, 25 mm (1.0 in). This comforms to ASTM specifications for small size specimens, which are standard round tension test specimens proportional to the full size standard 12.5 mm (0.5 in) diameter and 50 mm (2.0 in) gage length.

The tensile testing took place at Metlab in Tulsa. Room temperature tests were done on a SATEC system with a Baldwin load frame. The system was calibrated by Texas Calibration Co.. All strength testing followed ASTM specifications (ASTM A370, ASTM E8).

Charpy Impact Tests

Toughness is becoming more important as the service conditions in areas such as aerospace become more demanding. ASTM specifications are available for fracture toughness testing to obtain K_{Ic} and J_{Ic} values (ASTM E399, ASTM E813). Although these values are themselves valuable as material properties, they are not easily applied to CF3M investment castings which normally have much smaller section thicknesses than the toughness testing requires. Even for compact J_{Ic} specimens, which have a less stringent size

requirement, a CF3M specimen of over one inch thickness is needed for plane strain conditions (ASTM E813). For K_{Ic}, the thickness needed is over three inches (ASTM E399). All of the austenitic stainless steels are too tough for obtaining valid plane strain fracture toughness data on specimens of reasonable size (ASM 1982). This was confirmed by preliminary testing in our lab. Since toughness is becoming such an important issue in material quality, even for relatively tough materials, the thickness criterion is being questioned and other techniques are in the process of being developed and standardized to handle specimens of more reasonable and representative size (Robinson and Tetelman 1974, Bates et al 1981, Munz 1979, Priest 1986). Few values of K_{Ic} or J_{Ic} are available for investment cast CF3M.

The most widely used toughness related test is Charpy impact (ASTM E23). With Charpy testing, the effects of the microstructure on impact energy, lateral expansion and fracture mode can be examined. As discussed in the literature survey, some Charpy data is available for CF3M. The Charpy test was chosen for this study to obtain quantitative data on the as-cast CF3M and to complement the existing data on heat treated CF3M that is available in the literature.

Twenty specimens were obtained from the uninsulated castings and twenty from the insulated castings, as described above. Charpy test temperatures for the as-cast material included -196°C, -70°C, 0°C and 20°C to examine any transition temperature effects that the presence of bcc ferrite may have. Charpy tests for the heat-treated material were performed at -196°C and 20°C. Table 7 outlines the Charpy testing regimen.

TABLE 7

CHARPY IMPACT REGIMEN
UNINSULATED AND INSULATED MOLD SPECIMENS

TEST TEMPERATURE (degrees C)	-196	-70	0	20
AS-CAST	X	X	X	X
HEAT TREATED (min)				
5	X			X
15	X			X
30	X			X
60	X			X

Charpy impact testing took place in the Civil Engineering Laboratories at Oklahoma State University on a Satec Systems Inc. Model S1-1C3 which had been recently calibrated. Impact energy, lateral expansion and observations of the fracture surface were collected.

Microstructural Analysis

Light Microscopy

The Charpy impact bars provided heat treatment specimens which were used for microstructural evaluation. The location and orientation of the specimens were shown in Figure 9. Mechanical polishing to 0.05 micron was followed by electroetching with CrO_3-Acetic acid (Vander Voort 1984). This was found to be the best combination to reduce unwanted scratches and outline the delta ferrite without excessive relief which would interfere with the estimate of ferrite content. The manual point count method, ASTM E562-83, was used to determine the ferrite content. Ferrite morphology was also evaluated to further document the changes in ferrite with heat treatment time. Micrographs were taken for comparison among as-cast and heat-treated conditions.

Electron Microscopy

Scanning electron microscopy was used to further evaluate the fracture surfaces. The JOEL JSM-35 Scanning Microscope at the Electron Microscopy Laboratory at Oklahoma State University was used to examine and document the fracture surfaces of the Charpy and tensile specimens.

A CAMECA CAMEBAX SX50 with wavelength spectroscopy capability at the University of Oklahoma Microprobe Laboratory was used to document microsegregation in the as-cast CF3M.

To examine the the composition of inclusions, X-ray spectroscopy was done on an EDAX system at Mercury Marine division of Brunswick Corporation in Stillwater, Oklahoma.

CHAPTER V

RESULTS

As-cast Microstructure

The microstructure is the key link between processing and final properties. A detailed microstructural examination was done for both the as-cast and heat treated conditions of the material cast in the insulated and uninsulated molds.

The test slab castings were designed to produce a uniform microstructure throughout the Charpy specimens. Modeling of the solidification heat transfer indicated isotherms parallel to the mold wall indicating the microstructure should not vary significantly over the length of the slab. The uniformity was confirmed by microscopic examination of the three planes. This was consistent with other investigations using comparable conditions (Leger 1982, Durham and Cohen 1989).

After the as-cast Charpy impact testing was completed, the impact specimens provided material for heat treatment and microstructual examination. All micrographs are taken on the plane shown in Figure 9 of the previous chapter. This plane is perpendicular to the riser which is the cross sectional plane of the Charpy specimens. The apparent differences in the structures are due to orientation variations in the dendrites.

Figures 10 and 11 show typical as-cast CF3M microstructures from the uninsulated and insulated molds. The darker narrow regions are ferrite along the dendrite cores and the lighter matrix is austenite.

Figure 10 shows the finer structure resulting from solidification in the uninsulated molds. The mean dendrite arm spacing for the uninsulated specimens is 18.5 microns (s=1.43).

Figure 11 shows the coarser structure resulting from the slower solidification rate in the insulated molds. The mean dendrite arm spacing for the insulated specimens is 31.9 microns (s=5.5); about 72% wider spacing than in the uninsulated specimens.

The mean as-cast ferrite contents from 18 specimens were 10.6% for the uninsulated molds and 9.6% for the insulated molds. Although there was a significant difference between the mean values by t-test, the mean values on individual specimens had 95% confidence intervals of about 1.0-1.6% so the statistical difference in the overall means is misleading. Realistically, the manual point count method cannot resolve a 1% difference in ferrite.

Wavelength spectroscopy was used to demonstrate the steep concentration gradients established during solidification. Keeping in mind that chromium and molybdenum are ferritizers and nickel is an austenitizer, Figure 12 shows a line scan through three ferrite areas. The areas of high chromium and molybdenum and low nickel correspond to the ferrite. The scan was done on an etched specimen. The lack of symmetry of the peaks in Figure 12 is due to the height changes of the specimen as the beam tranverses the two phases.

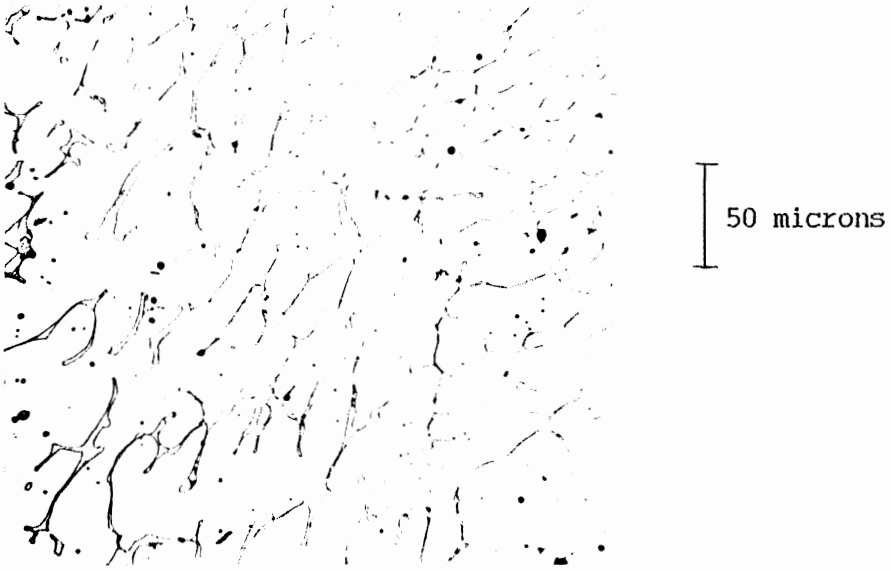

Figure 10. As-cast Microstructure from Uninsulated Mold.

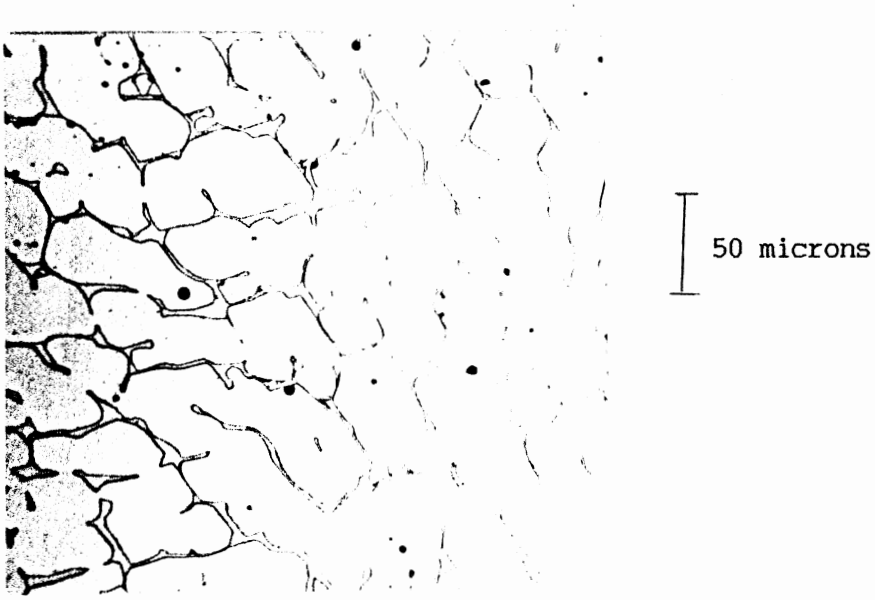

Figure 11. As-cast Microstructure from Insulated Mold.

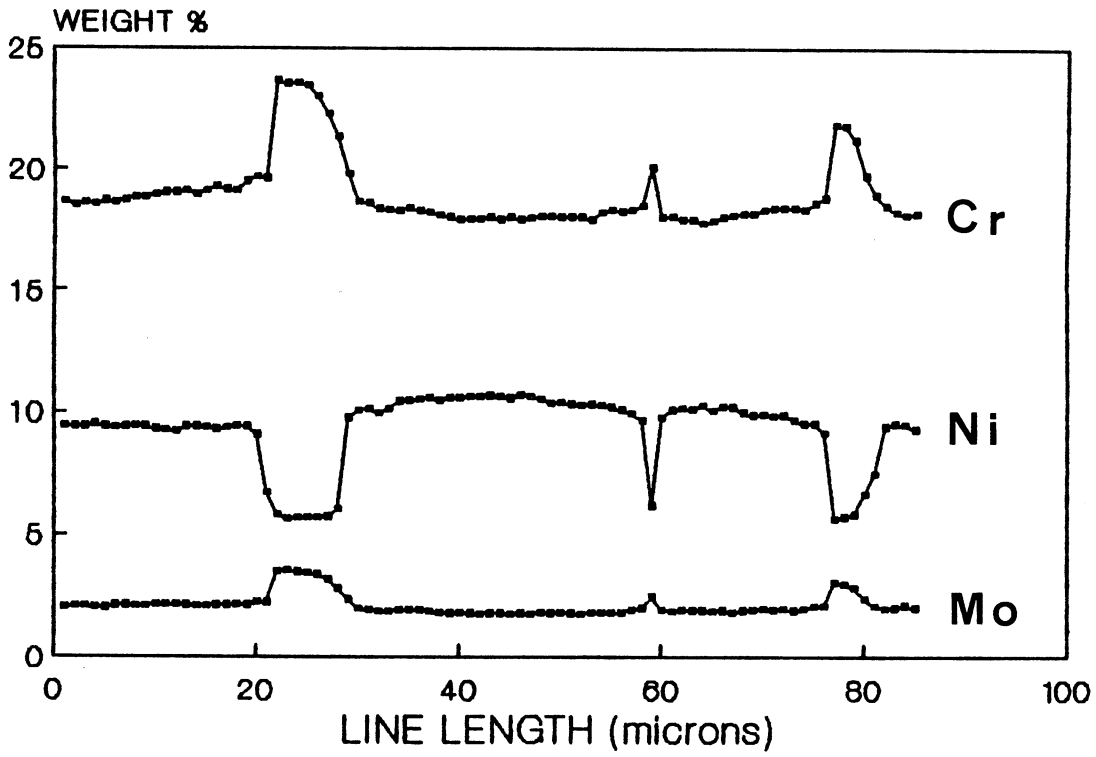

Figure 12. Wavelength Spectroscopy Line Scan.

Heat-treated Microstructure

The present study contains a detailed examination of the microstructural response of one pour of CF3M to heat treatment at the highest recommended heat treatment temperature, 1121°C (2050°F).

Figure 13 shows the results of heat treatment Series 1, which included heat treatment times from 2 to 480 minutes. The fraction of ferrite remaining is expressed as a ratio of the ferrite content to the ferrite content for that specimen in the as-cast condition. By 2-5 minutes, there was an increase in ferrite content of about 20-40%. This corresponds to an increase in volume % from the as-cast value of 10% to the heat treated value of 12% for the uninsulated molds and 8% to 11% for the insulated molds.

The data from Series 1 suggested that there may be another increase in ferrite after about 20-30 minutes of heat treatment. A second heat treatment series examined the behavior of the microstructure in more detail during the first 30 minutes of heat treatment. Figure 14 shows the results of heat treatment Series 2. Series 2 also showed the increase in ferrite during the first few minutes of heat treatment. The presence of another increase in ferrite at 20-30 minutes could not be confirmed. In both heat treatment series, after 30-50 minutes of heat treatment, ferrite content dropped below the as-cast value, indicating ferrite dissolution.

While the amount of ferrite is changing, the morphology also changes. Figure 15 illustrates these changes with a series of micrographs from heat treatment Series 2. The ferrite pools go from

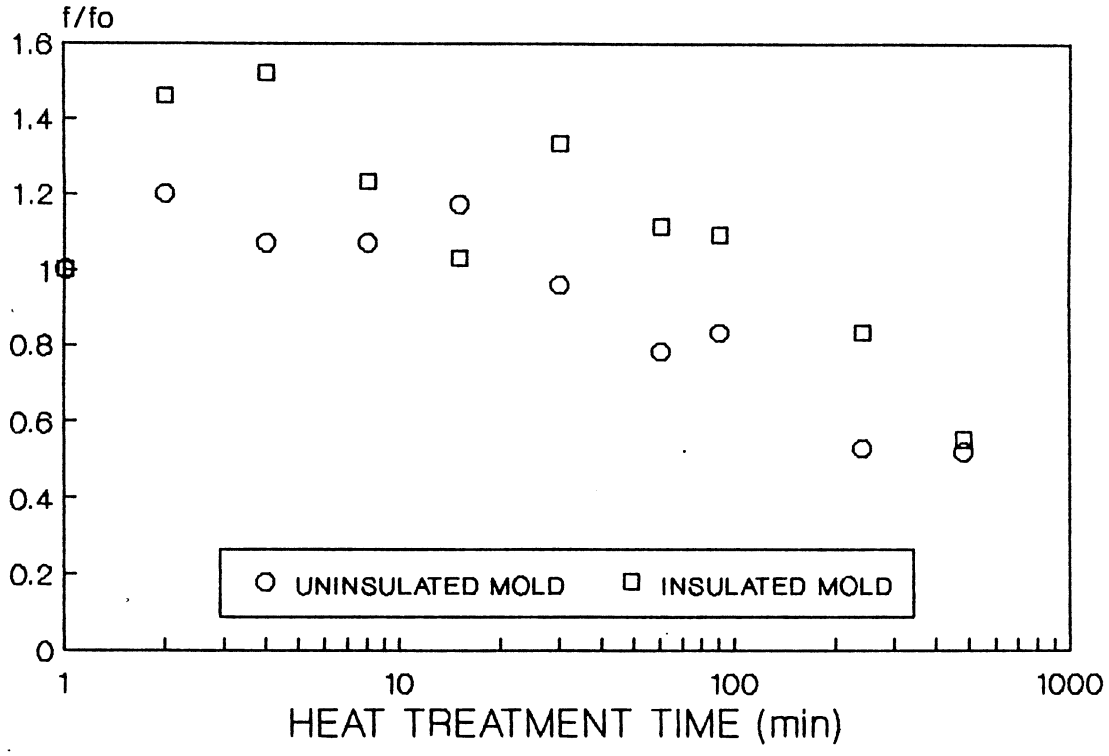

Figure 13. Changes in Ferrite Content, Series 1.

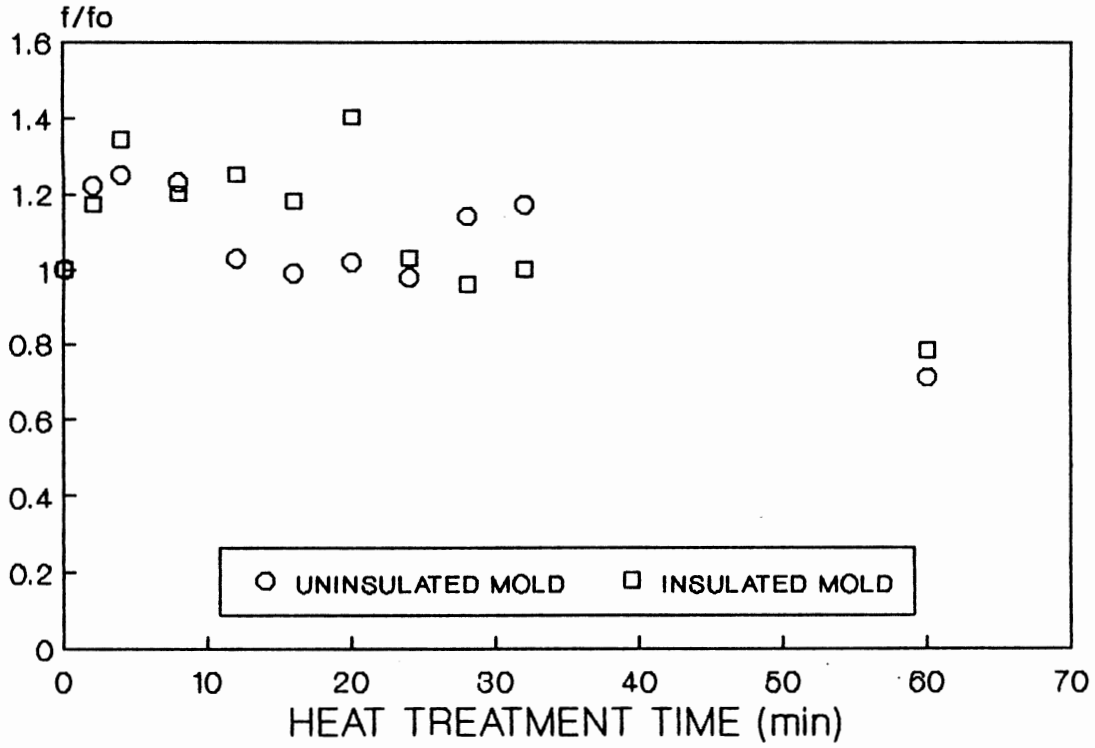

Figure 14. Changes in Ferrite Content, Series 2.

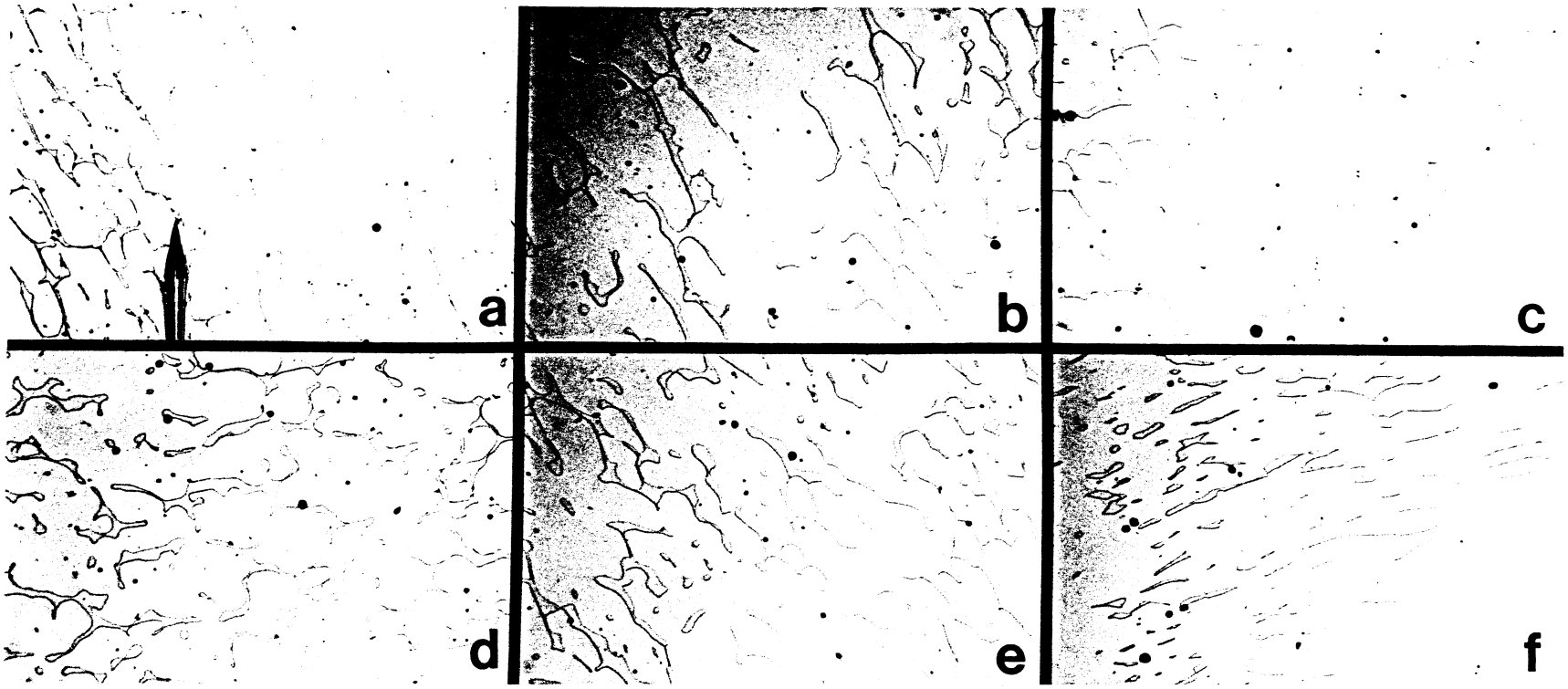

Figure 15. Changes in Ferrite Morphology. a) as-cast, b) 2 min, c) 4 min, d) 16 min, e) 28 min, f) 60 min. 270X reprinted .65X

a nearly continuous network with sharp corners in the as-cast condition to a more rounded and broken up structure as heat treatment progresses. A complete set of micrographs showing as-cast and heat treated structures for each specimen is included in Appendix B.

There were significant changes in the ferrite morphology after only two minutes of heat treatment. Figure 16 points out the major changes by comparing the as-cast structure to the same area of the specimen after two minutes of heat treatment. The most important change is the loss of the thin, continuous areas of ferrite indicated by arrows on the micrographs. There is also some rounding of sharp corners of the ferrite and what appears to be thickening of some areas.

Counts of the thin, threadlike ferrite areas were conducted using the micrographs from heat treatment Series 2. Measurements were taken on the same specimen before and after heat treatment. Table 8 shows the values for the uninsulated and insulated mold material. Although this one set of measurements cannot be considered statistically significant, the difference between the as-cast and heat treated values does reflect the thickening and rounding of the ferrite.

Rockwell Hardness

Rockwell B hardness measurements (HRB) were taken on the as-cast and heat treated specimens. The reported HRB hardnesses are averages of five or six measurements per specimen. These averages are tabulated in Appendix C.

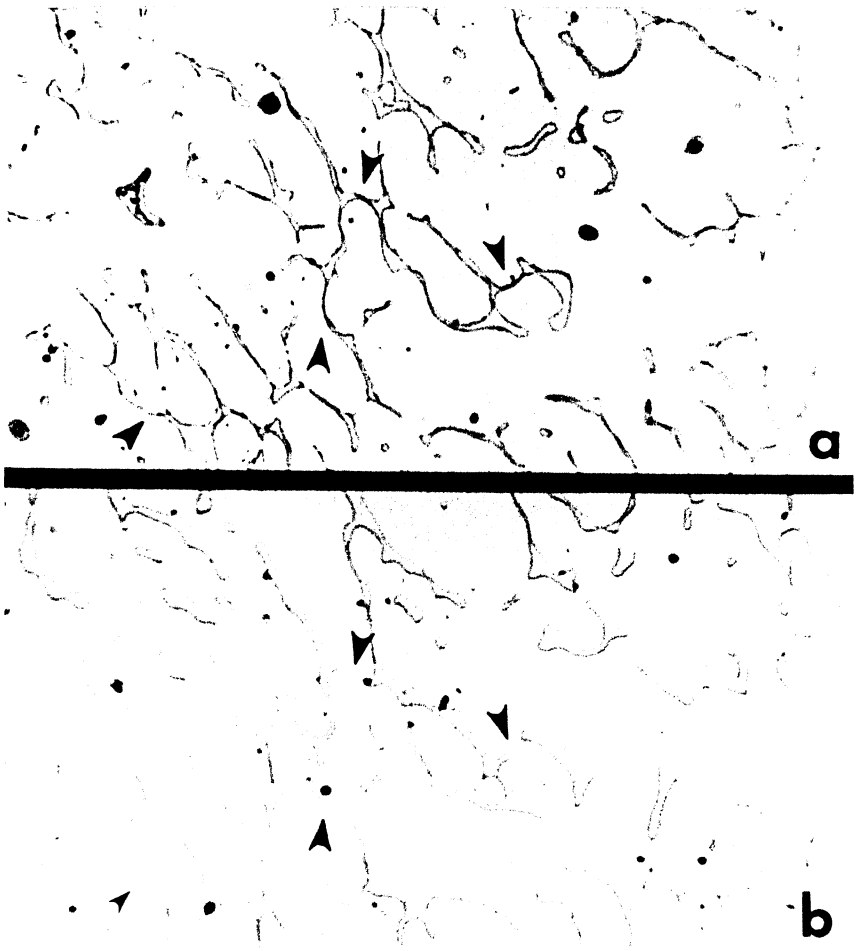

Figure 16. Detail of Ferrite Morphology Changes After Two Minutes. 270X reprinted 2X

TABLE 8

COUNTS OF THREADLIKE FERRITE

HEAT TREATMENT TIME (min)	UNINSULATED		INSULATED	
	AS-CAST	HEAT TREATED	AS-CAST	HEAT TREATED
2	15	3	13	1
4	14	2	10	2
8	12	4	8	2
12	16	5	9	2
16	14	1	10	1
20	15	4	8	1
24	12	1	9	5
28	13	0	13	2
32	12	1	11	4
60	12	0	12	2

Hardness measurements were made on all Charpy bars machined from the test slabs to examine any variation in the as-cast hardness. There was no significant differences in hardness from one end of a test slab to the other or between the upper and lower test slabs of each casting. Also, there was no significant difference between the specimens from insulated and uninsulated molds. The uninsulated mold specimens averaged HRB 91, compared to HRB 90 for the insulated mold specimens.

Hardness measurements were also taken on the heat treated specimens. As shown in Figure 17, the HRB measurements declined slightly but not significantly with heat treatment and did not change significantly as heat treatment progressed for 60 minutes. In addition, the insulated and uninsulated specimens behaved essentially the same.

Tensile Tests

Mechanical Data

Room temperature tensile tests were performed on the specimens in the as-cast and heat-treated conditions. Figure 18 shows a typical load-displacement curve obtained for the test specimens. The tensile data are tabulated in Appendix C.

Figure 19 shows UTS vs. heat treatment time. As with the hardness values described above, after a small decrease with heat treatment the tensile strength levels off at approximately 620 MPa

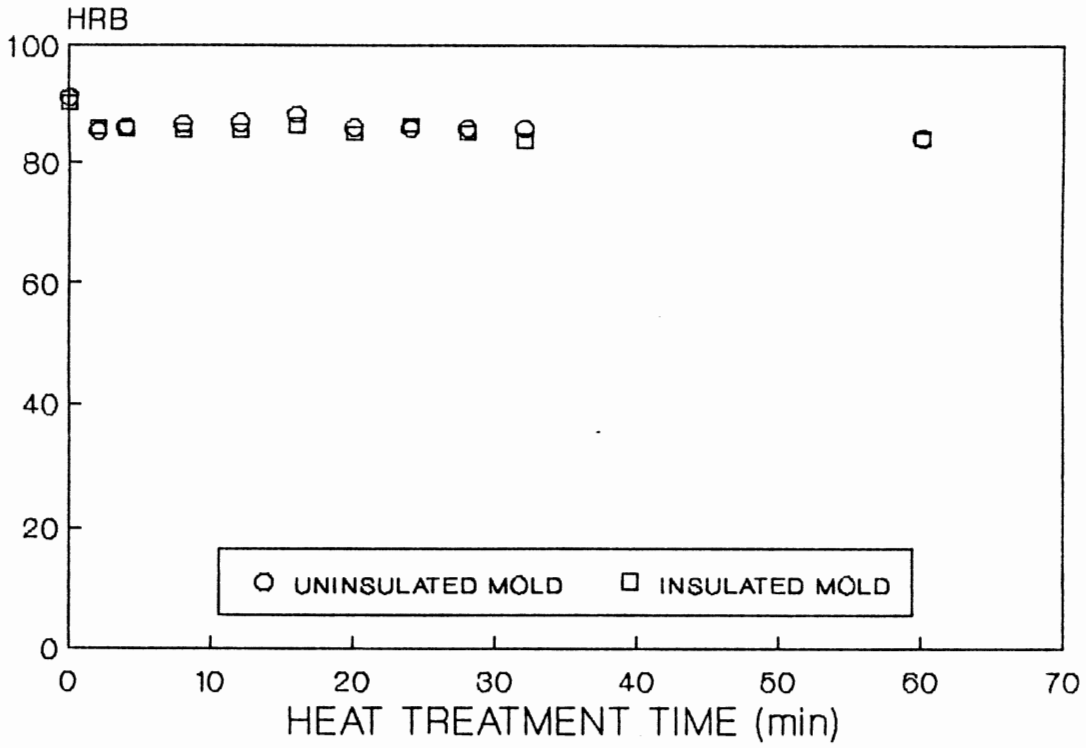

Figure 17. Rockwell B Hardness Measurements.

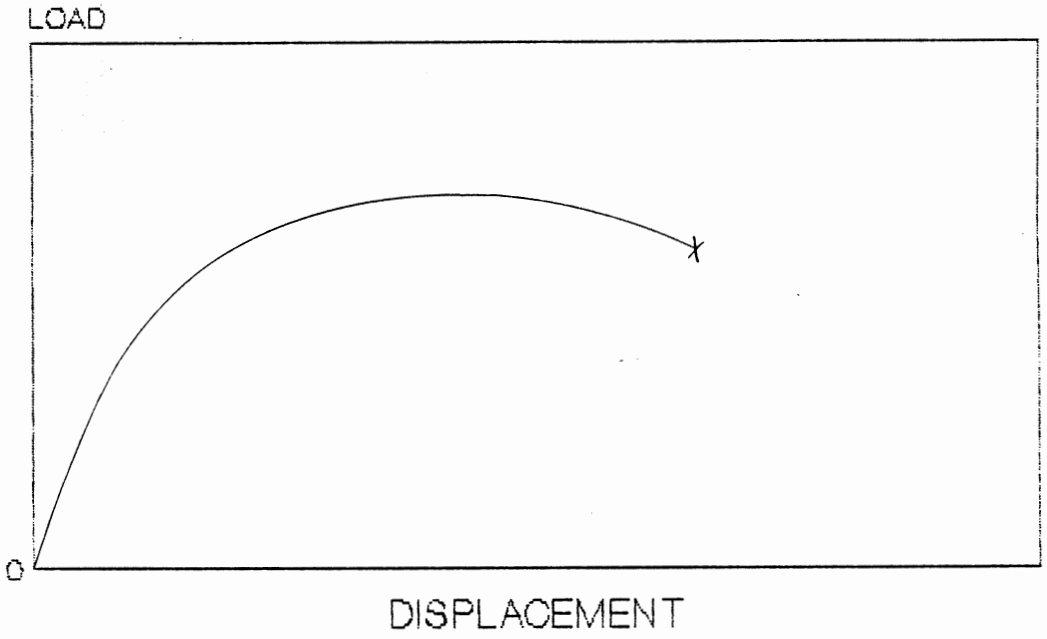

Figure 18. Typical Load-displacement Curve.

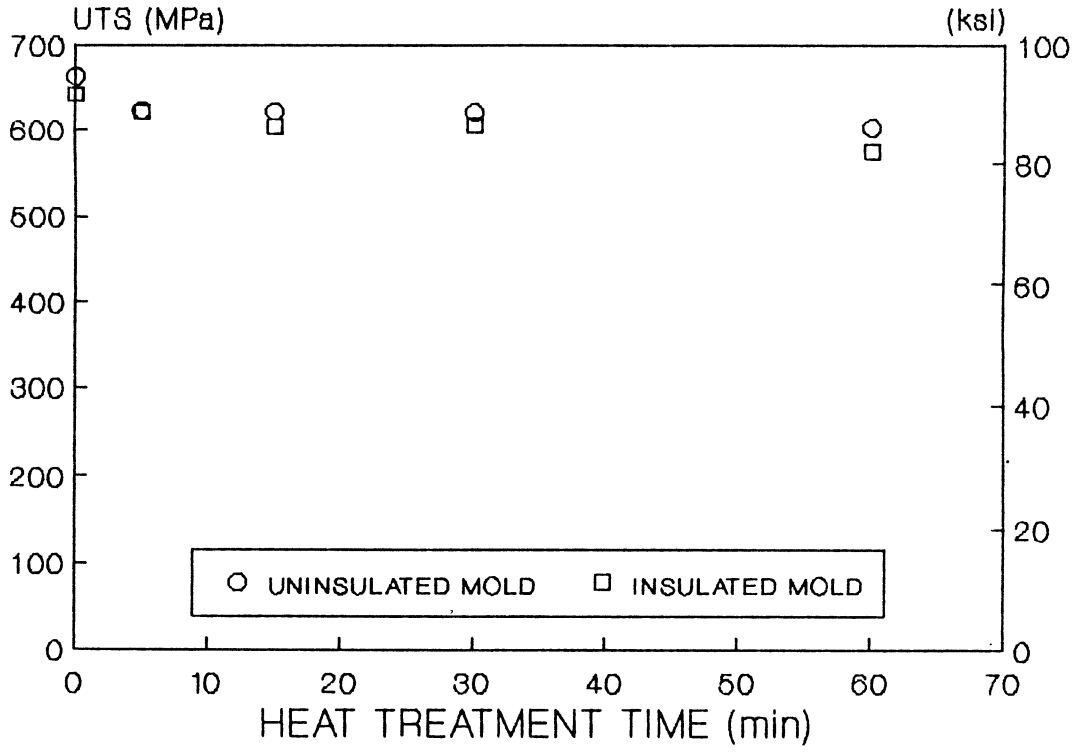

Figure 19. Ultimate Tensile Strength.

(90 ksi). Yield strengths were difficult to measure on some of the plots, but were in the range of 276-310 MPa (40-45 ksi).

Figure 20 shows % elongation vs. heat treatment time. As expected, the as-cast values are the lowest at about 30%. The % elongation increases to about 50% with heat treatment. The apparent differences in % elongation between the uninsulated and insulated material cannot be considered statistically significant. Each point is one measurement on one specimen. An error of about 5% elongation was found when a measure was repeated. This error is large enough to eliminate any apparent differences the plot may infer. ASTM specifications for % elongation state a minimum value only as shown in Table 1.

Fractography

Figure 21 compares 500X scanning electron micrographs from the central regions of the tensile specimens. The uninsulated specimens are shown above the insulated specimens. In the as-cast condition, both the uninsulated and insulated specimens show rough, irregular microvoids with some secondary cracking. The uninsulated specimen has a finer structure which reflects the finer spacing of the dendrites.

After only 5 minutes of heat treatment, obvious changes occur in the fracture surface. The microvoids become more equiaxed and the porosity of the specimen becomes more apparent. Typical microvoid sizes are 6 microns for the uninsulated mold specimen and 12 microns

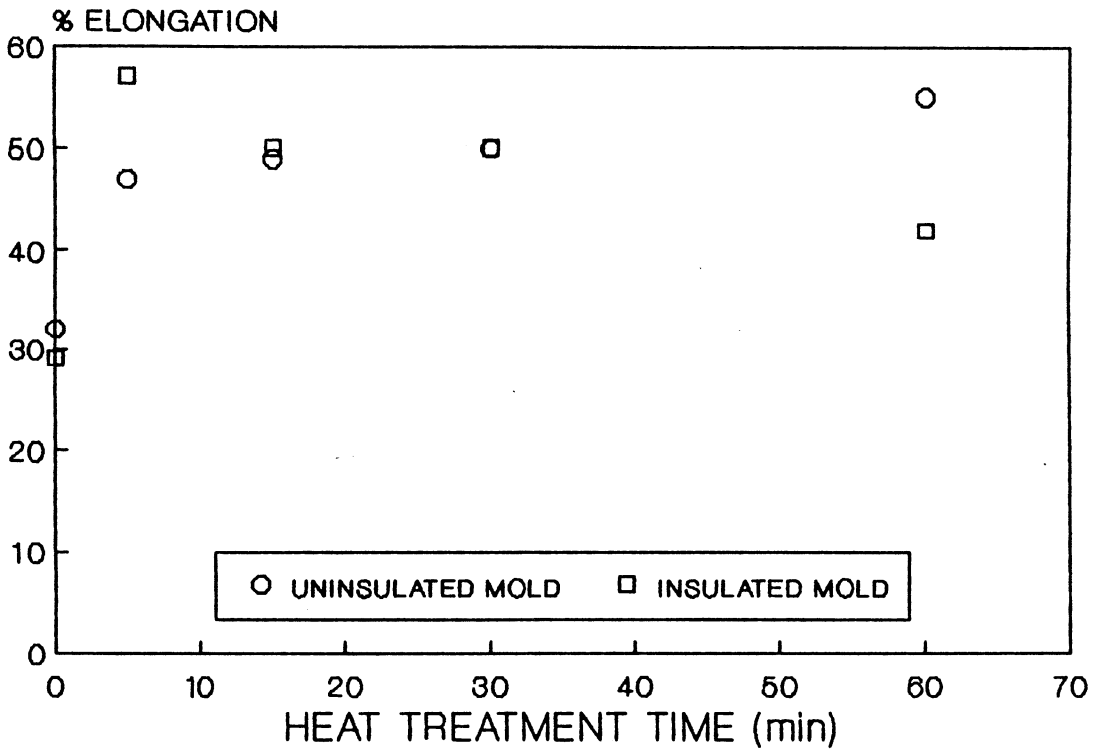

Figure 20. % Elongation.

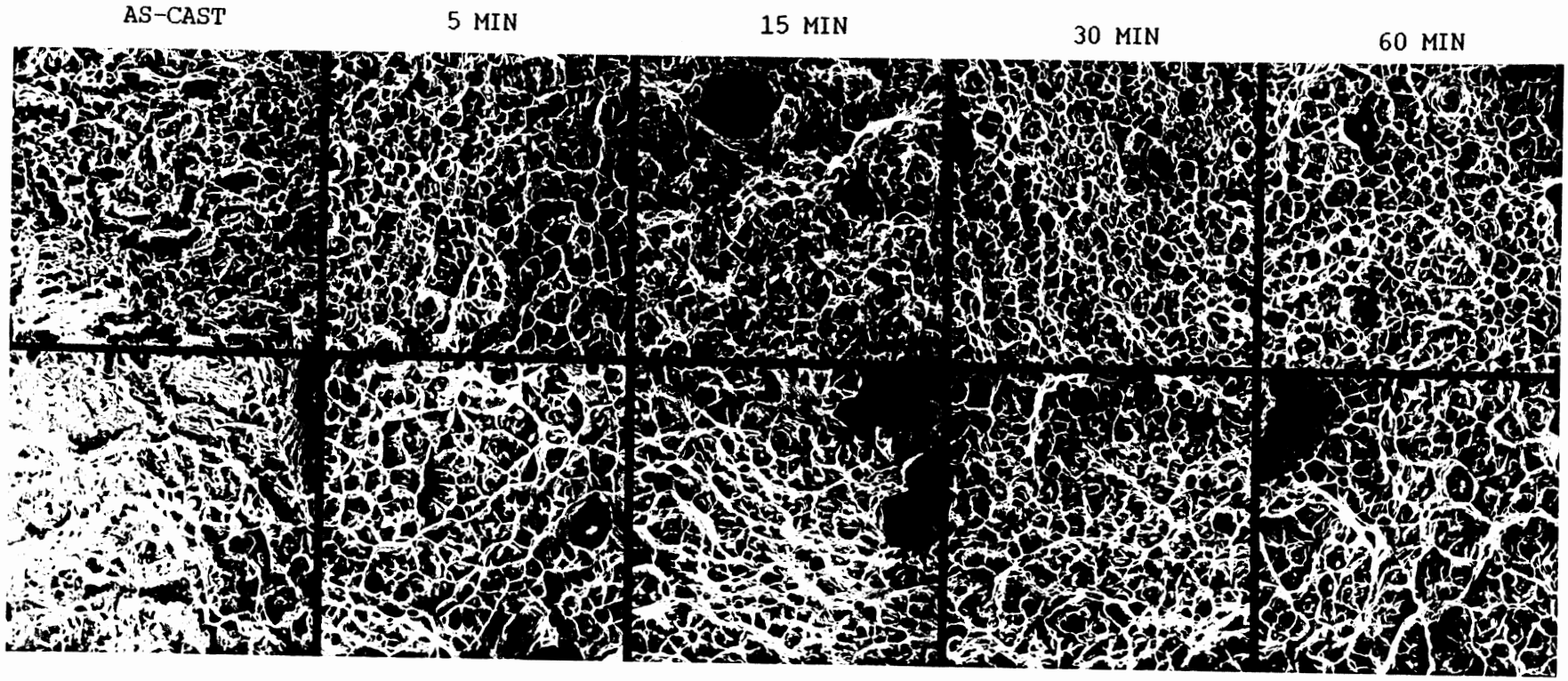

Figure 21. Tensile Specimen Microvoids. 500X reprinted .5X
Uninsulated Mold (top), Insulated Mold (bottom)

for the insulated specimen, again, reflecting the microstructural differences documented with light microscopy.

After 15 minutes of heat treatment, typical microvoid sizes for the uninsulated and insulated specimens are 6 and 8 microns respectively. At the 30 and 60 minute heat treatment times, the microvoids are becoming more uniform in size. Solidification porosity is still apparent. Typical microvoid size goes from 4 to 7 microns for the uninsulated specimen and 8 to 12 microns for the insulated. Figure 22 shows the trend in typical microvoid size for the uninsulated and insulated conditions. Each point is an average of 12 measurements. The averages and standard deviations are tabulated in Appendix C. The trend is similar for the uninsulated and insulated material but with a significant difference in microvoid size as expected from the microstructural characterization discussed above.

Charpy Impact

Mechanical Data

Figure 23 shows Charpy impact energy vs. test temperature for the as-cast CF3M. Figure 24 shows the corresponding lateral expansion measurements. In the as-cast condition, there was no significant difference in the Charpy impact behavior between the uninsulated and insulated specimens. Both sets showed reductions in impact energy and lateral expansion as the test temperature decreased, demonstrating the influence of the bcc ferrite transition behavior.

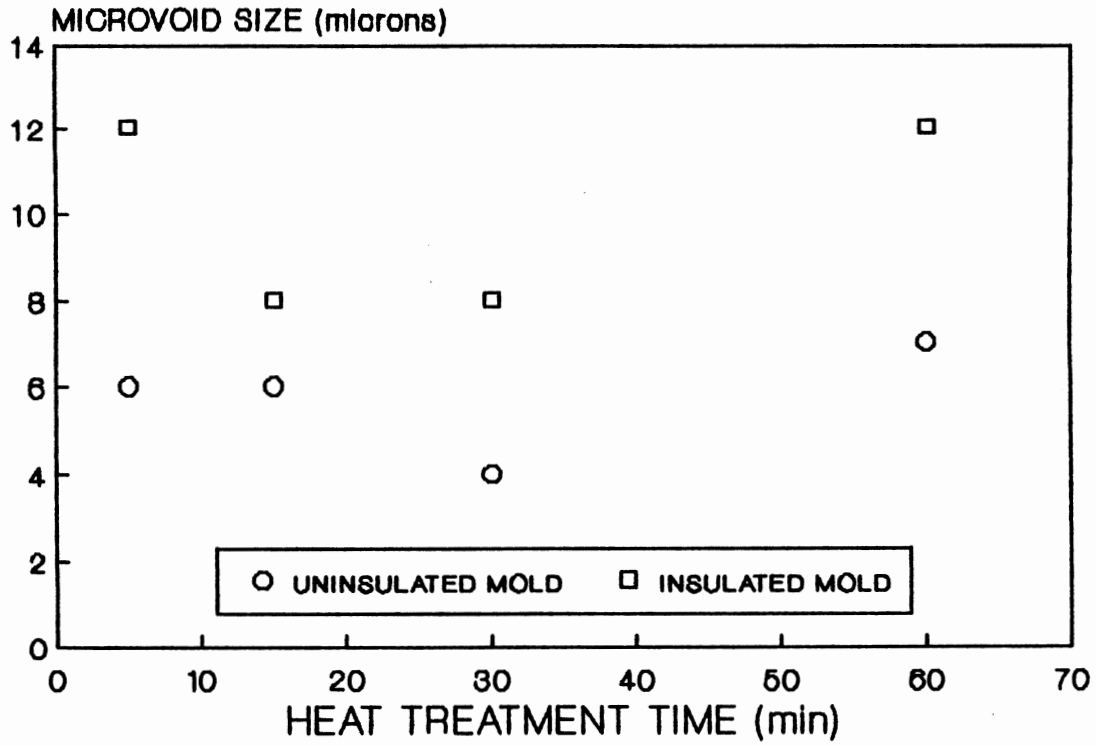

Figure 22. Changes in Microvoid Size.

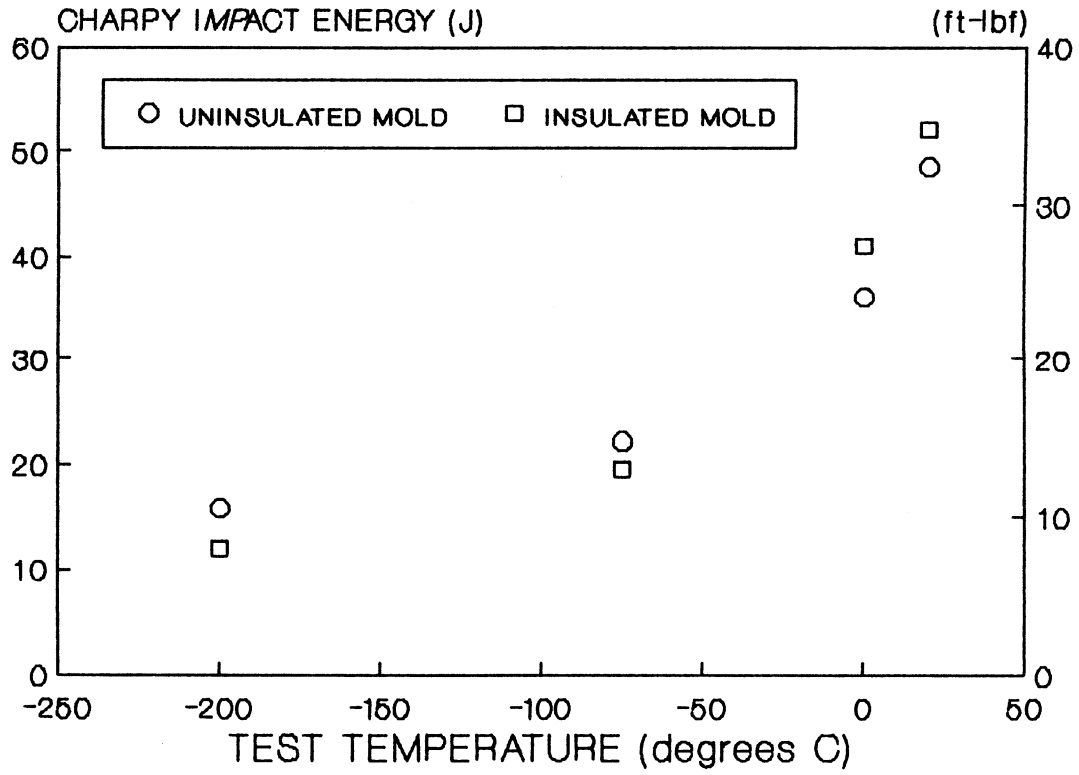

Figure 23. As-cast Charpy Impact Tests.

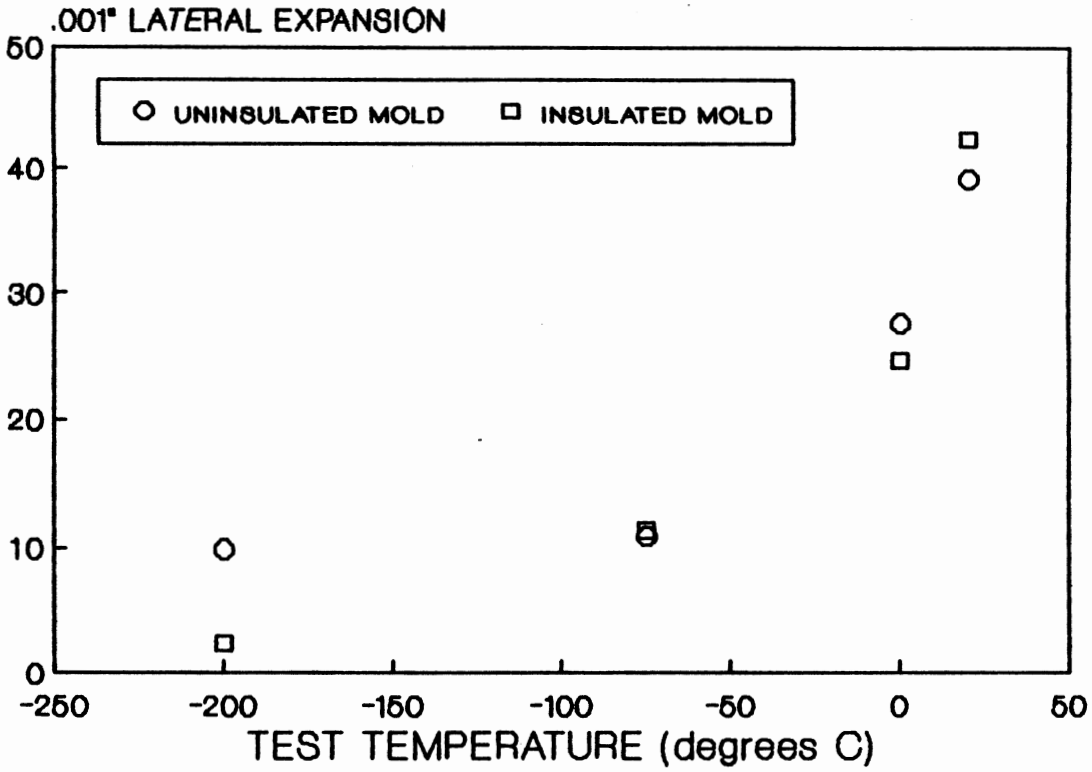

Figure 24. As-cast .001" Lateral Expansion.

The heat treated specimens were tested at -196°C and 20°C. After only five minutes of heat treatment at 1121°C, large increases in Charpy impact energy and .001" lateral expansion took place. Figures 25 and 26 show the response of 20°C Charpy impact energy and .001" lateral expansion to heat treatment. After 5 minutes of heat treatment, 20°C Charpy impact energy increased approximately 4X from the as-cast condition. In addition, the difference between the uninsulated and insulated material increases to about 40 J from the negligible difference in the as-cast condition. This difference in the 20°C impact energy persists at 15 and 30 minutes of heat treatment but disappears at 60 minutes.

The Charpy impact tests at -196°C behaved differently than the tests at 20°C as shown in Figures 27 and 28. After 5 minutes of heat treatment there was approximately a 13X increase in impact energy over the as-cast condition. The difference between the uninsulated and insulated material persisted through the 60 minute heat treatment time although the difference reduced from about 50 J to 30 J. Repeated measures on lateral expansion showed differences up to 0.015" so no statistical conclusions can be drawn from Figures 24, 25 or 26. Data used in the plots are tabulated in Appendix C.

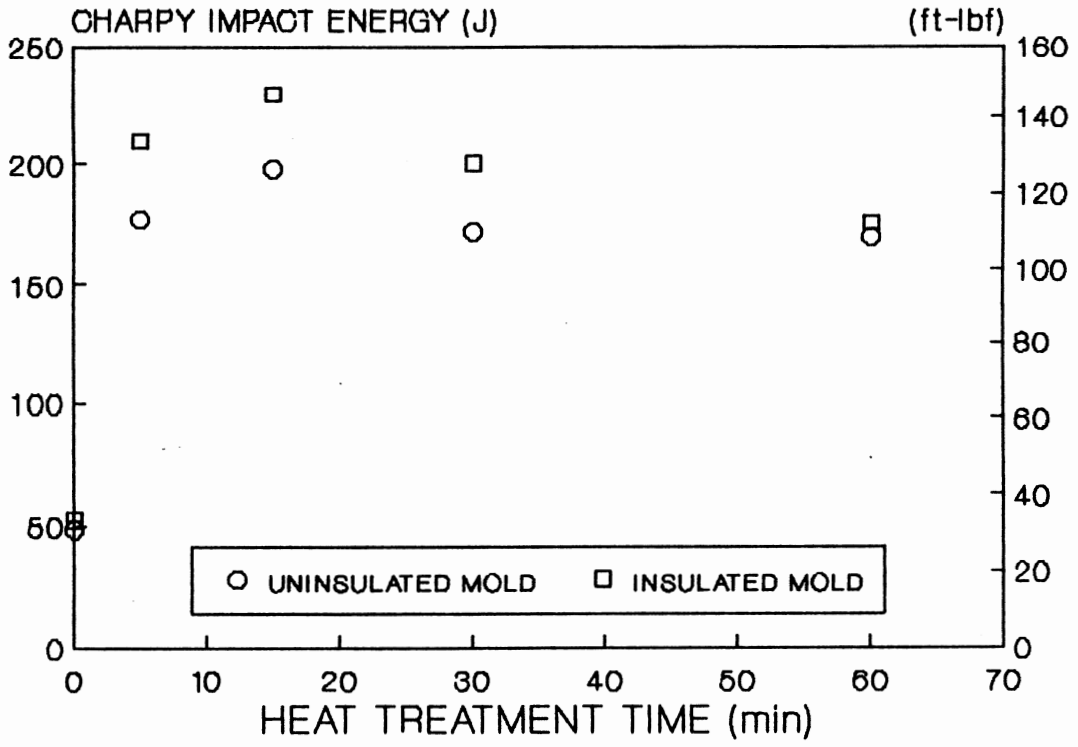

Figure 25. 20°C Charpy Impact Tests.

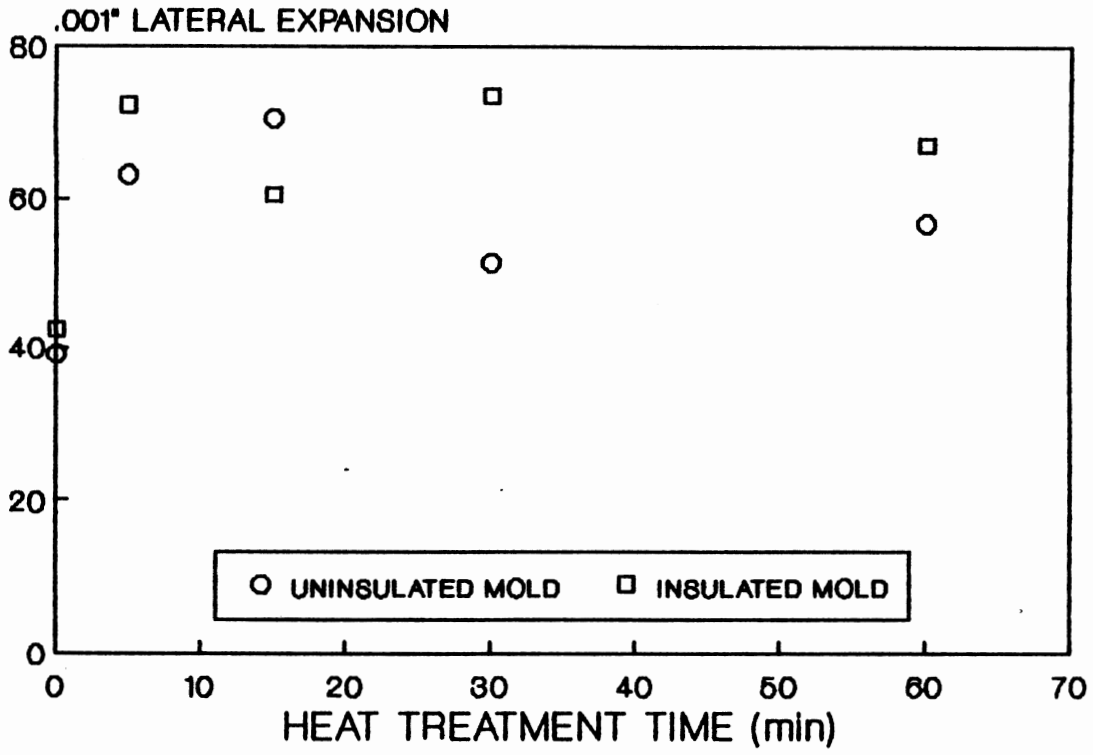

Figure 26. 20°C .001" Lateral Expansion.

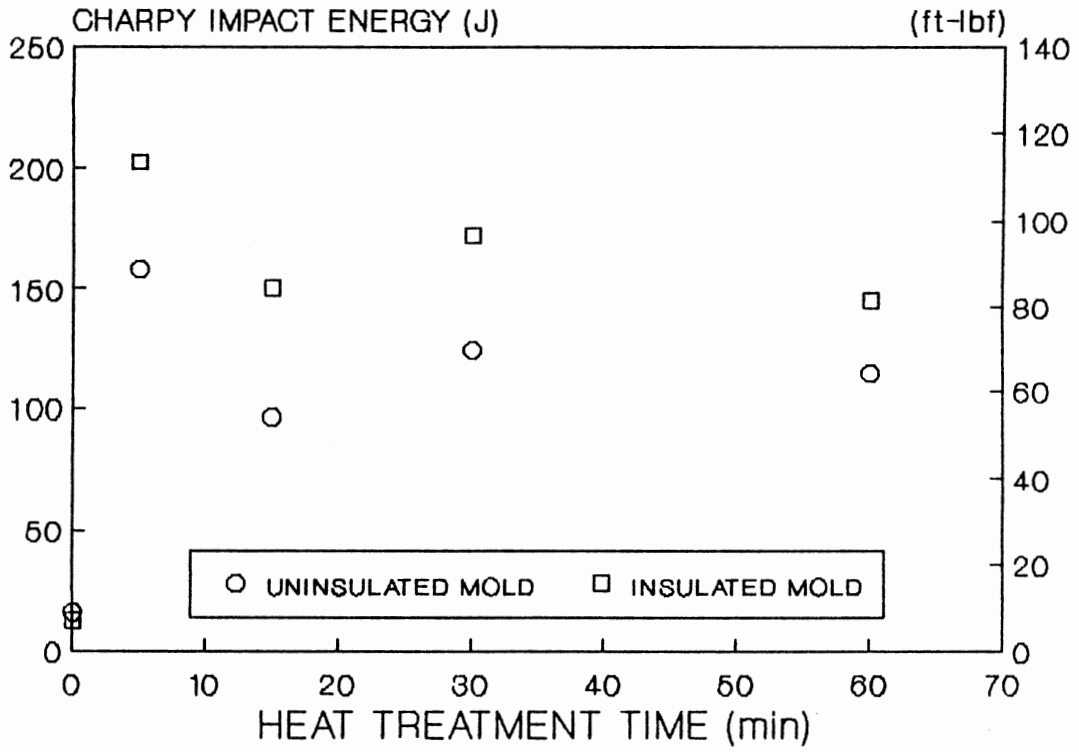

Figure 27. -196°C Charpy Impact Tests.

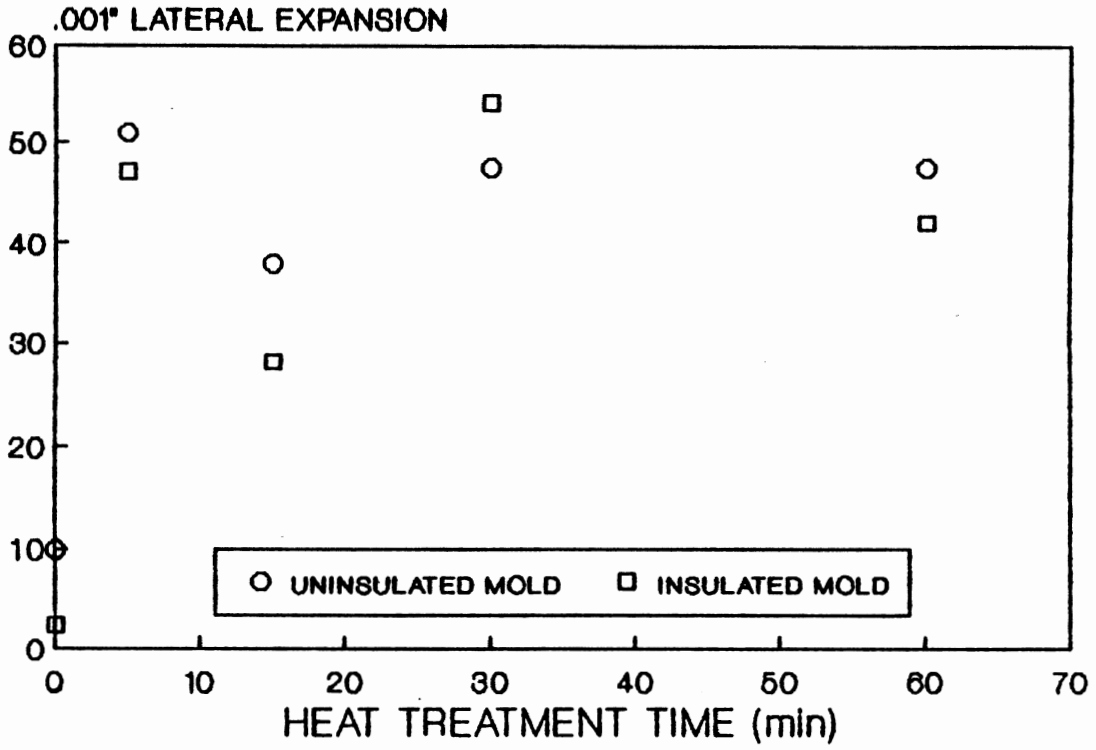

Figure 28. -196°C .001" Lateral Expansion.

Fractography

Detailed macro and micro examinations of the fracture surfaces were done. Overall, the fracture surfaces ranged from partially cleavage or quasi cleavage at the most severe conditions to completely fibrous ductile failure as heat treatment time and test temperature increased.

Figure 29 compares the macroscopic appearances of the 20°C Charpy series with the -196°C series for the uninsulated mold specimens. Figure 30 shows the comparison for the insulated mold specimens. The most dramatic changes occurred between the as-cast and 5 minute heat treatment samples. The 5 minute samples show much more flare, reflecting the lateral expansion data. The as-cast fracture surfaces are flatter and show more directional and stepped areas. By 5 minutes, there are few flat areas and the surface appears primarily fibrous.

A series of comparisons were made at 500X on the SEM. Figures 31 and 32 show the micrographs for the uninsulated mold specimens and the insulated mold specimens respectively. All photographs are representative of microvoids in the central regions of the fracture surface. Note that these microvoids are larger than the tensile specimen microvoids due to the larger section size of the Charpy test slabs resulting in a coarser structure.

Even at the extreme condition of as-cast, -196°C Charpy testing, the samples showed some microvoid areas. As seen in Figures 31 and 32, all the as-cast samples were extremely heterogeneous and showed predominantly cleavage or quasi cleavage. By 5 minutes, the

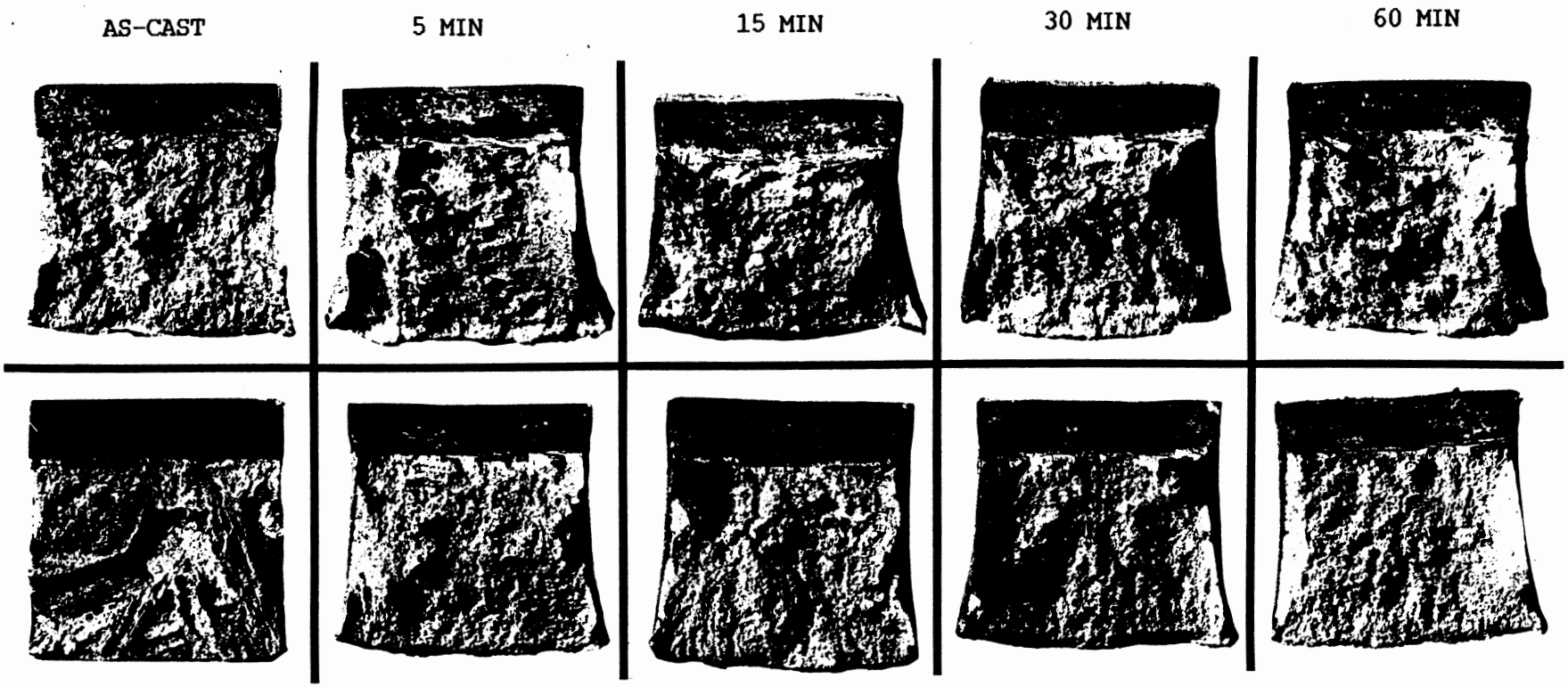

Figure 29. Uninsulated Mold Charpy Impact Fracture Surfaces.
20°C Tests (top), -196°C Tests (bottom).
10 cm x 10 cm Specimens.

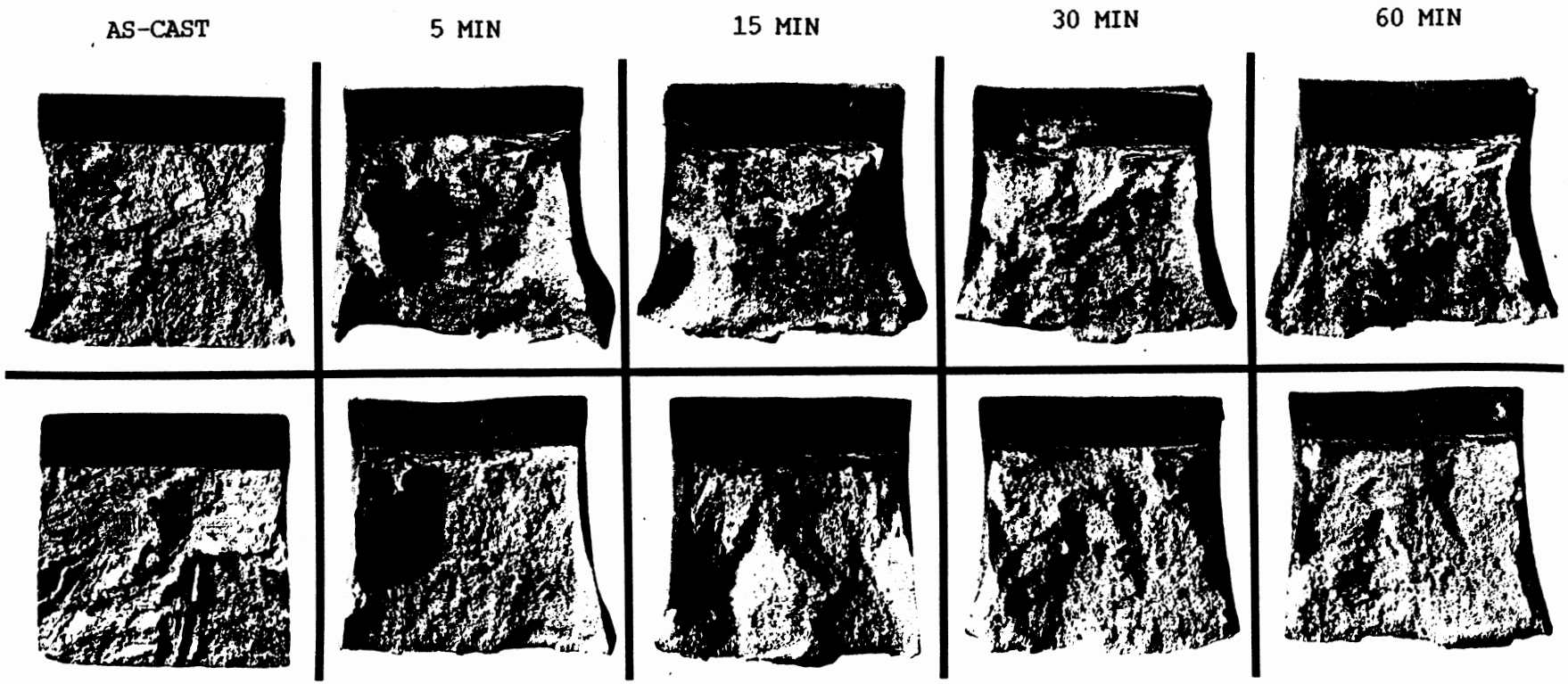

Figure 30. Insulated Mold Charpy Impact Fracture Surfaces.
20°C Tests (top), -196°C Tests (bottom).
10 cm x 10 cm Specimens.

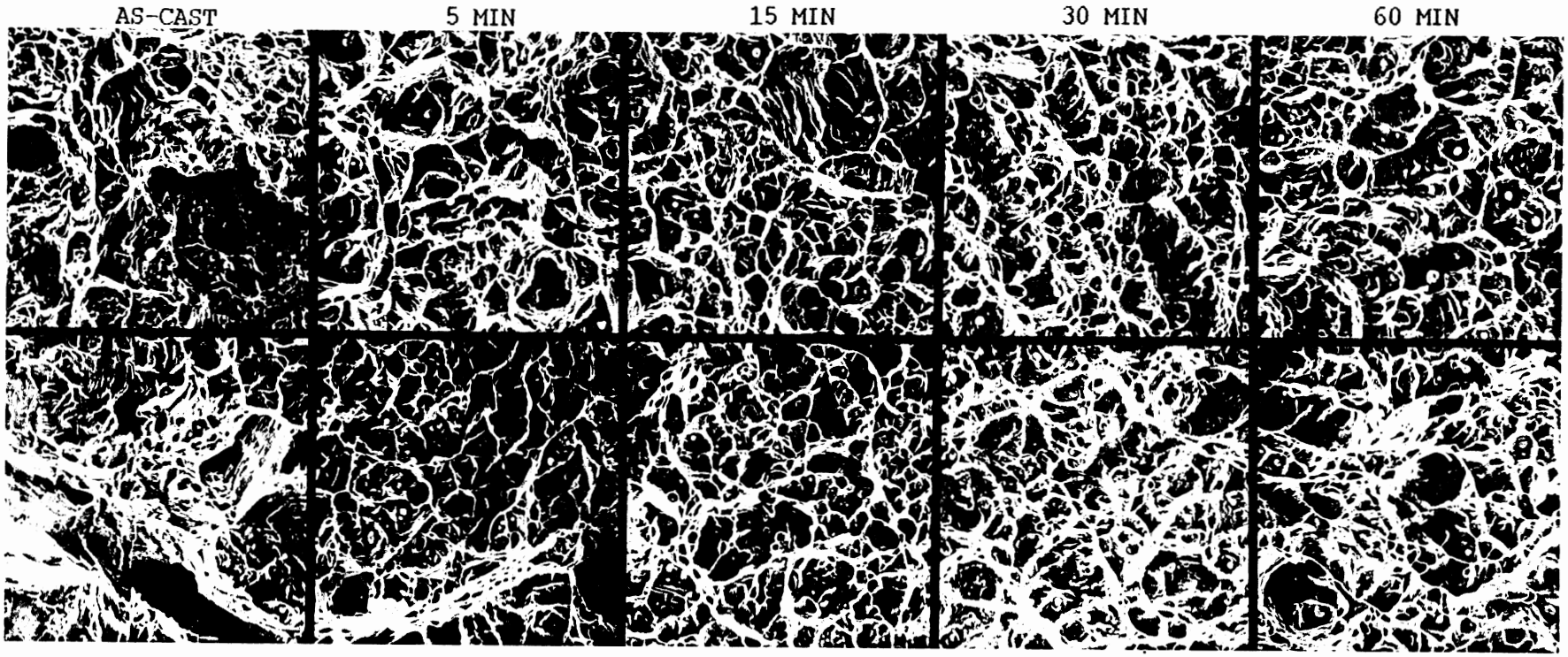

Figure 31. Uninsulated Mold Charpy Specimen Microvoids.
20°C Tests (top), -196°C Tests (bottom).
500X reprinted .5X

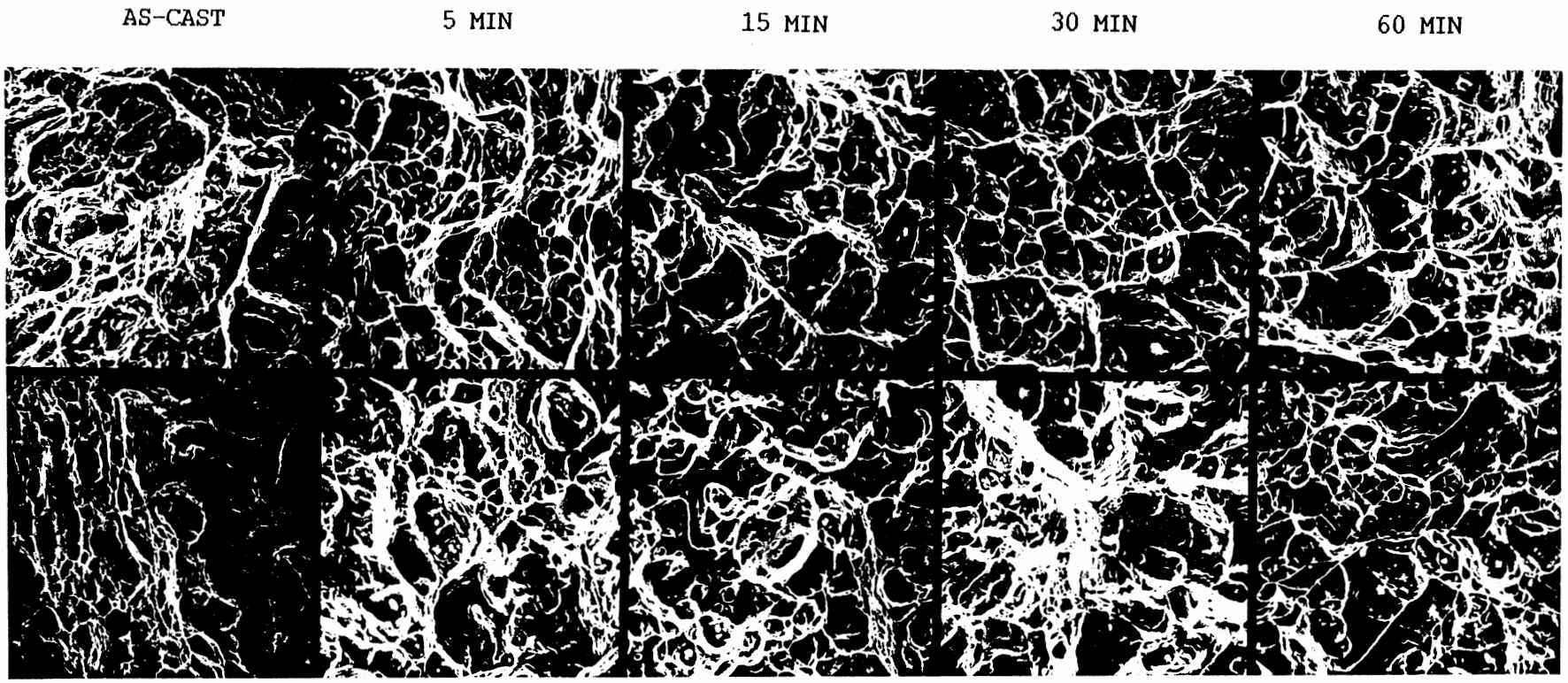

Figure 32. Insulated Mold Charpy Specimen Microvoids.
20°C Tests (top), -196°C Tests (bottom).
500X reprinted .5X

samples move toward a more homogeneous appearance. Two size populations of microvoids seem to develop. A larger diameter group, often with spherical inclusions, and a very small diameter group usually in narrow fibrous regions between the larger microvoid or quasi cleavage areas.

X-ray analysis by EDAX was done on inclusions in a polished surface and on a fracture surface. Besides the major alloying elements, iron, chromium, nickel and molybdenum; silicon, calcium and manganese were detected. The inclusions are very likely manganese silicide which have been detected in austenitic stainless steels by other investigators (Marshall 1984, Mills 1988).

Figures 33 and 34 show details of the as-cast -196°C Charpy fracture surface for the uninsulated and insulated specimens. In Figure 33a, the machined notch of the Charpy specimen is at the top of the photograph. The surface is primarily a series of flat steps separated by fibrous areas where larger changes in height occur. Figure 33b takes a closer look at the region near one of the fibrous steps. Figure 33c and 33d show in finer detail the cleavage areas, with some very small microvoids in the fibrous area along the changes in height.

Figure 34 is a similar series for the insulated mold, -196°C Charpy test. In Figure 34a the machined notch is to the right. As in the uninsulated mold specimen in Figure 33a, there are many flat areas with a directional appearance. Figure 34b and 34f show the extreme contrast present. Even the as-cast specimen had fibrous looking areas such as in Figure 34b. Upon closer examination, this fibrous area contained regions of cleavage along with regions of very

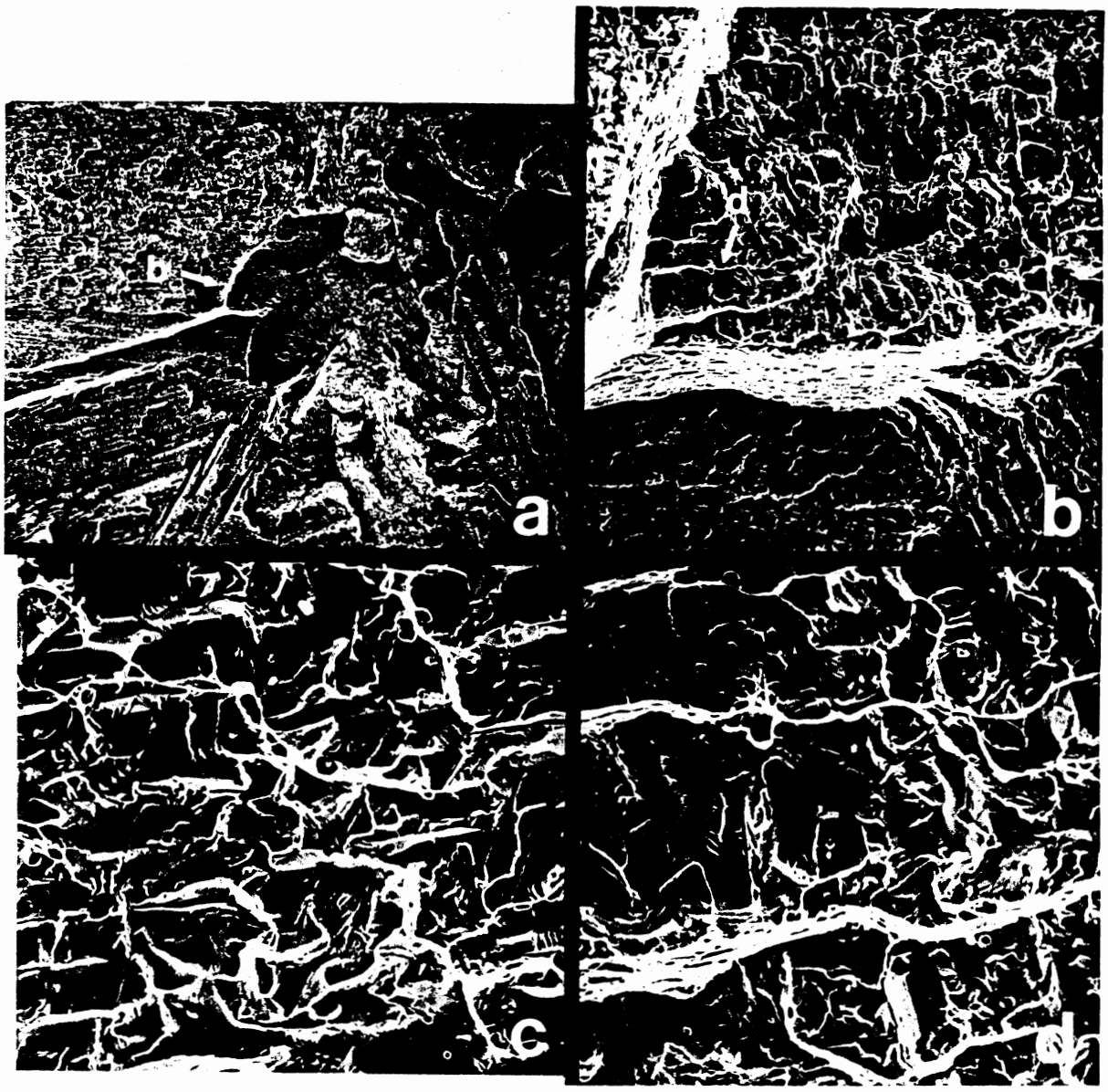

Figure 33. Details of As-cast -196°C Charpy Fracture Surface. Uninsulated Mold. a) 10X reprinted .8x, b) 100X reprinted .9X, c) and d) 500X reprinted .9X

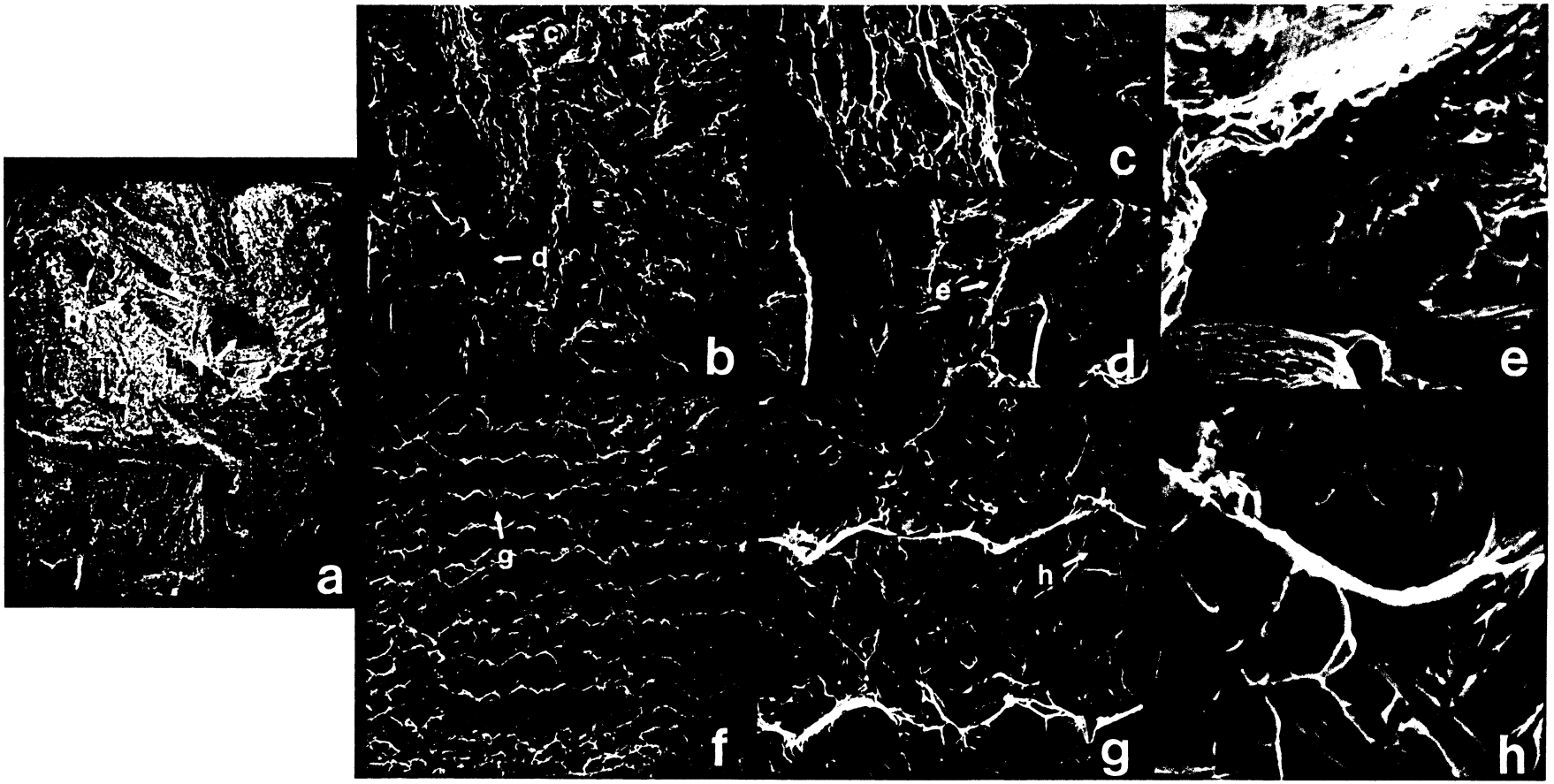

Figure 34. Details of As-cast -196°C Charpy Fracture Surface.
Insulated Mold. a) 10X reprinted .7X,
b) and f) 100X reprinted .6X,
c), d) and g) 500X reprinted .7X
e) and h) 2000X reprinted .7X

small microvoids (Figures 34c and 34d). In Figure 34d and 34e, the lighter stringy areas are spaced similarly to the spacing on the light micrographs. This supports Mills' description of microvoid failure or dimple rupture occurring at silicate inclusions, ferrite particles or local rupture of the ferrite (Mills 1988). He found that the ferrite particles are often found along the dimple cusps, not at the bottom of the microvoids where inclusions are often seen.

All the specimens show solidification porosity. An extreme example of this is shown in Figure 35. Note the areas of microvoids and ductile tearing. This sample is an insulated mold, 5 minute heat treatment, 20°C Charpy.

The solidification porosity is useful for comparing the spacing in the uninsulated and insulated molds. The light microscopy showed the insulated specimens to have approximately 2X the dendrite arm spacing of the uninsulated specimens. We can see in Figures 36 and 37 that the relationship is confirmed by SEM. The uninsulated specimens at the top of the figures show dendrite areas about half the size of the insulated specimens in the bottom photographs. Although the spacing is different, Figure 37 shows that the mechanism of failure is similar. Both specimens are 20°C Charpy, 60 minute heat treatment. Along the edges of the exposed dendrite areas, both specimens show ductile tearing and microvoids.

The areas along the exposed dendrites are useful for examining the difference in fracture mode between the as-cast and heat treated condition. Figure 38 shows this comparison for 20°C Charpy uninsulated mold conditions. The top photograph is the as-cast specimen showing small microvoids along the edge of the fracture.

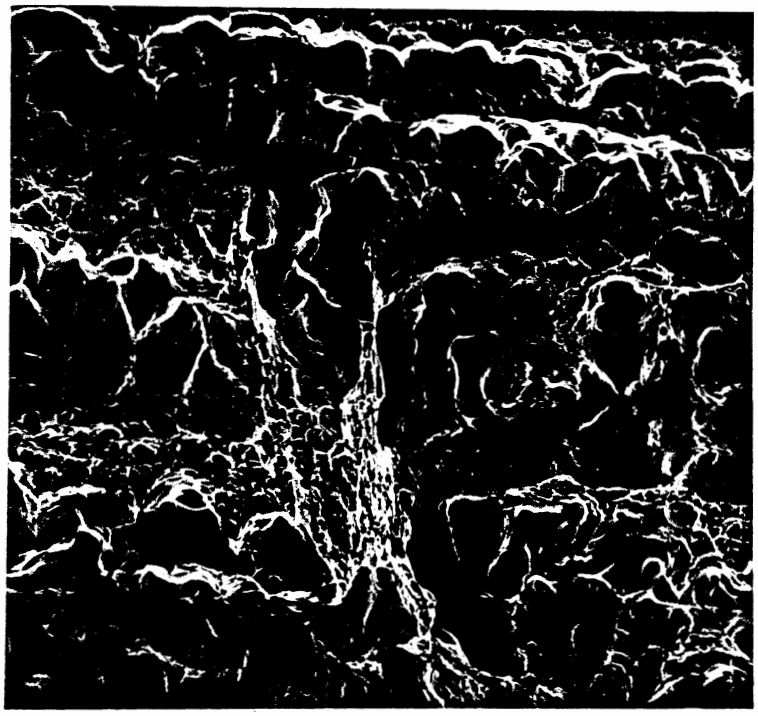

Figure 35. Extreme Example of Solidification Porosity. Insulated Mold, 5 min Heat Treatment. 100X

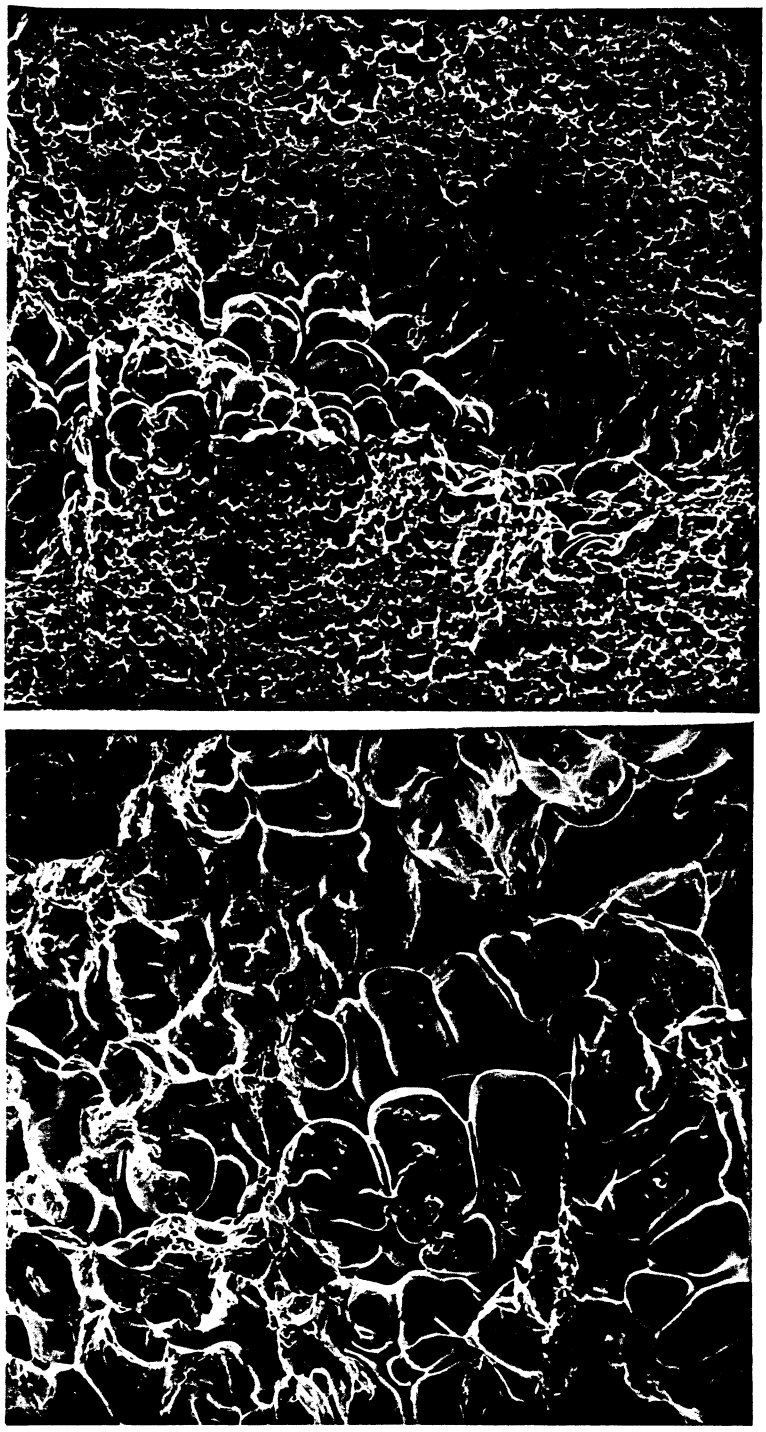

Figure 36. Comparison of Dendrite Sizes. 100X
Uninsulated Mold, 5 min Heat Treatment (top)
Insulated Mold, 60 min Heat Treatment (bottom)

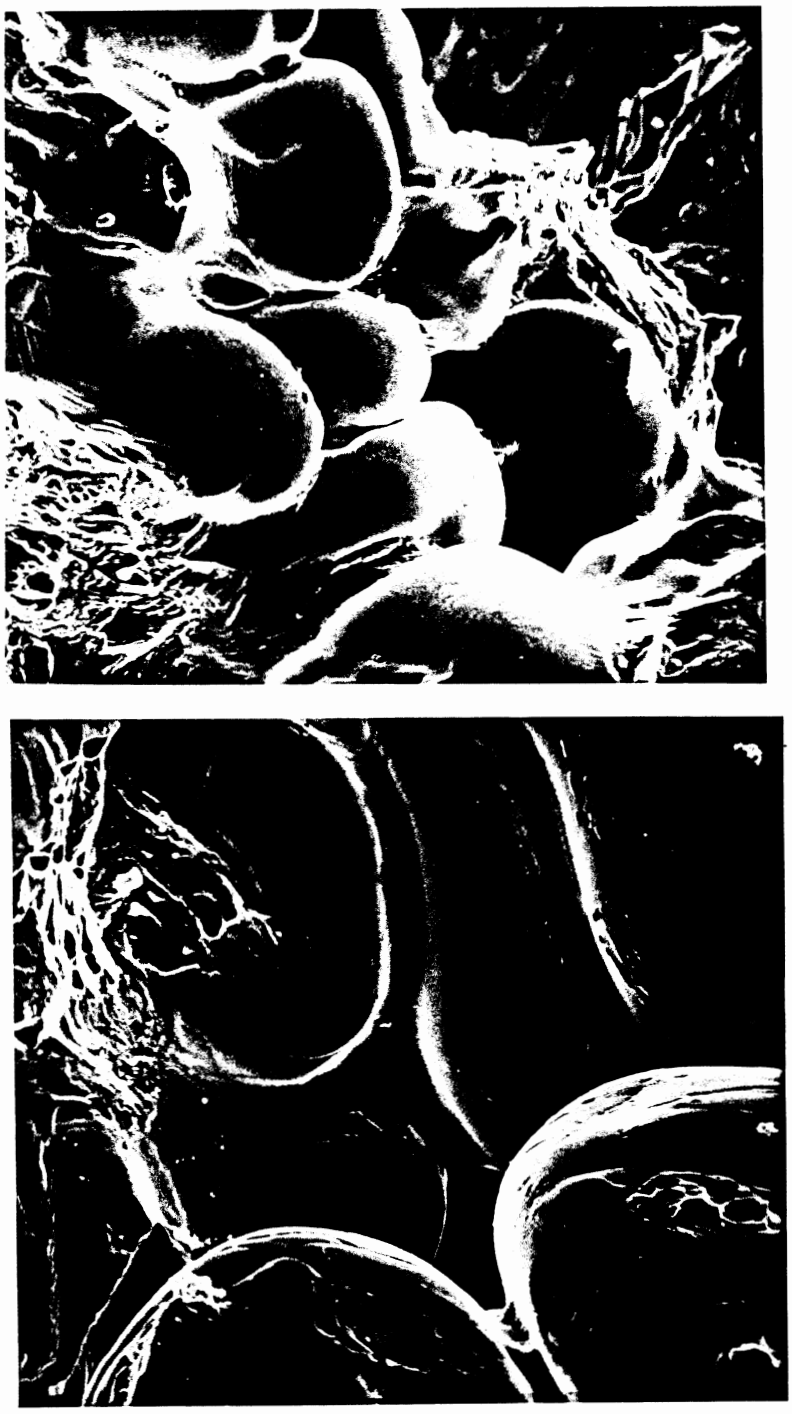

Figure 37. Dendrites Showing Fracture Mode. 500X
Uninsulated Mold (top)
Insulated Mold (bottom)
Both 60 min Heat Treatment.

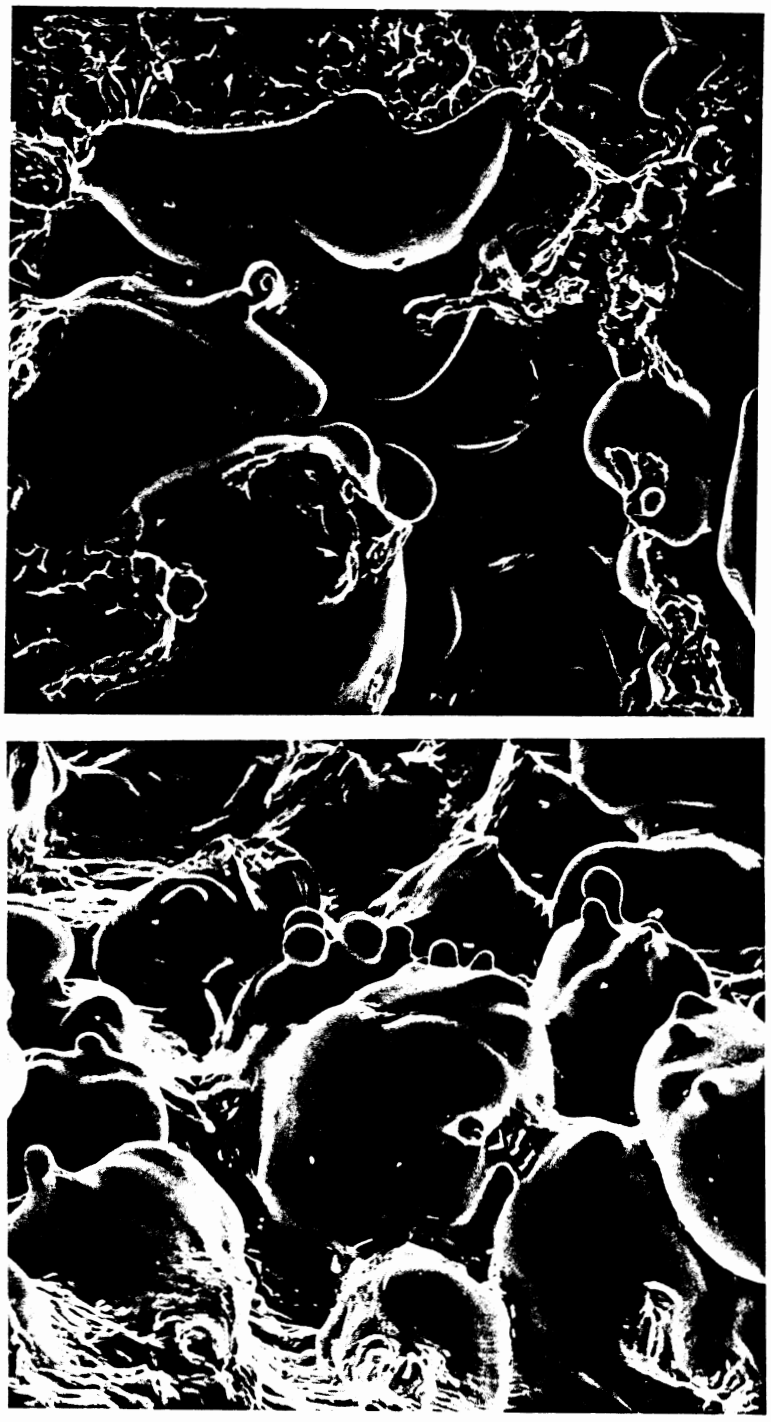

Figure 38. Fracture Modes Along Dendrites, 20°C Charpy. 500X
Uninsulated Mold, As-cast (top)
Uninsulated Mold, 60 min Heat Treatment (bottom)

The bottom specimen, heat treated for 60 minutes, shows ductile tearing and stretching.

As expected with a primarily austenitic structure, microvoid coalescence was the major fracture mode with the microvoids nucleating at inclusions and associated with ferrite pools. Microvoids were present even at the extreme condition of as-cast -196°C Charpy testing. The uninsulated and insulated specimens showed similar fracture modes with differences in the sizes of some features which reflects the influence of the different solidification conditions.

CHAPTER VI

DISCUSSION

Microstructural Response to Heat Treatment

Ferrite Content

After only five minutes of heat treatment, the ferrite content appeared to increase approximately 25%. Even though this increase was observed in both heat treatment series, there are limitations in methods used to measure ferrite content which must be discussed.

The manual point count method of measurement of ferrite content is often used as a standard to calibrate other methods, but there are limitations which are important when comparing small changes in ferrite content such as in this study. Results can vary with etching techniques, microscopic resolution and the conversion of a planar measurement to a volume % (Aubrey et al 1982). One group of investigators suggested precision limits of + or - 3% for ferrite levels of about 10% as in this project (Gunia and Ratz 1969).

Instrumental methods are often worse. For example, the Ferritescope has been found to be dependent on ferrite morphology (Leger 1982). Another instrument, the Magne-Gage, is also affected by the size, shape and orientation of the ferrite (Aubrey et al 1982). Other methods such as Leger's dilatometry are very

interesting and are reported to give results to an accuracy of 2%, but are simply not readily available.

If the guidelines in ASTM E526 are followed, the manual point count method is still considered the most consistent method and it needs little specialized equipment. As image analysis systems become more affordable and easier to use, they may extend the accuracy of the point count method with the increased sampling capacity of a computer.

The increase in ferrite observed in this study is near the limit of detection of the manual point count method. All specimens were etched and examined in the same way, so although the increase can be questioned, a possible explanation of the ferrite increase follows.

The thermal energy of heat treatment promotes diffusion of solute atoms, the most important, in this case, being chromium and nickel. Carbon can also affect steel microstructure but the effect is minimal at the low carbon level of 0.03% in this CF3M pour.

Table 9 shows the diffusion coefficients for chromium and nickel in ferrite and austenite at the heat treatment temperature of 1121°C (Honeycombe 1981). Both chromium and nickel have higher diffusion coefficients in ferrite. Movement is more rapid in ferrite because the bcc lattice is more loosely packed than the fcc austenite. The looser structure responds more readily to thermal energy and allows easier movement through the lattice.

In addition to the diffusion through the lattice there can also be grain boundary diffusion and diffusion along dislocations. Grain boundary and dislocation diffusion dominate at low temperatures. Above about 0.5Tm, where Tm in the equilibrium melting temperature in

TABLE 9

DIFFUSIVITIES OF CHROMIUM AND NICKEL
IN FERRITE AND AUSTENITE
AT 1121°C

	DIFFUSION COEFFICIENT (cm^2/s)	
	FERRITE	AUSTENITE
CHROMIUM	4.15×10^{-9}	1.18×10^{-11}
NICKEL	2.06×10^{-9}	2.45×10^{-11}

degrees Kelvin, the contribution of dislocation diffusion becomes negligible and above about 0.75-0.8Tm the contribution of grain boundary diffusion also becomes negligible (Porter and Easterling 1981). The heat treatment temperature used in this study, 1121°C, is approximately 0.82Tm so the lattice diffusion dominates.

If we recall the WDS scan in the results section, as expected in the as-cast material, the ferrite is chromium-rich and nickel-poor with very steep concentration gradients at the phase boundaries. Instead of ferrite dissolution, in this CF3M pour we saw an increase in ferrite before dissolution began. If we look at the movement of the chromium we can see that as the chromium atoms move through the ferrite toward the region of less concentration, the austenite, they will diffuse more slowly once in the austenite. This may act to establish a relatively high chromium content in the austenite adjacent to the ferrite, changing the Cr/Ni ratio enough to move the ferrite boundaries outward resulting in the increase in ferrite content. The steep nickel gradient at the boundaries is opposite that of chromium and no steep concentration differences will be created because the nickel moves faster in the ferrite than in the austenite. Eventually, as the chromium gradients flatten out, the Cr/Ni ratio in the ferrite near the boundaries will decrease enough to begin the dissolution process.

The question remains as to whether the lattice diffusion alone controls the increase in ferrite content with very short heat treatment times. Can the chromium and nickel diffuse far enough in a few minutes to have any detectable effect on the ferrite content?

Although finding a specific solution for the diffusion equation is extremely complex, Appendix D contains calculations using a diffusion model. The model is based on a pair of semi-infinite solids in contact. The calculations show that five minutes is enough time for the chromunm and nickel to travel 2-3 microns in the austenite and cause an increase in the Cr/Ni near the interface. There are limitations to this model which are discussed in the Appendix. The calculations support the conclusion that sufficient diffusion can occur in five minutes to move the ferrite-austenite interface an amount detectable by light microscopy. Although the diffusion calculations support a change in the ferrite within five minutes, the manual point count method limits the size of the change that can be measured. This problem could be addressed in more detail by taking repeated WDS scans on as-cast and heat treated specimens to map the movement of the major alloying elements in the areas near ferrite-austenite interfaces; a very expensive and time consuming project. This mapping, along with computer imaging estimates of ferrite content, would characterize the diffusion-boundary movement question more completely.

Ferrite Morphology

The gradual spheroidizing and dissolution of ferrite with heat treatment has been well described in this laboratory as well as by other investigators (Ratke 1987, Ratke et al 1989, Durham and Cohen 1989). The addition that the present study offers is the documentation of the change in ferrite with extremely short times at temperature. In the as-cast specimens, the ferrite is nearly

continuous. The pools are joined by very thin strands of ferrite. After only two minutes of heat treatment these very thin areas are nearly gone. The ferrite pools are also rounding and breaking apart. The significance of this very fast change in the microstructure becomes apparent when the mechanical properties are considered.

Microstructure and Mechanical Properties

No large differences in ferrite content could be produced under the conditions of this study. Since ferrite is the main strengthening mechanism in CF3M, this explains the lack of significant changes in hardness or tensile strength. This turned out to be an advantage because it allowed the ferrite morphology to be isolated as being responsible for the changes in mechanical properties.

The microstructure had two major influences on the mechanical properties in this study. The first influence concerned the spacing of the ferrite. The wider spacing in the uninsulated mold specimens had higher Charpy impact values although significant differences in hardness, tensile strength or ferrite content were not found. This contradicts that, in general, finer microstructures result in more desirable mechanical properties. Recall that CF3M contains a higher strength bcc ferrite network in a ductile fcc austenite matrix. The ferrite acts as a strengthening mechanism. Strength is a component of impact energy since toughness is the area under the stress-strain curve. Since ferrite content was essentially the same for the uninsulated and insulated molds, the influence of ferrite content on

impact properties was eliminated in this study. One explanation of the higher impact values follows.

As discussed in the results, the ferrite particles were often associated with the edges of microvoids. One possible process could start with a microvoid nucleating at an inclusion. It grows until it impinges on another void or on ferrite pools. In the case of larger spacing, voids would grow more in the ductile austenite before hitting the more brittle ferrite. Larger microvoids indicate more energy absorbed in the austenite and higher Charpy impact values. As the heat treatment time increased, the microstructure in the uninsulated mold and insulated mold materials became more homogeneous and the difference in the Charpy impact values decreased.

The second influence of the microstructure on the mechanical properties also concerned the ferrite morphology. There was a 4 to 13X increase in impact energy after only two minutes of heat treatment. The loss of the continuous ferrite network appears to be responsible for the increased Charpy values. The explanation is similar to the argument presented above. In addition, the rounding of the ferrite would reduce the nucleation of microvoids at sharp corners of ferrite.

After five minutes of heat treatment, CF3M showed a UTS of 620 MPa (90 ksi). This value is well above the minimum requirements shown in Table 1. The 20°C Charpy impact was about 200 J (148 ft-lbs), also well above the typical value given in Table 1. In addition, the investment cast CF3M showed a combination of mechanical properties superior to the material used by the investigators whose data is summarized in Table 4. None of these investigators used the

investment casting method or tested as-cast material. All material was keel block cast and solution heat treated at least one hour.

The superior performance of the investment cast CF3M with 10% ferrite after only five minutes of heat treatment demonstrates the critical role of processing on the final mechanical properties. The smaller section sizes combined with the lower solidification rates of investment casting produces a more homogeneous structure than in other casting methods. Differences in chemical composition, ferrite content and hardness have been observed from the top and bottom of cast keel blocks and slabs and from the inner and outer diameters of centrifugally cast pipes (Chopra and Chung 1987).

The studies in Table 4 all used keel block castings. They also changed the ferrite contents by changing the chemistry and in turn identified the differences in ferrite content as responsible for the changes in mechanical properties. By holding the chemistry and ferrite content constant, this study was able to show that ferrite morphology has a significant influence on mechanical properties at 10% ferrite. This data demonstrated that in investment cast CF3M, a superior combination of tensile and impact strength can be obtained with very short heat treatment times.

This work specifically addressed the investment casting process. Very little information is available on how the mechanical properties of an investment casting compare to other cast or wrought material. Certainly, more work is needed to see if the morphology has a large influence at other ferrite contents. At the ferrite content in this study, differences were observed in microvoid sizes between the

tensile and Charpy fracture surfaces, suggesting that section size may influence morphology more than mold insulation.

The methods of measuring ferrite morphology and content must be improved. Microstructural characterization is often too time consuming for practical use in the foundry. The results of studies like this take steps towards process improvement in the investment casting industry.

CHAPTER VII

CONCLUSIONS AND RECOMMENDATIONS

Conclusions

1. No significant difference in ferrite content was produced under the normal foundry conditions used in this study; hot insulated mold and uninsulated mold. However, slower solidification in insulated molds resulted in larger spacing.

2. The larger spacing of the insulated mold material showed superior impact properties without reductions in tensile strength.

3. Ferrite morphology was significantly changed within five minutes of heat treatment. The loss of continuous ferrite and the rounding of sharp edges was responsible for significant improvements in Charpy impact energy for both the uninsulated and insulated mold material.

4. Heat treatment times over five minutes offered no significant improvements in mechanical properties.

Recommendations

1. The changes in the concentration gradients of alloying elements would help define the movement of the ferrite-austenite boundary in the first few minutes of heat treatment. Instruments such as the microprobe WDS system could be used to quantitatively document the diffusion of chromium and nickel.

2. More accurate measures of ferrite content are needed to enable small changes to be reliably measured. Computer image analysis systems could provide a way to process the volume of data needed to obtain reliable chemistry-ferrite relationships.

3. Since the ferrite morphology has been shown to have a significant influence on mechanical properties, quantitative measures of morphology need to be developed. Computer imaging systems would again be useful as described above.

4. The effects of short heat treatment times on other material properties, most notable corrosion resistance, must be examined.

5. More studies of prosessing-microstructure-property relationships and better transfer of this data into standardized practices are needed. The ranges of alloying elements allowed in the ASTM specification for CF3M result in the production of material with

a wide range of microstructures and properties. As the demand increases for certified, high quality, uniform products, these ranges should be reduced. Improvements are needed such as an additional identifying number or letter representing a certain class of ferrite content and morphology, taking a specific heat treatment into consideration.

REFERENCES

ASM, Metals Handbook-Properties and Selection of Stainless Steels, Tool Materials and Special Purpose Metals. 9th ed. Vol. 3, American Society for Metals, Metals Park, Ohio, 1980

ASTM A167-89a, "Standard Specification for Stainless and Heat-Resisting Chromium-Nickel Steel Plate, Sheet and Strip", 1990 Annual Book of ASTM Standards, Vol. 1.03, American Society for Testing and Materials, Philadelphia, 1990

ASTM, A370-88, "Standard test methods and definitions for mechanical testing of steel products", 1989 Annual Book of ASTM Standards, Vol. 01.02, American Society for Testing and Materials, Philadelphia, 1989

ASTM, A743-88, "Standard specifications for castings, iron-chromium, iron-chromium-nickel, corrosion resistant, for general application", 1990 Annual Book of ASTM Standards, Vol. 01.02, American Society for Testing and Materials, Philadelphia, 1990

ASTM, A744-88a, "Standard specifications for castings, iron-chromium, iron-chromium-nickel, corrosion resistant, for severe service", 1990 Annual Book of ASTM Standards, Vol. 01.02, American Society for Testing and Materials, Philadelphia, 1990

ASTM, E8-88, "Standard methods for tension testing of metallic materials", 1989 Annual Book of ASTM Standards, Vol. 01.02, American Society for Testing and Materials, Philadelphia, 1989

ASTM, E23-88, "Standard test methods for notched bar impact testing of metallic materials", 1989 Annual Book of ASTM Standards, Vol. 03.01, American Society for Testing and Materials, 1989

ASTM E399-83, "Standard test method for plane-strain fracture toughness of metallic materials", 1989 Annual Book of ASTM Standards, Vol. 03.01, American Society for Testing and Materials, Philadelphia, 1989

ASTM, E562-83, "Standard practice for determining volume fraction by systematic manual point count", 1989 Annual Book of ASTM Standards, Vol. 03.01, American Society for Testing and Materials, Philadelphia, 1989

ASTM E813-87, "Standard method for J_{Ic}, a measure of fracture toughness", 1989 Annual Book of ASTM Standards, Vol. 03.01, American Society for Testing and Materials, Philadelphia, 1989

Aubrey, L.S., Wieser, P.F., Pollard, W.J., and Schoefer, E.A., "Ferrite Measurement and Control in Cast Duplex Stainless Steels", in Stainless Steel Castings. ASTM STP 756, V.G. Behal and A.S. Melilli, Eds., American Society for Testing and Materials, Philadelphia, pp. 126-164, 1982.

Bates, C.E., Heger, J.J., and Patterson, B.R. Influence of Section Size on the Mechanical Properties of Cast and Wrought Stainless Steels, Special Report No. 18, Steel Founders' Society of America, Rocky River, Ohio, 1981

Beck, F.H., Schoefer, E.A., Flowers, J.W. and Fontana, M.G. "New cast high-strength alloy grades by structure control", in ASTM STP 369, Advances in the technology of stainless steels and related alloys, American Society for Testing and Materials, Philadelphia, 1965

Campbell, J.E., Gerberrich, W.W., and Underwood, J.H., Eds., Application of Fracture Mechanics for Selection of Metallic Structural Materials, American Society for Metals, Metals Park, Ohio, 1982

Carr, F.L., Biehler, D., Connolly, A., Dragen, R., Faller, J., Johari, O., Morais, R., Parker, M.T. and Sailors, R.H., "Correlation of Microfractography and Macrofractography of AISI Steel-A Report of ASTM E-24/II Task Force", in ASTM STP 493, Applications of Electron Microfractography to Materials Research, American Society for Testing and Materials, Philadelphia, 1971

Chapman, A.J. Heat Transfer, Macmillan Publishing Co., New York, 1984

Chopra, O.K. and Chung, H.M. "Effect of Low Temperature Aging on the Mechanical Properties of Cast Stainless Steel", in ASME MPC-Vol. 26, PVP-Vol. 132, Properties of Stainless Steels in Elevated Temperature Service, M. Prager, Ed., American Society of Mechanical Engineers, New York, pp. 79-105, 1987

Cottrell, A., An Introduction to Metallurgy, Edward Arnold Ltd., London, 1975

David, S.A. "Ferrite morphology and variations in ferrite content in austenitic stainless steel welds", Welding Journal, Vol. 60, pp. 63s-72s, April 1981

DeLong, W.T. "Ferrite in austenitic stainless steel weld metal", Welding Journal, Vol. 53, pp. 273s-286s, July 1974

Durham, D.R. and Cohen, R.E. "Control of Microstructural Development in Investment Casting of Austenitic Stainless Steel, CF-3M", in Microstructural Development and Control, MD Vol. 14, D.R. Durham and A. Saigal, Eds., American Society of Mechanical Engineers, New York, 1989

Flemings, M.C. Solidification Processing, McGraw Hill, New York, New York, 1974

Garrow, E. "Heat treatment of investment cast stainless steels and high temperature alloys", Modern Casting, pp. 58-64, December 1966

Hertzberg, R.W. Deformation and Fracture Mechanics of Engineering Materials, 3rd Edn., John Wiley & Sons, New York, 1989

Holman, J.P. Heat Transfer, McGraw-Hill Book Co., New York, 1972

Honeycombe, R.W.K. Steels, Microstructure and Properties, Edward Arnold, London, 1981

Klemp, T. and Sikkenga, S.L. "Effect and control of delta ferrite in cast stainless steel", Investment Casting Institute Annual Meeting Proceedings, 1986

Kurz, W. and Fisher, D.J. Fundamentals of Solidification, Trans Tech Publications, Aedermannsdorf, Switzerland, 1984

Leger, M.T. "Predicting and Evaluating Ferrite Content in Austenitic Stainless Steel Castings", in Stainless Steel Castings, ASTM STP 756, V.G. Behal and A.S. Melilli, Eds., American Society for Testing and Materials, Philadelphia, pp.105-125, 1982

Leone, G.L. and Kerr, H.W. "The ferrite to austenite transformation in stainless steels", Welding Journal, Vol. 61, pp. 13s-21s, January 1982

Lippold, J.C. and Savage, W.F. "Solidification of austenitic stainless steel weldments: Part I-A proposed mechanism", Welding Journal, Vol. 58, pp. 362s-374s, December 1979

Marshall, P. Austenitic Stainless Steels, Microstructure and Mechanical Properties, Elsevier Applied Science Publishers, London, 1984

Mills, W.J., "Fracture Toughness of Stainless Steel Welds", in Fracture Mechanics: Nineteenth Symposium, ASTM STP 969, T.A. Cruse, Ed., American Society for Testing and Materials, Philadelphia, pp. 330-355, 1988

Munz, D. "Minimum Specimen Size for the Application of Linear-Elastic Fracture Mechanics", in Elastic-Plastic Fracture, ASTM STP 668, J.D. Landes, J.A. Begley and G.A. Clarke, Eds., American Society for Teasting and Materialss, pp. 406-425, 1979

Peckner, D. and Bernstein, I.M. Handbook of Stainless Steels, McGraw Hill Inc., New York, 1977

Porter, D.A. and Easterling, K.E. Phase Transformations in Metals and Alloys, Van Nostrand Reinhold Co. Ltd., Wokingham, England, 1981

Priest, A.H., "Size effects in fracture toughness testing procedures", in Size Effects in Fracture, MEP Institution of Mechanical Engineers, London, 1986

Raghunathan, V.S., Seetharamen, V., Venkdesan, S. and Rodriquez, P. "The influence of post weld heat treatments on the structure, composition and amount of ferrite in type 316 stainless steel welds", Metallurgical Transactions A, Vol. 10A, pp. 1683-1689, November 1979

Ratke, P.D. "A study of the effects of heat treatment on delta ferrite in cast austenitic stainless steel", Master's Thesis, Oklahoma State University, 1987

Ratke, P., Cohen, R.E. and Durham, D.R. "Delta-Ferrite Morphology in Austenitic Stainless Steel Investment Castings in the As-cast and Heat Treated Condition", AFS Transactions, Vol. 118, pp. 195-200, 1989

Riihimaki, A. "Metallurgical properties and applications of duplex cast stainless steels", in Advanced Casting Technology, Conference Proceedings, J.Easwaran, Ed., American Society for Metals, Metals Park, Ohio, 1987

Robinson, J.N. and Tetelman, A.S. "Measurement of K_{Ic} on Small Specimens Using Critical Crack Tip Opening Displacement", in ASTM STP 559, Fracture Toughness and Slow-Stable Cracking, American Society for Testing and Materials, Philadelphia, 1974

Rohsenow, W.M. and Hartnett, J.P., Eds., Handbook of Heat Transfer, McGraw-Hill Book Co., New York, 1973

Shendye, S.B, Devletian, J.H. and Wood, W.E. "Weldability and mechanical properties of cast stainless steels after elevated temperature aging", in ASME MPC-Vol. 26, PVP-Vol. 132, Properties of Stainless Steels in Elavated Temperature Service, M. Prager, Ed., American Society of Mechanical Engineers, New York, 1987

Shewmon, P.G. Diffusion in Solids, McGraw-Hill Book Co. Inc., New York, 1963

Shewmon, P.G. Transformations in Metals, McGraw-Hill Book Co. Inc., New York, 1969

Steel, R.G.D. and Torrie, J.H., Principles and Procedures of Statistics, McGraw-Hill Book Company Inc., New York, 1960

Takalo, T., Suutala, N. and Moisio, T. "Influence of ferrite content on its morphology in some austenitic stainless steel welds", Metallurgical Transactions A, Vol. 11A, pp. 1591-1592, October 1976

Vander Voort, G.F. Metallography, Principles and Practice, McGraw-Hill Book Company Inc., New York, 1984

Wieser, P.F., Ed. Steel Castings Handbook, 5th ed., Steel Founders' Society of America, Rocky River, OH, 1980

Wieser, P.F., Beck, F.H., Fontana, M.G. and Schoefer, E.A., "A survey of mechanical and corrosion properties of selected cast, stainless steels", in ASME MPC-2 Metal Properties for the Petroleum and Chemical Industries, A.O. Schaefer, Ed., American Society of Mechanical Engineers, New York, pp. 61-121, 1976

APPENDIXES

APPENDIX A

HEAT TRANSFER CALCULATIONS

Heat treatment specimens of 1 cm x 1 cm x 1 cm were subjected to radiation and convection on five sides and conduction on the sixth side. The overall heat transfer,

$$q = q_{conv} + q_{rad} + q_{cond} \qquad [1]$$

If the contributions of convection, radiation and conduction are calculated, q can be used to model the temperature change with time in the specimen.

For convection,

$$q_{conv} = h_c A_1 (T_1 - T_2) \qquad [2]$$

where h_c is the convective heat transfer coefficient, A_1 is the surface area of the body, T_1 is the temperature of the body, and T_2 is the temperature of the surrounding convective fluid.

Analogous to convection, a radiation heat transfer coefficient, h_r can be defined,

$$q_{rad} = h_r A_1 (T_1 - T_2) \ . \qquad [3]$$

In this case T_1 and T_2 are the temperatures of the two bodies exchanging heat by radiation.

If it is assumed that the second radiation exchange surface is an enclosure and it is at the same temperature as the convective fluid, then the heat transfer for convection and radiation can be summed (Holman 1972). The expression for the combined convection and

radiation heat transfer becomes

$$q_{conv + rad} = (h_c+h_r)A_1(T_1-T_2) \quad . \qquad [4]$$

The radiation heat transfer coefficient can be calculated from the expressions for radiation between two infinite parallel planes.

$$h_r = \frac{\sigma (T_1^2+T_2^2)(T_1+T_2)}{1/e_1+(A_1/A_2)(1/e_2-1)} \qquad [5]$$

where σ is the Boltzmann constant, 5.67×10^{-8} W/m^2-K^4, e_1 and e_2 are the emisssivity of the specimen and furnace walls respectively. The emissivity of the specimen will change from about .2 to .8 as the surface oxidizes. Since a visible oxide film has been observed within seconds of exposure to the furnace air atmosphere, .5 was chosen as a reasonable value. The emissivity of the furnace, .8, is based on .75 for firebrick and about .9 for various silicon materials, since the ten molybdenum disilicide heating elements form a SiO_2 layer above 800°C.

The surface area of the five sides of the cube subject to convection and radiation is 5×10^{-4} m^2 and the surface area of the five corresponding five sides of the furnace is 0.145 m^2. The temperature of the furnace is 1394 K and the specimen is at 293 K. Substituting in equation [5],

$$h_r = 97 \text{ W/m}^2\text{-K} \quad .$$

For the convection in the furnace air, a conservative value of 20 W/m^2-°C was chosen. This value overlaps the value ranges for forced convection in air, 10-500 W/m^2-°C, and free convection in air, 5-25 W/m^2-°C (Chapman 1984).

With the combined convection-radiation heat transfer coefficient of 117 W/m^2-°C the contribution of the convection and radiation

to the overall heat transfer can be estimated using equation [4]. Substituting in equation [4],

$$q_{conv + rad} = -64 \text{ W} \quad .$$

The specimens were placed on a block of stainless steel which was at 1121°C. The interface values for steel to steel in air are so high as to give negligible resistance to heat flow (Rohsenow and Hartnett 1973). Assuming negligible interface resistance, the contribution of the conduction to the overall heat transfer can be estimated by

$$q_{cond} = - \frac{kA}{\Delta x} (T_1 - T_2) \quad . \qquad [6]$$

Using conductivity, k = 24 W/m-°C, and substituting in equation [6] for a location, 0.005 m, at the center of the cube

$$q_{cond} = -529 \text{ W} \quad .$$

Summing the contributions of convection, radiation and conduction

$$q = -593 \text{ W} \quad .$$

The time to temperature can be estimated using

$$q = \rho c V \frac{dT}{dt} \quad . \qquad [7]$$

where ρ is density, 7817 kg/m³, c is specific heat, 460 J/kg-°C and V is volume, 1 x 10^{-6} m³ .

Solving equation [7]

$$\frac{dT}{dt} = 165 \quad .$$

After one second the temperature of the specimen has increased 165°C from 20°C to 185°C. This new temperature is used in equations [4] and [6] to calculate an updated q for the next one second time step. Repeating this procedure at one second intervals

gives a temperature-time profile for the center of the specimen. This profile is conservative because it does not consider the increse in the h_r with increasing T_1.

Figure 38 shows that the specimen reached within 1°C of the test temperature after 40 seconds exposure to the furnace environment. The timing of the heat treatments began approximately one minute after the specimens were placed in the furnace. This assured that the specimens would be at the test temperature when timing of the heat treatment began.

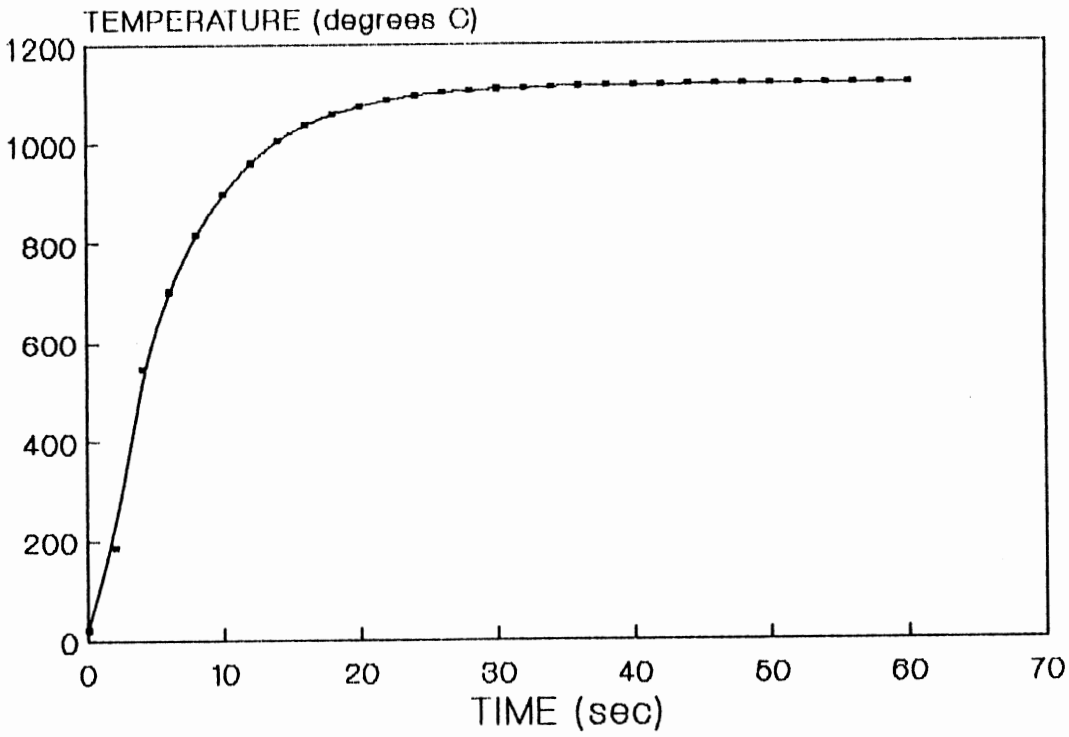

Figure 39. Model of Temperature Response of Specimens.

APPENDIX B

HEAT TREATMENT SERIES 2 MICROGRAPHS

The following series of micrographs show the changes in the microstructure as heat treatment progresses. All were taken at the same magnification; 270X, 1 cm on the print = 37 microns on the specimen. The heat-treated photographs were taken as close as possible to the as-cast photograph location. There was some difficulty in maintaining the location markers after repolishing.

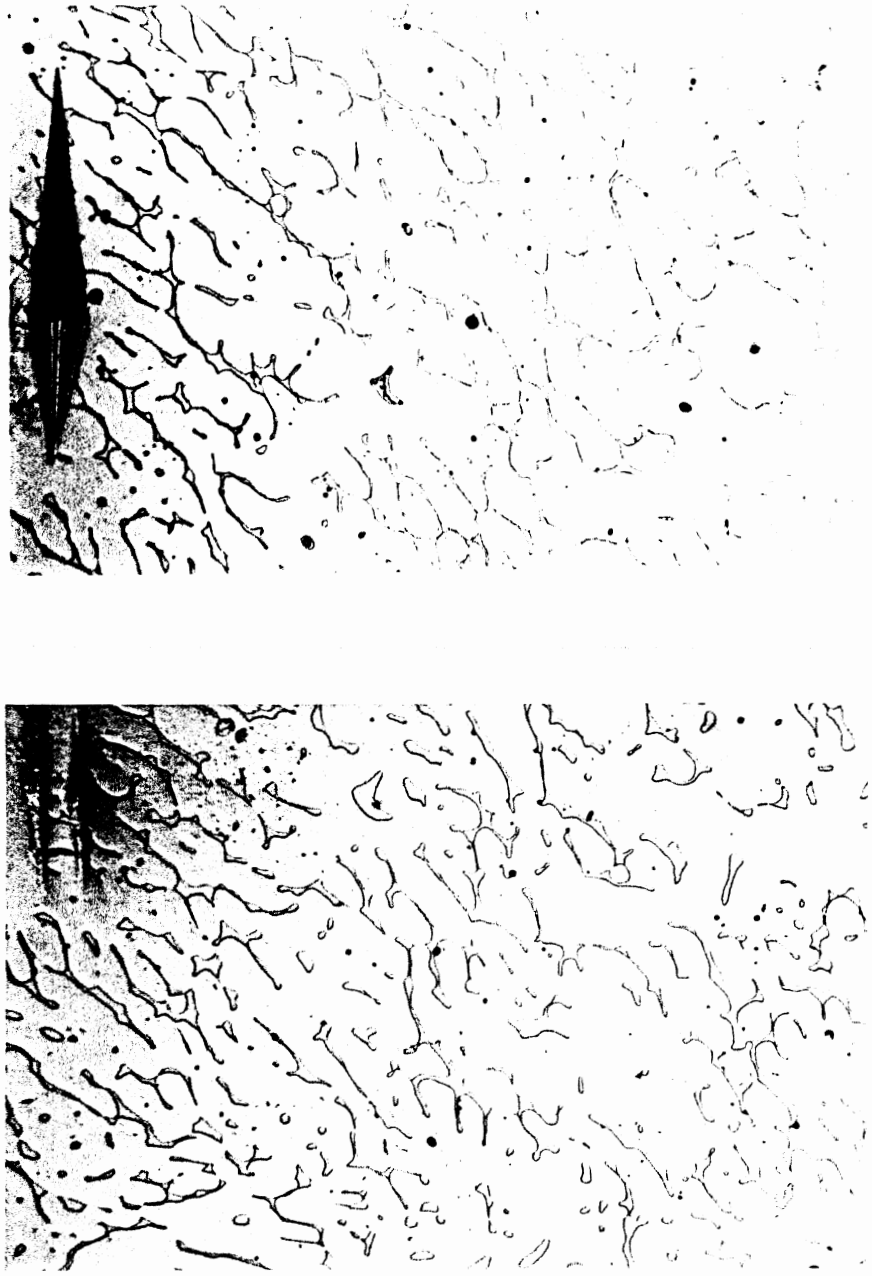

Figure 40. Uninsulated Mold, Two Minutes Heat Treatment.
As-cast (top), Heat Treated (bottom).

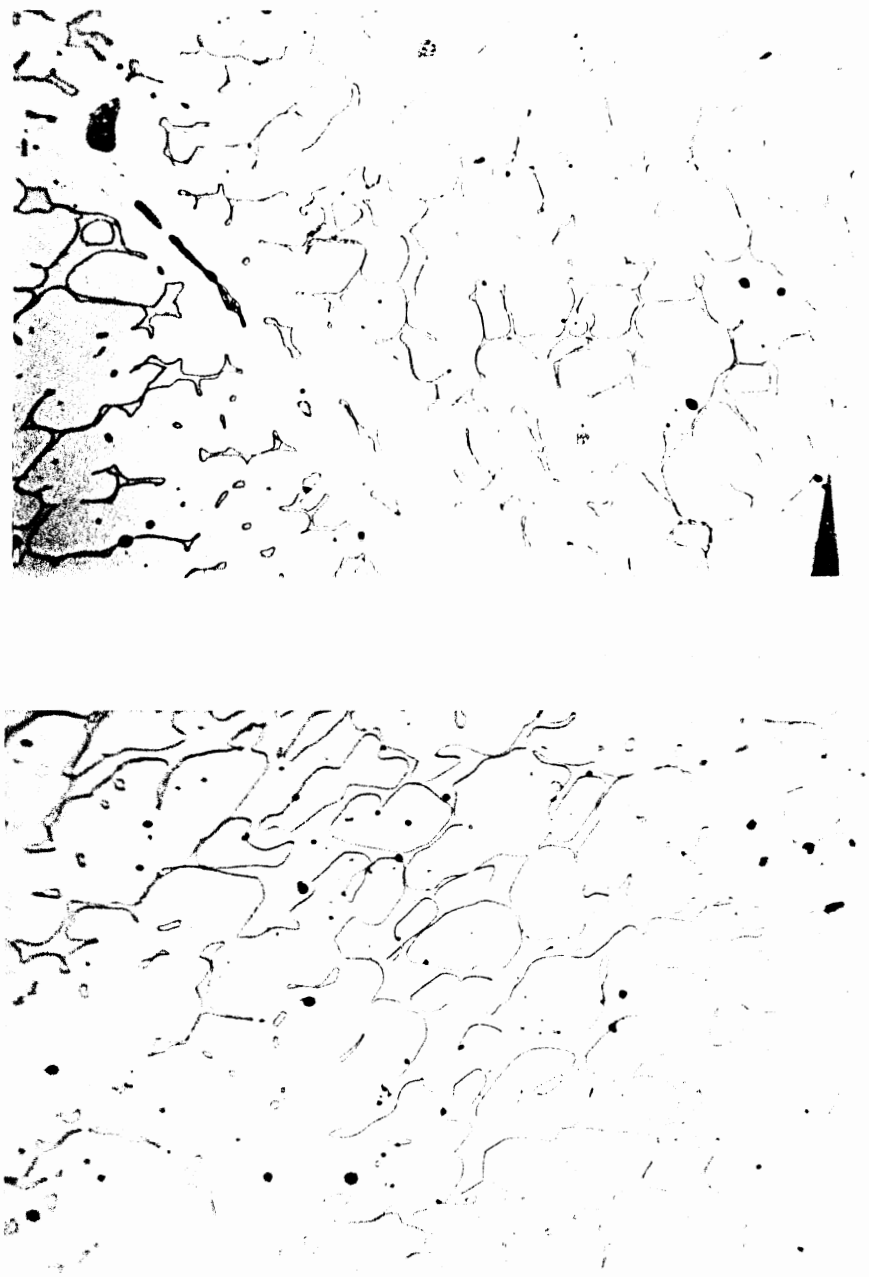

Figure 41. Uninsulated Mold, Four Minutes Heat Treatment. As-cast (top), Heat Treated (bottom).

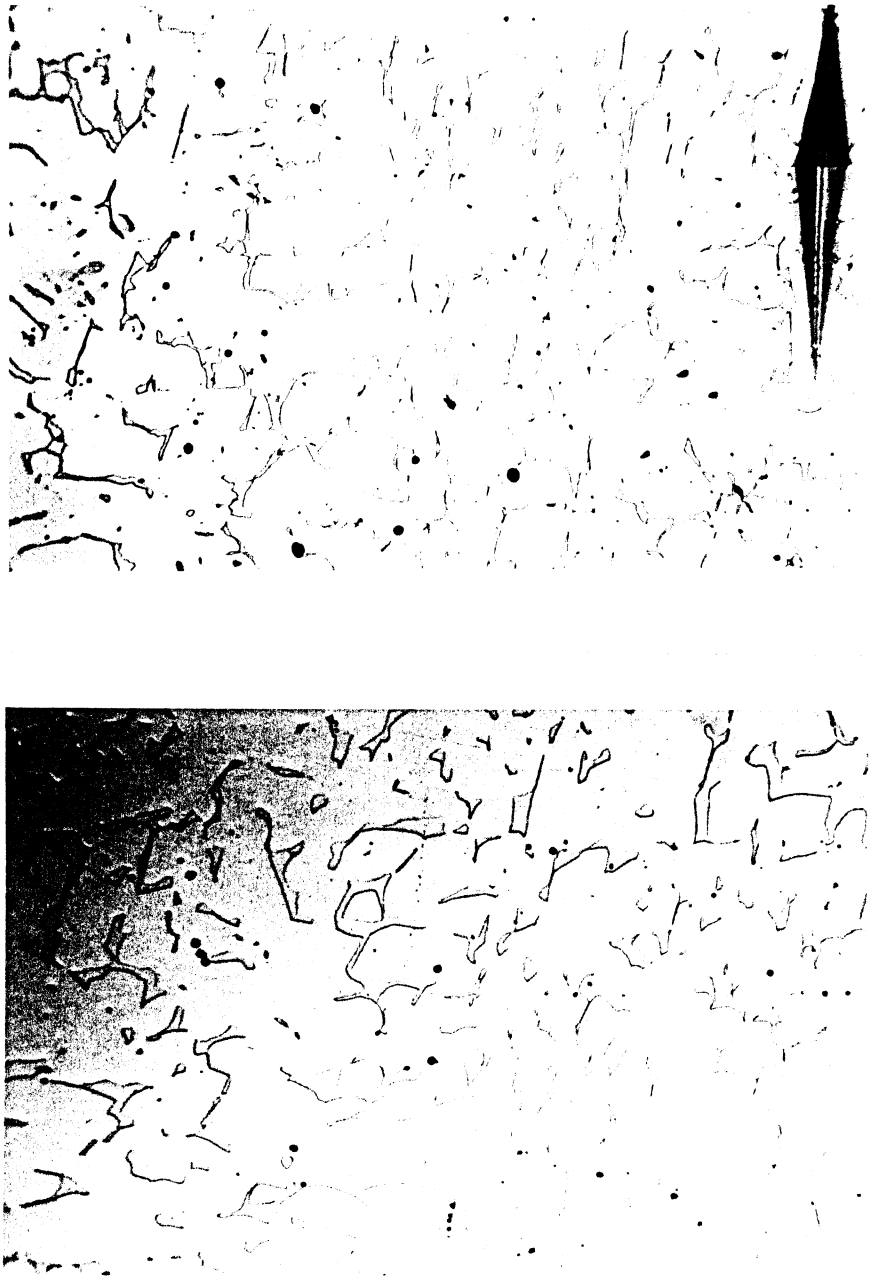

Figure 42. Uninsulated Mold, Eight Minutes Heat Treatment. As-cast (top), Heat Treated (bottom).

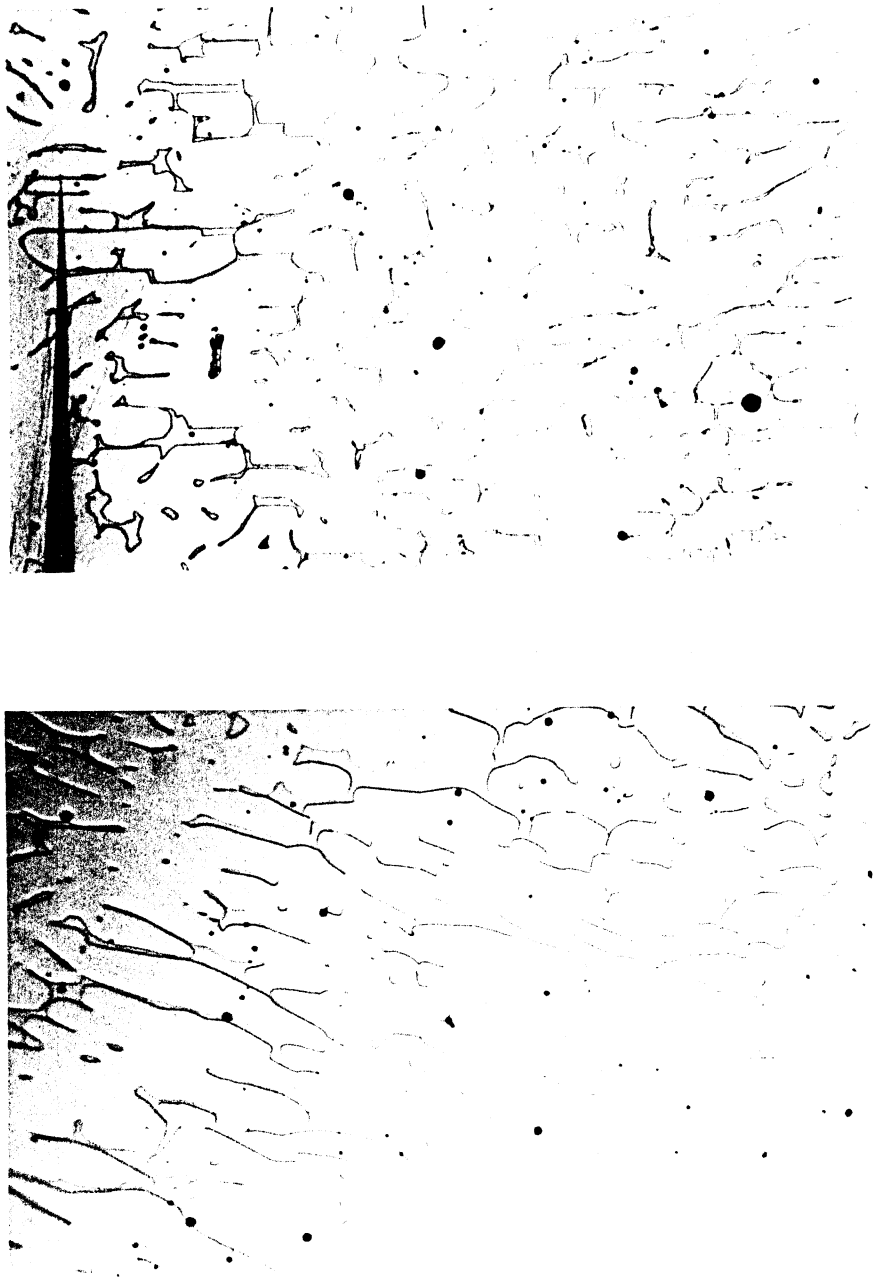

Figure 43. Uninsulated Mold, 12 Minutes Heat Treatment. As-cast (top), Heat Treated (bottom).

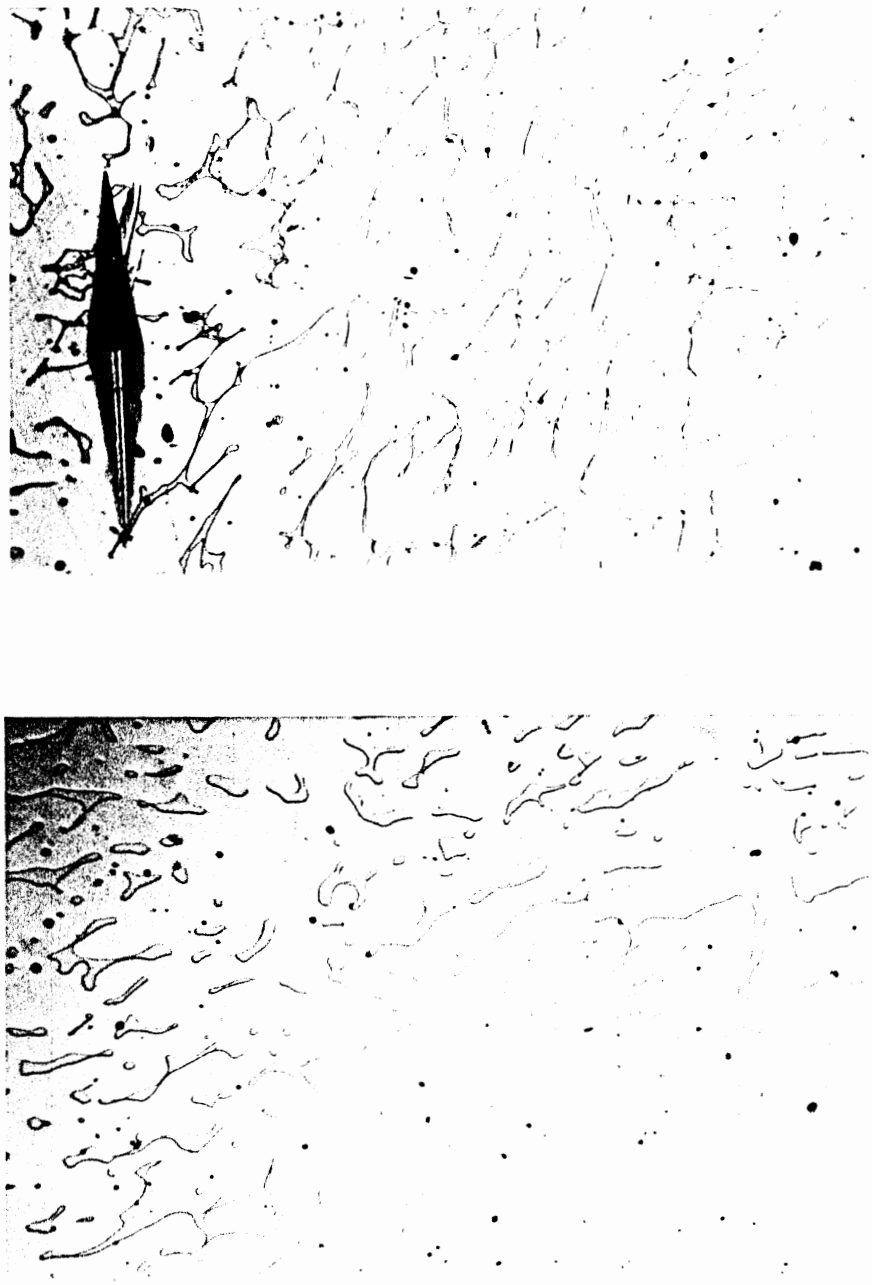

Figure 44. Uninsulated Mold, 16 Minutes Heat Treatment. As-cast (top), Heat Treated (bottom).

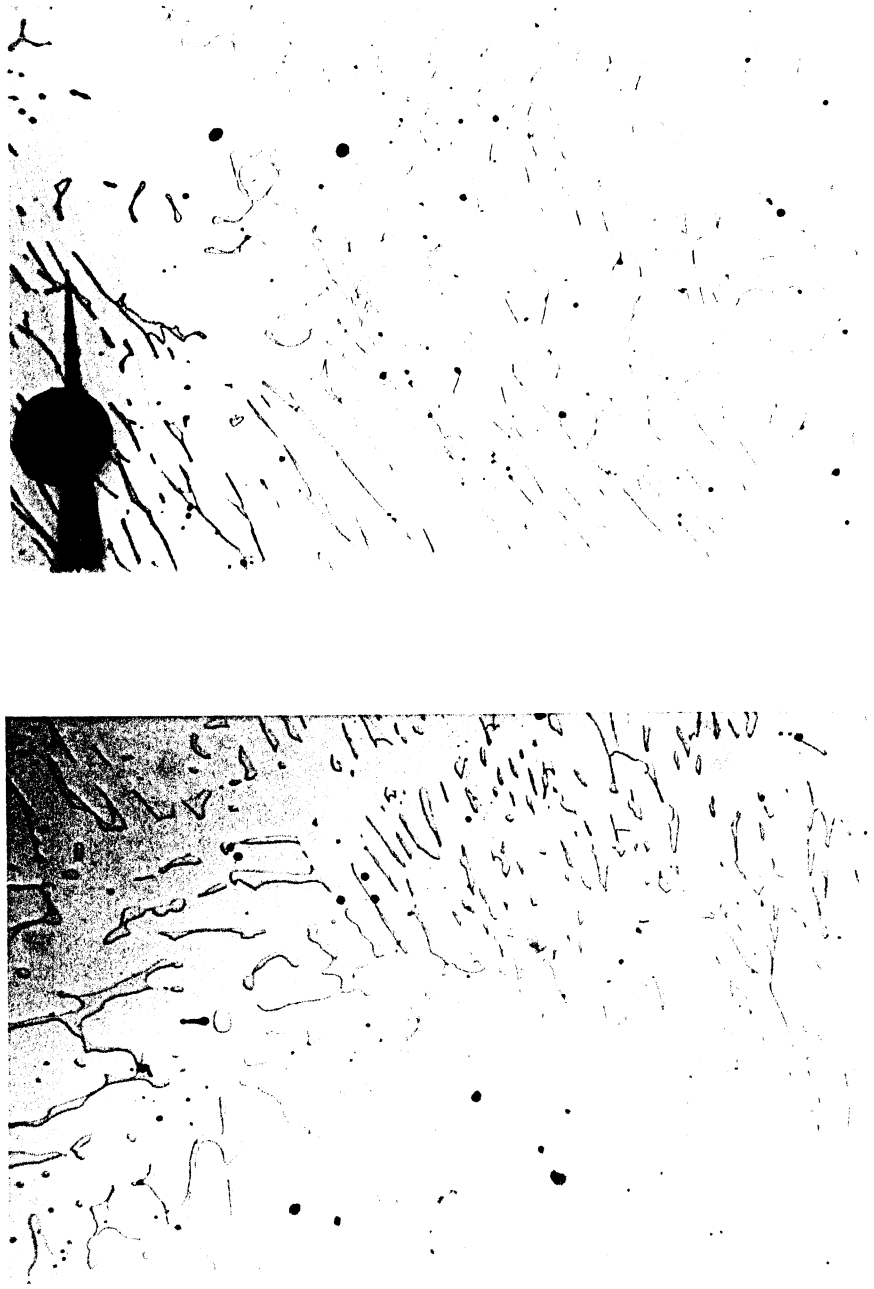

Figure 45. Uninsulated Mold, 20 Minutes Heat Treatment. As-cast (top), Heat Treated (bottom).

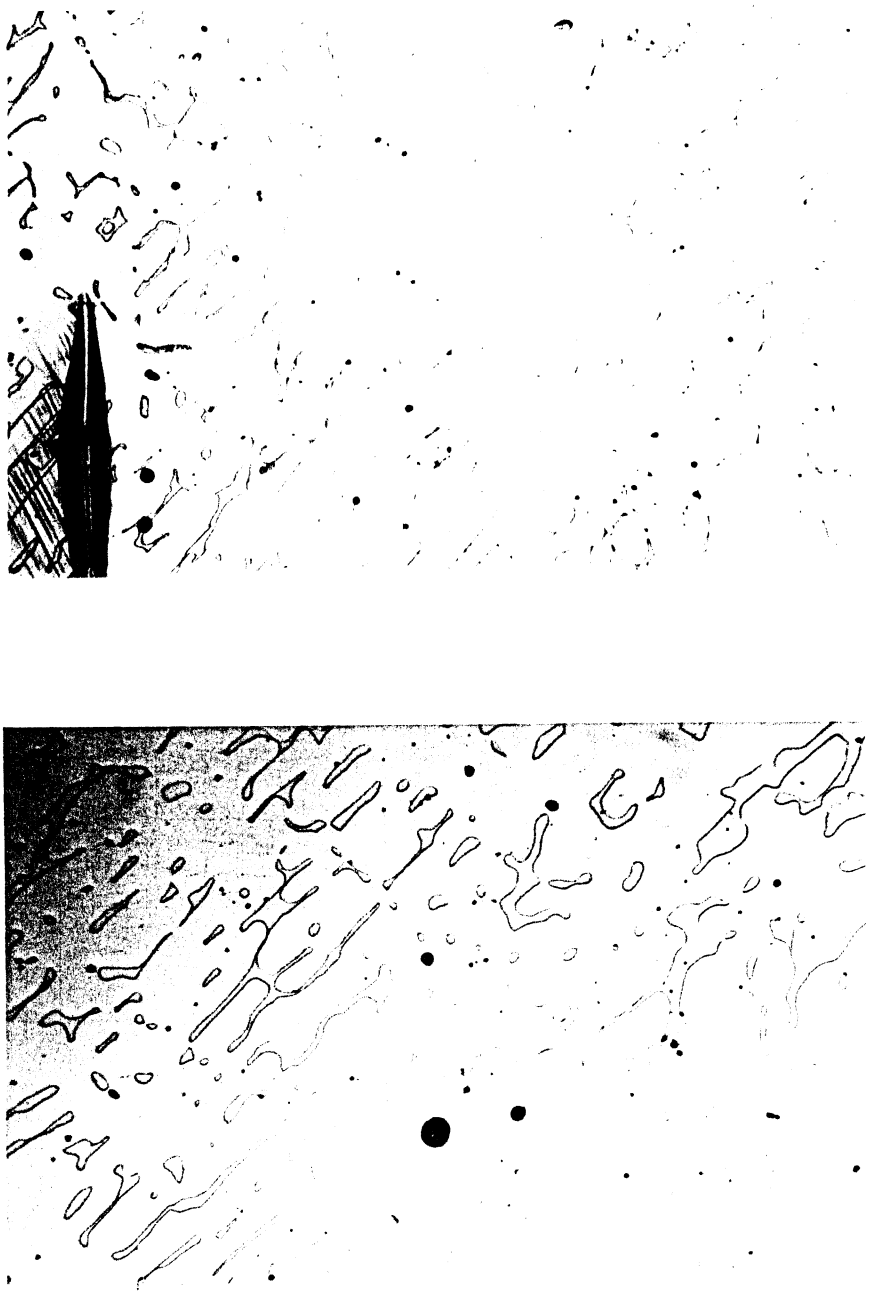

Figure 46. Uninsulated Mold, 24 Minutes Heat Treatment. As-cast (top), Heat Treated (bottom).

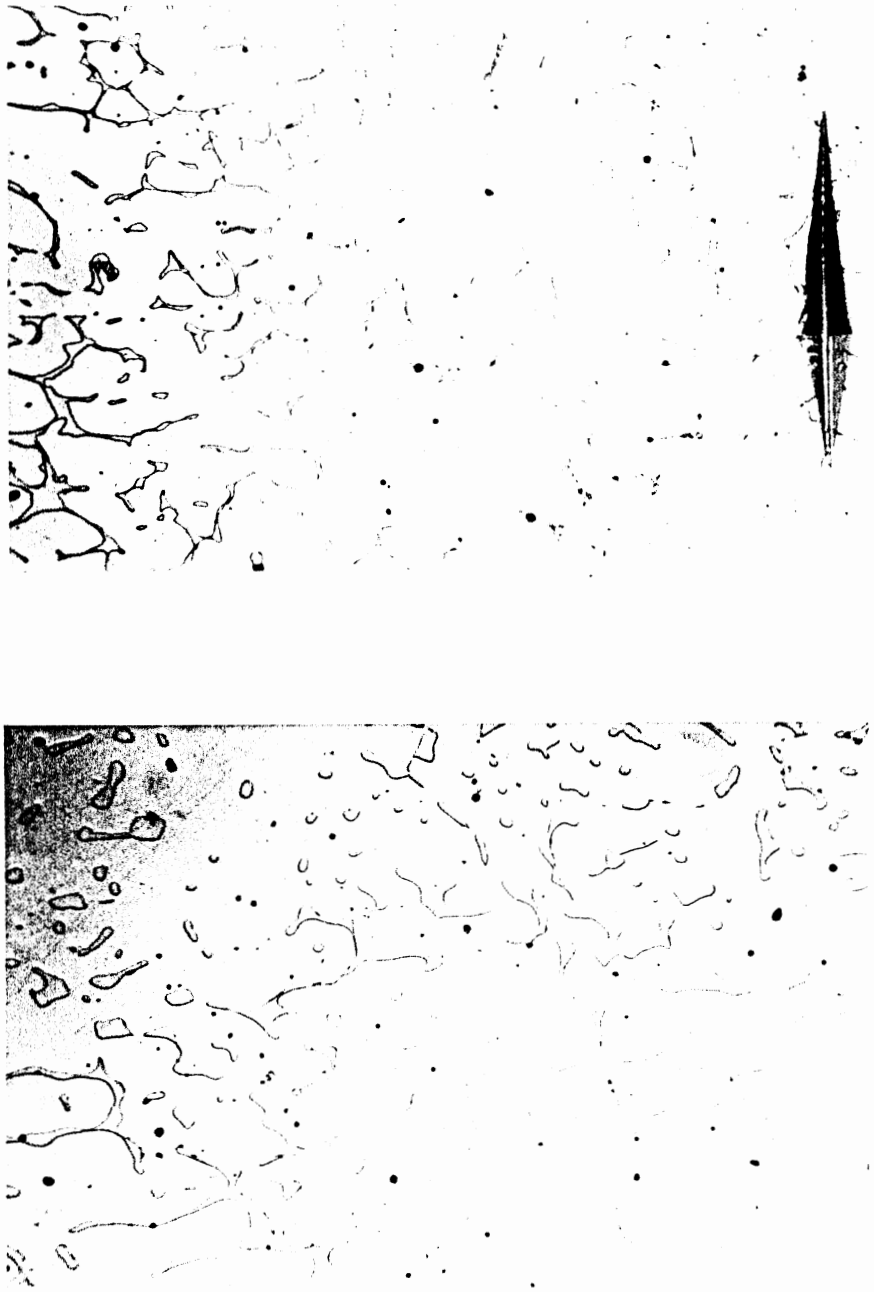

Figure 47. Uninsulated Mold, 28 Minutes Heat Treatment. As-cast (top), Heat Treated (bottom).

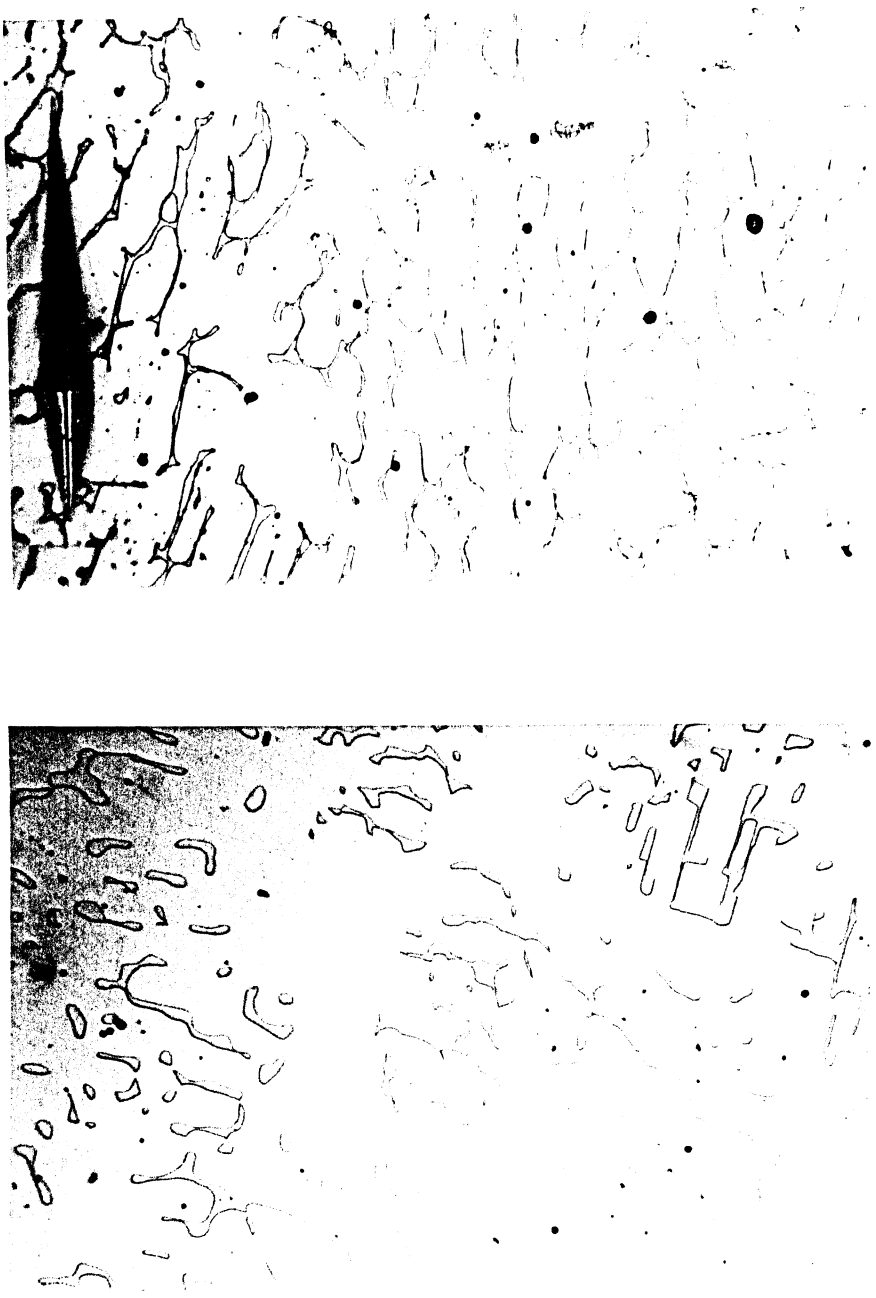

Figure 48. Uninsulated Mold, 32 Minutes Heat Treatment. As-cast (top), Heat Treated (bottom).

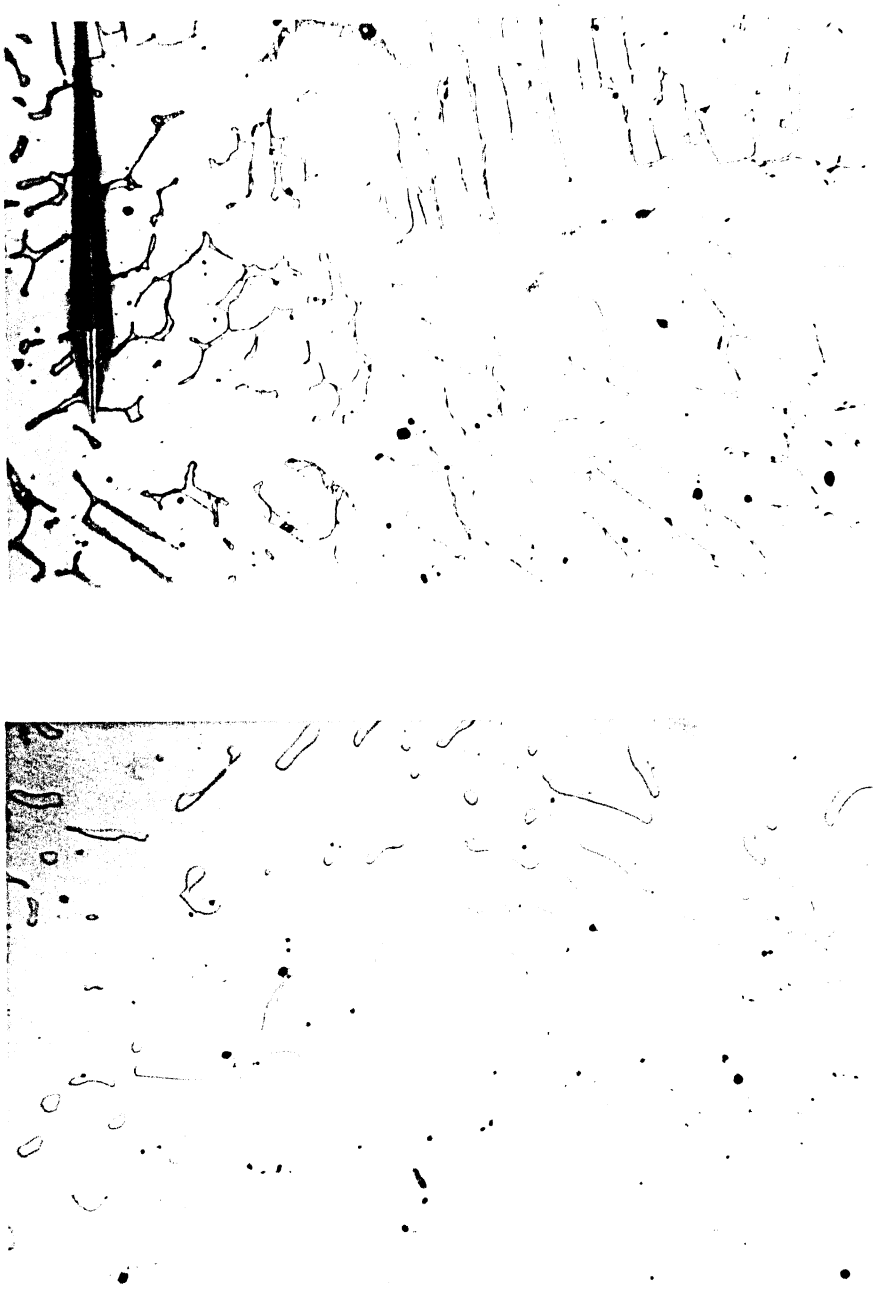

Figure 49. Uninsulated Mold, 60 Minutes Heat Treatment. As-cast (top), Heat Treated (bottom).

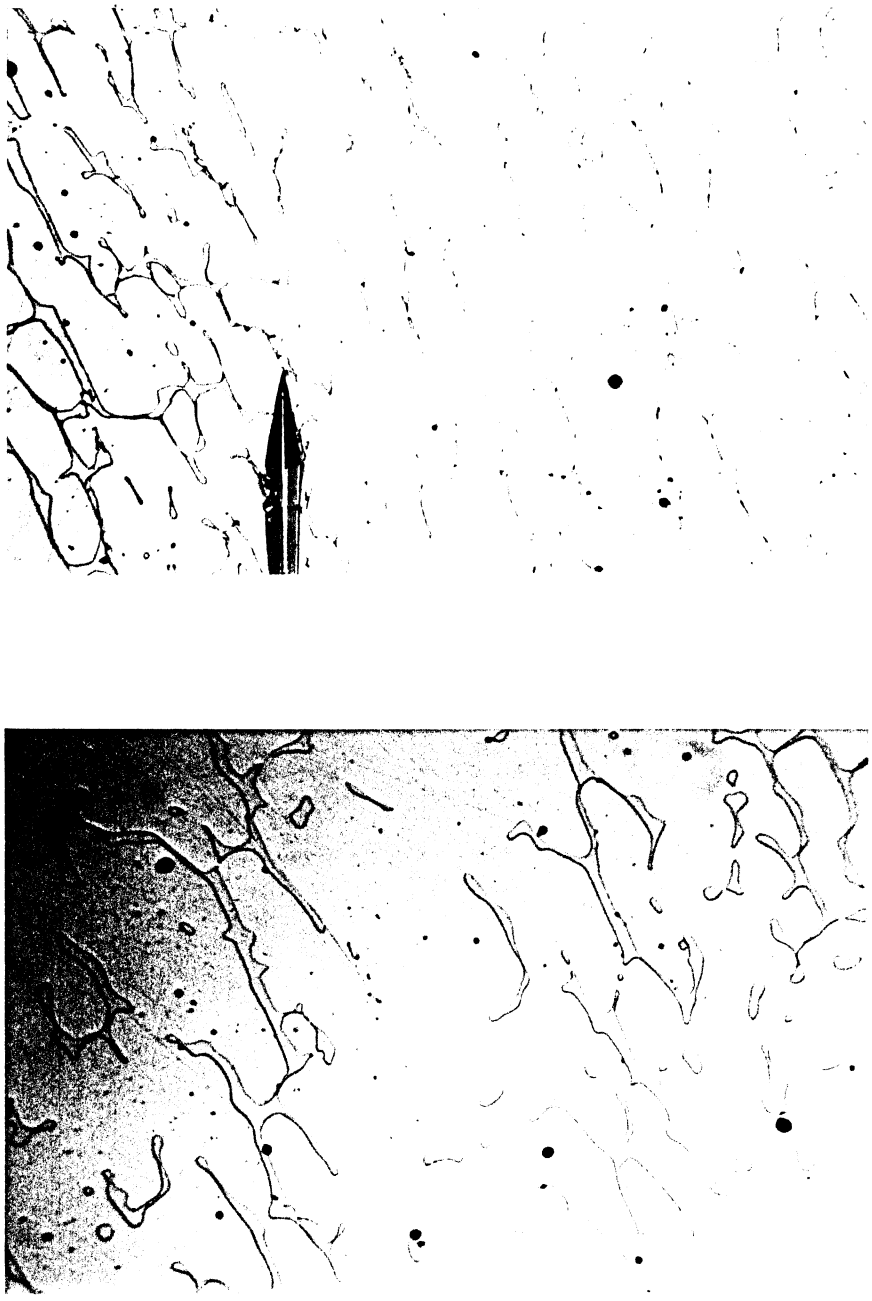

Figure 50. Insulated Mold, Two Minutes Heat Treatment. As-cast (top), Heat Treated (bottom).

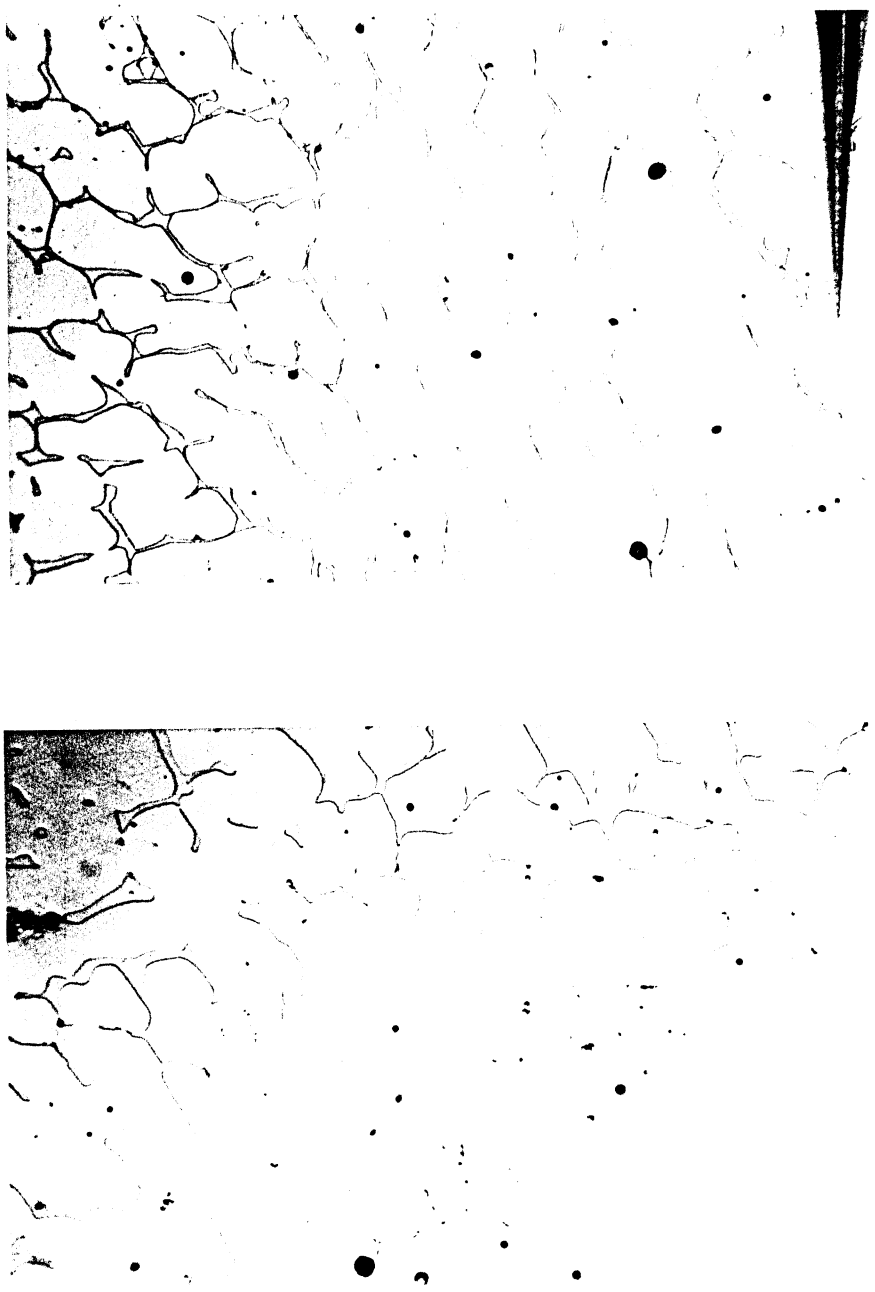

Figure 51. Insulated Mold, Four Minutes Heat Treatment. As-cast (top), Heat Treated (bottom).

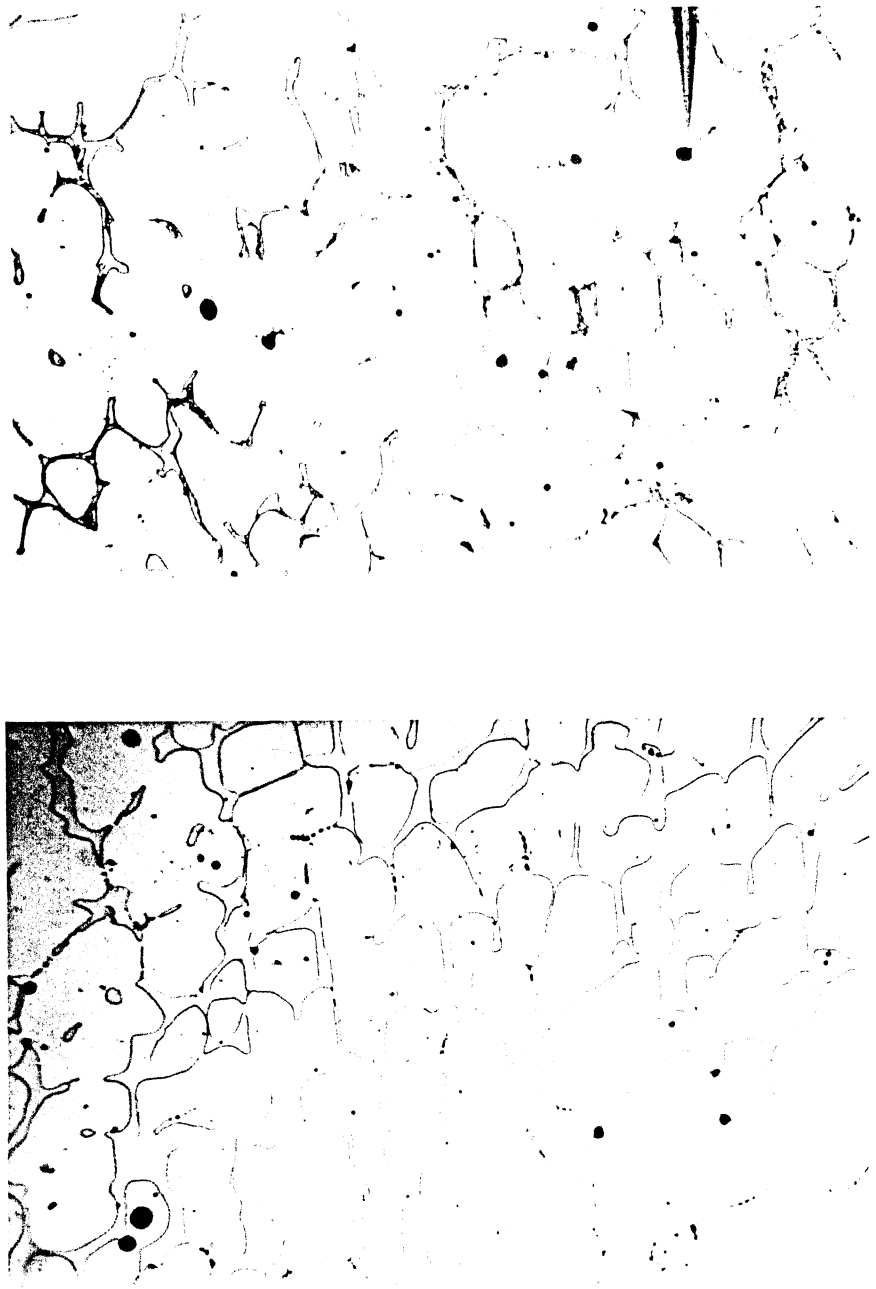

Figure 52. Insulated Mold, Eight Minutes Heat Treatment. As-cast (top), Heat Treated (bottom).

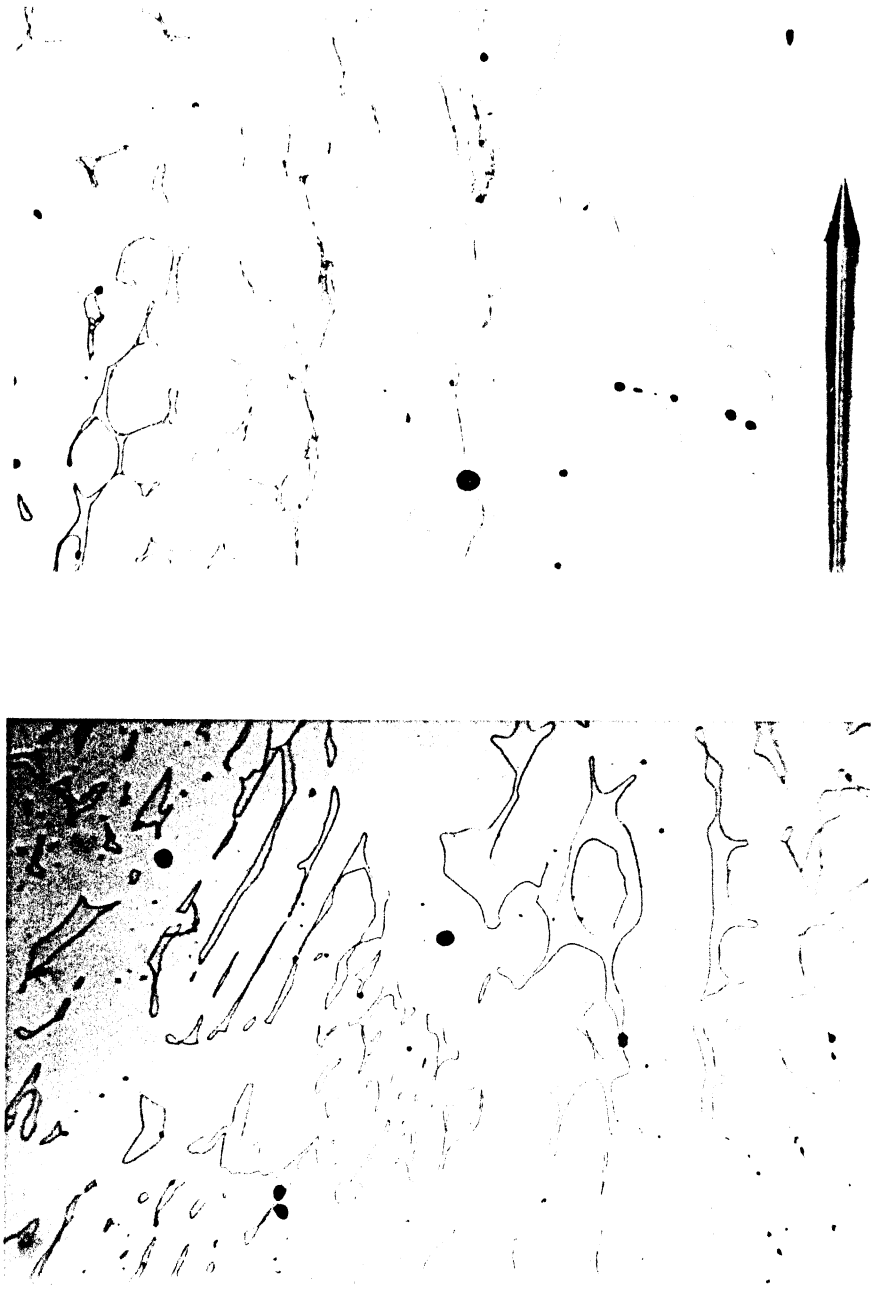

Figure 53. Insulated Mold, 12 Minutes Heat Treatment. As-cast (top), Heat Treated (bottom).

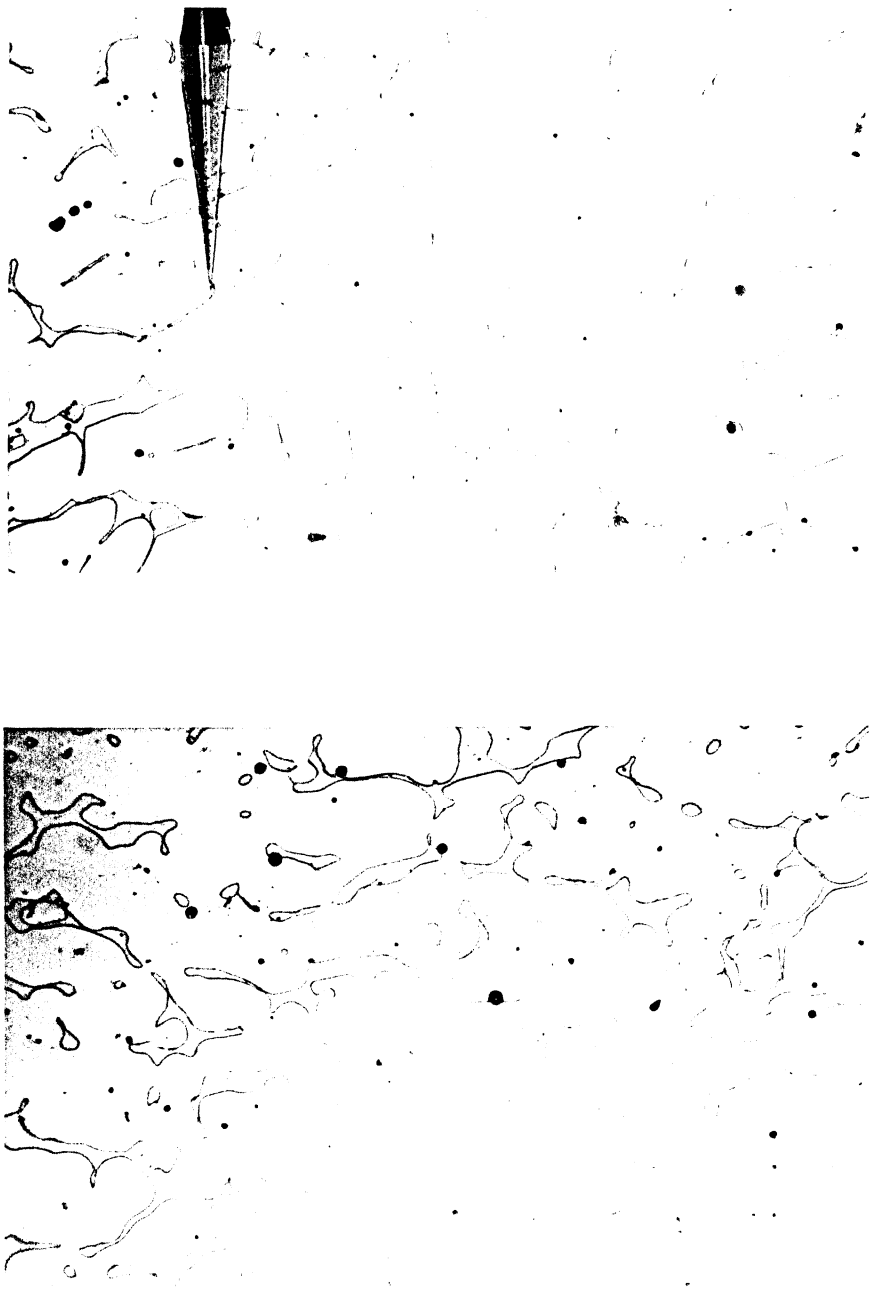

Figure 54. Insulated Mold, 16 Minutes Heat Treatment. As-cast (top), Heat Treated (bottom).

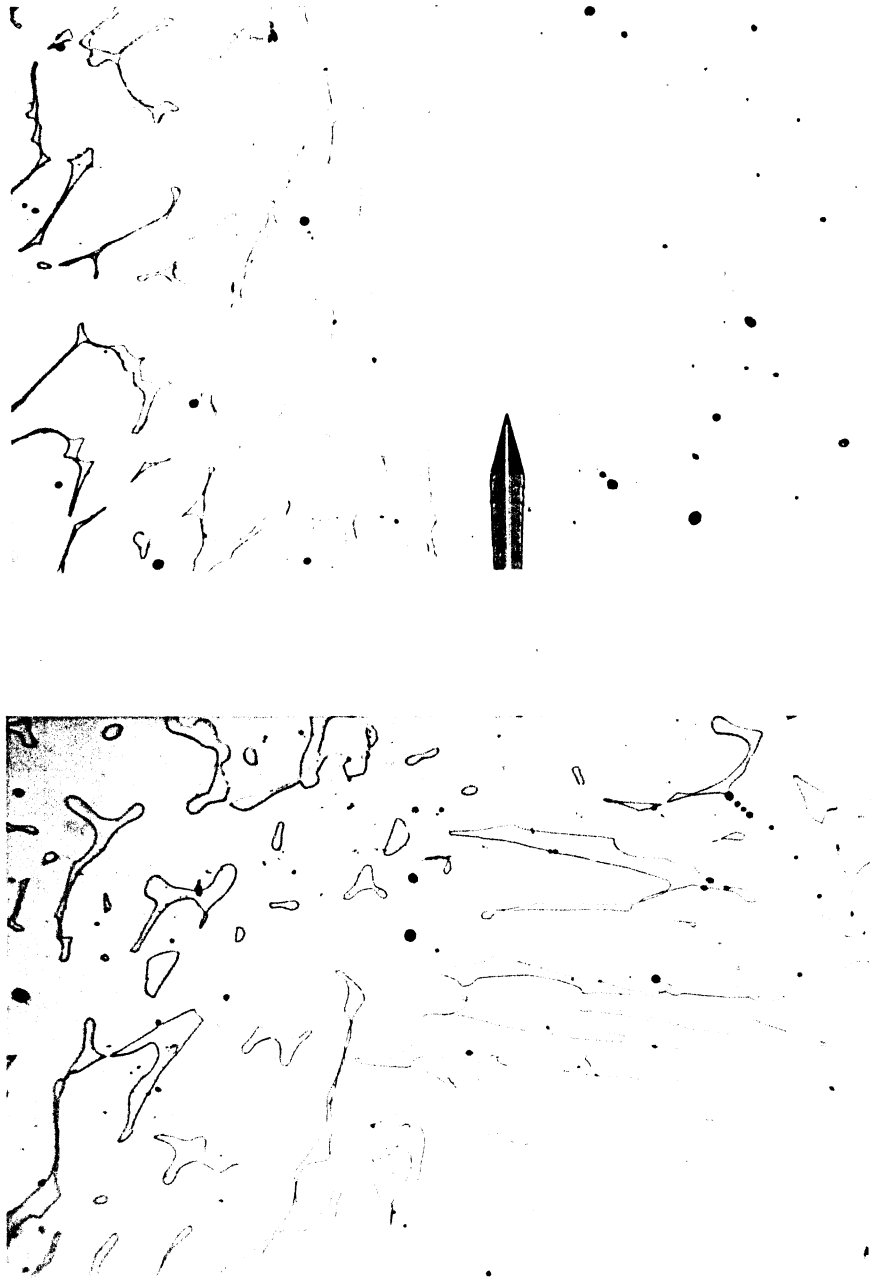

Figure 55. Insulated Mold, 20 Minutes Heat Treatment. As-cast (top), Heat Treated (bottom).

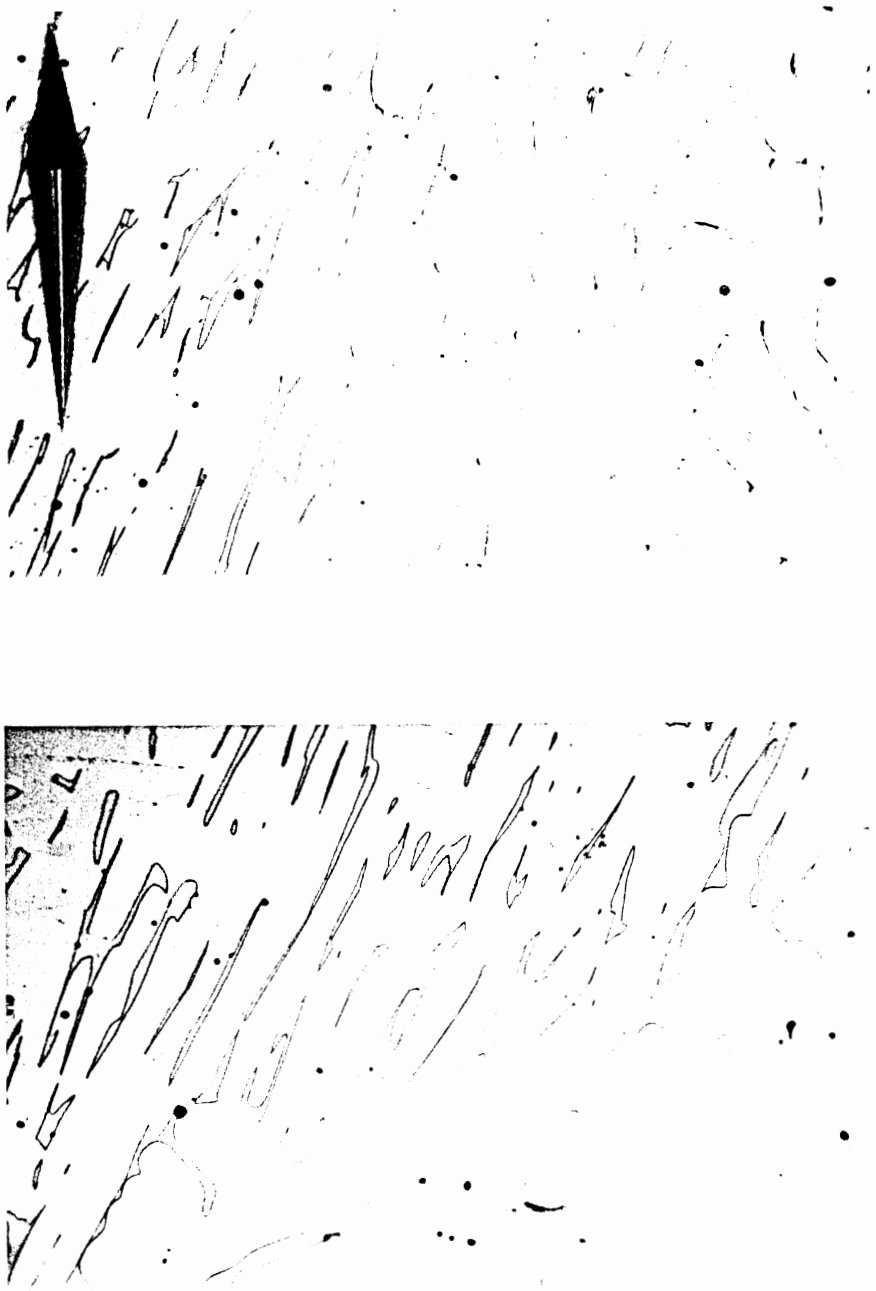

Figure 56. Insulated Mold, 24 Minutes Heat Treatment. As-cast (top), Heat Treated (bottom).

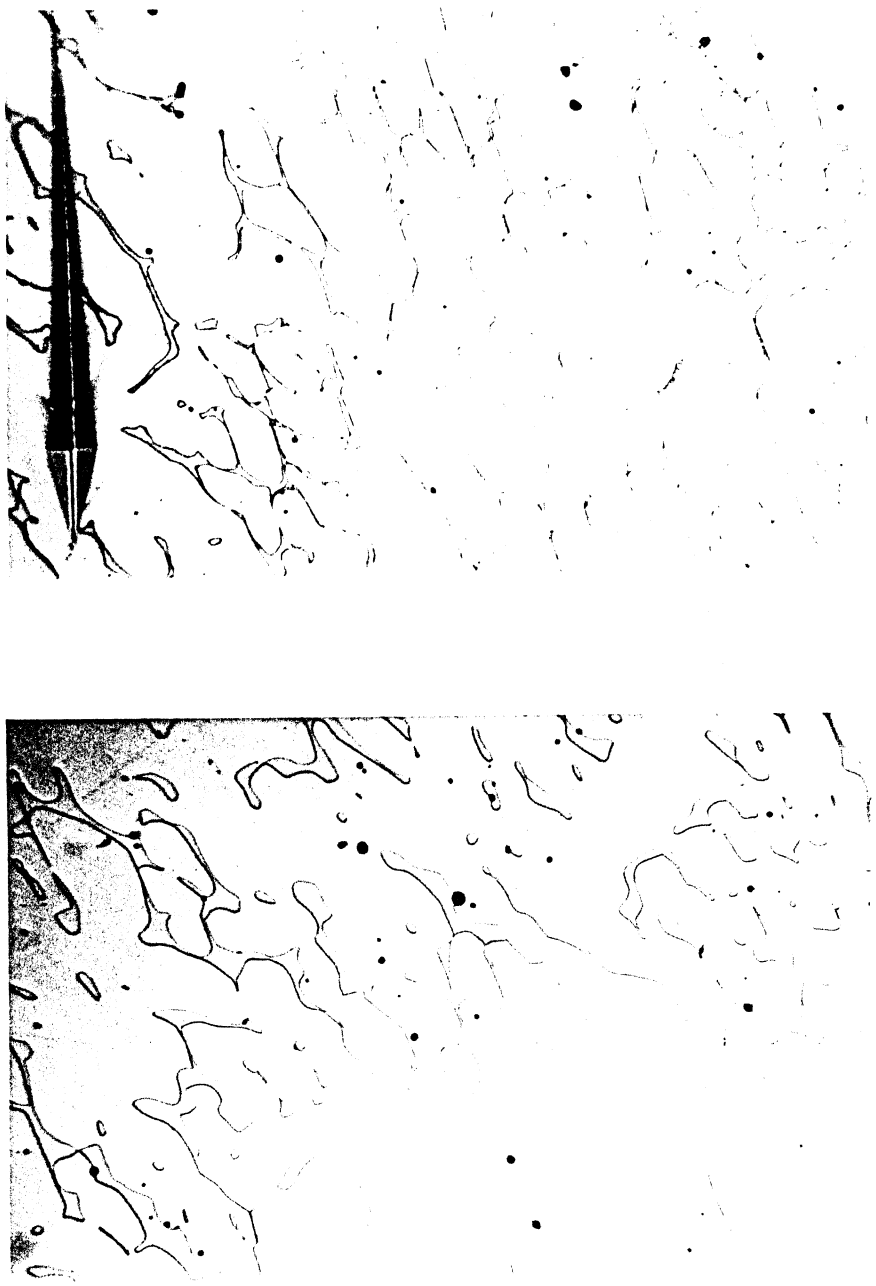

Figure 57. Insulated Mold, 28 Minutes Heat Treatment. As-cast (top), Heat Treated (bottom).

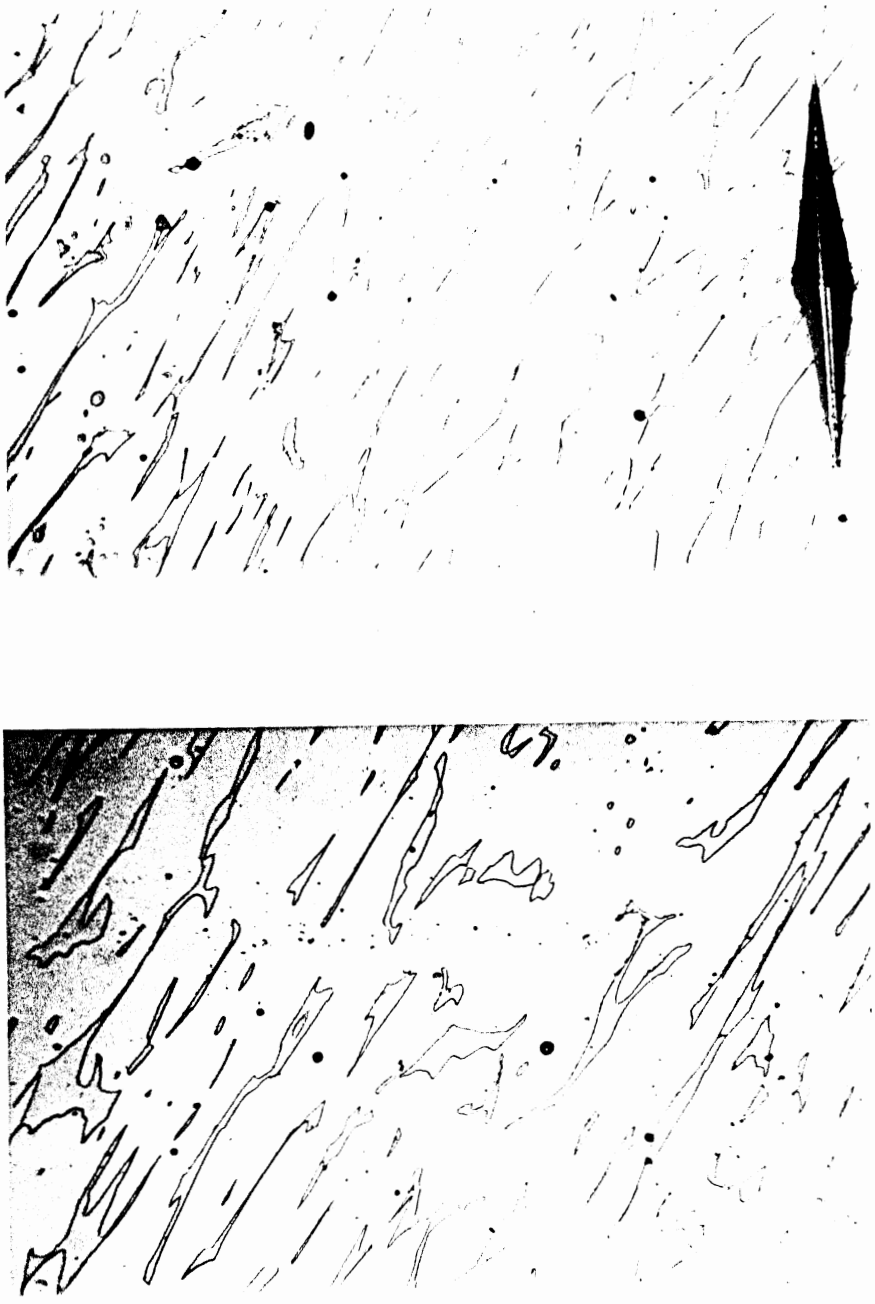

Figure 58. Insulated Mold, 32 Minutes Heat Treatment. As-cast (top), Heat Treated (bottom).

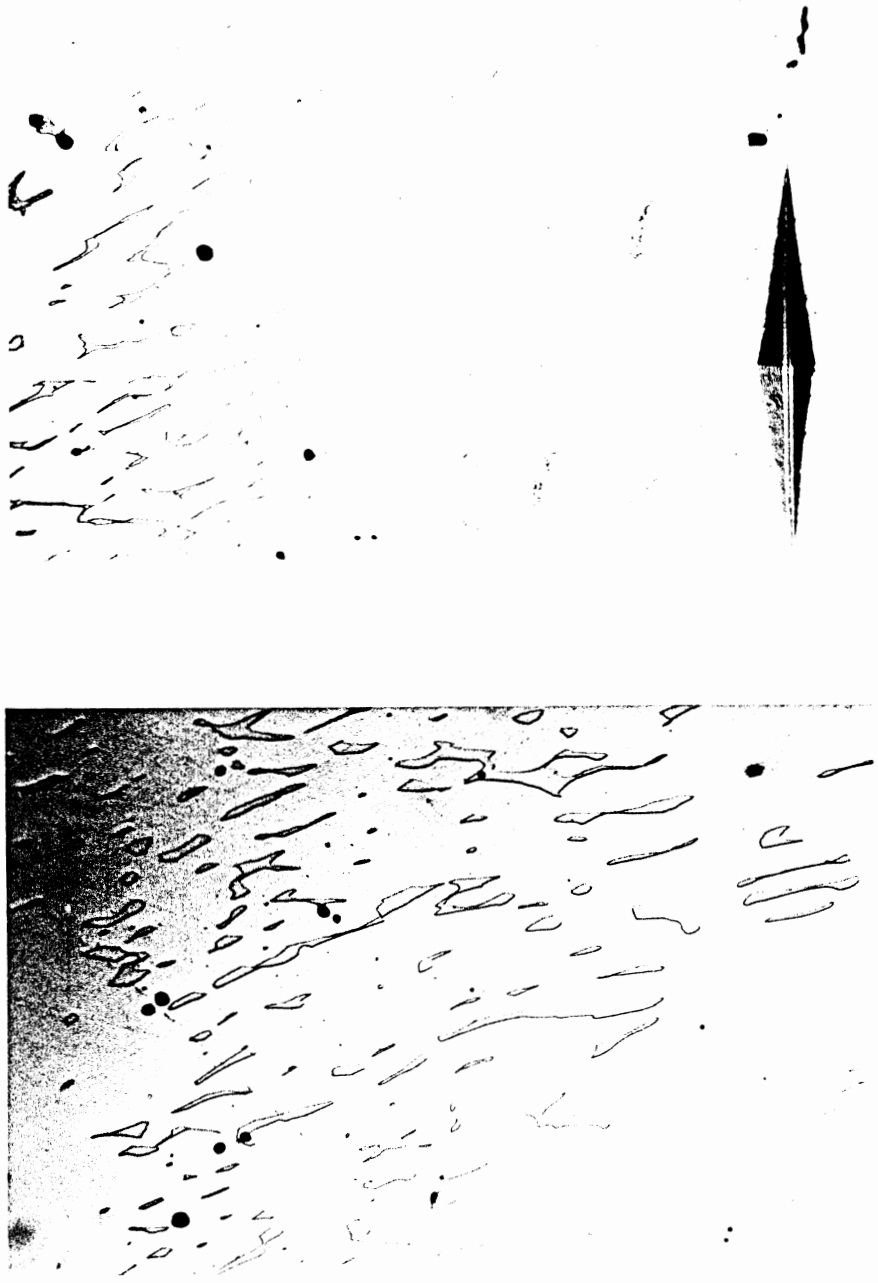

Figure 59. Insulated Mold, 60 Minutes Heat Treatment. As-cast (top), Heat Treated (bottom).

APPENDIX C

DATA TABLES

TABLE 10

ROCKWELL B HARDNESS
MEAN (STANDARD DEVIATION)

	UNINSULATED	INSULATED
As-cast	91.3 (1.2)	90.2 (1.9)
Heat treated (min)		
2	85.3 (0.7)	85.9 (0.2)
4	86.0 (1.1)	85.5 (0.6)
8	86.5 (1.2)	85.3 (0.7)
12	86.8 (0.7)	85.2 (0.5)
16	88.3 (0.3)	86.3 (0.7)
20	85.8 (0.9)	84.8 (0.7)
24	85.7 (1.4)	86.1 (0.7)
28	85.7 (1.1)	85.0 (1.1)
32	85.7 (1.0)	83.5 (0.9)
60	84.1 (0.7)	83.9 (0.7)

TABLE 11

ULTIMATE TENSILE STRENGTH
MPa (ksi)

	UNINSULATED	INSULATED
As-cast	653 (95)	631 (92)
Heat treated (min)		
5	613 (89)	611 (89)
15	612 (89)	593 (86)
30	610 (89)	595 (86)
60	592 (86)	564 (82)

TABLE 12

% ELONGATION

	UNINSULATED	INSULATED
As-cast	32	29
Heat treated (min)		
5	47	57
15	49	50
30	50	50
60	55	42

TABLE 13

TYPICAL TENSILE MICROVOID SIZE
MEAN (STANDARD DEVIATION)
MICRONS

	UNINSULATED	INSULATED
Heat treated (min)		
5	5.8 (1.6)	12.1 (3.6)
15	5.6 (2.0)	8.0 (1.4)
30	3.8 (1.7)	7.1 (1.0)
60	6.8 (1.8)	11.6 (2.4)

TABLE 14

AS-CAST CHARPY IMPACT ENERGY
J (FT-LBS)

Test Temperature (°C)	UNINSULATED	INSULATED
-196	16 (12)	12 (9)
-77	22 (16)	20 (14)
0	36 (27)	41 (31)
20	49 (36)	52 (38)

TABLE 15

AS-CAST LATERAL EXPANSION
.001"

Test Temperature (°C)	UNINSULATED	INSULATED
-196	9.8	2.3
-77	10.8	11.3
0	27.5	24.5
20	39.0	42.3

TABLE 16

-20°C CHARPY IMPACT ENERGY
J (FT-LBS)

	UNINSULATED	INSULATED
As-cast	49 (36)	52 (38)
Heat treated (min)		
5	177 (131)	209 (154)
15	198 (146)	228 (169)
30	172 (127)	200 (147)
60	170 (125)	175 (129)

TABLE 17

-20°C LATERAL EXPANSION
.001"

	UNINSULATED	INSULATED
As-cast	39.0	42.3
Heat treated (min)		
5	63.0	72.0
15	70.3	60.3
30	51.3	73.3
60	56.5	66.8

TABLE 18

-196°C CHARPY IMPACT ENERGY
J (FT-LBS)

	UNINSULATED	INSULATED
As-cast	16 (12)	12 (9)
Heat treated (min)		
5	158 (117)	202 (149)
15	96 (71)	150 (111)
30	124 (92)	172 (127)
60	114 (84)	145 (117)

TABLE 19

-196°C LATERAL EXPANSION
.001"

	UNINSULATED	INSULATED
As-cast	9.8	2.3
Heat treated (min)		
5	51.0	47.0
15	38.0	28.0
30	47.5	54.0
60	47.5	42.0

APPENDIX D

DIFFUSION CALCULATIONS

A diffusion model derived from Fick's second law was used to examine the changes in the ratio of chromium to nickel near the ferrite-austenite interface. The model uses a pair of semi-infinite solids in contact and the initial source of solute is assumed to be an extended one. In addition, the diffusion distances are assumed to be small relative to the length of the system (Shewmon 1963). Under these conditions the solution to Fick's second law becomes

$$C_x = C_2 + \frac{C_1 - C_2}{2}\left[1 - \mathrm{erf}(x/(2\sqrt{Dt}))\right]$$

where C_1 is the source concentration, C_2 is the base concentration, t in time in seconds and x is the distance from the interface in centimeters. The diffusivity, D, is assumed constant.

To more accurately represent the situation, the appropriate diffusivities were used depending on the situation. The values were shown in Table 8 and were considered constant for use in this model.

Two heat treatment times were examined, five minutes and 30 minutes. Figures 39 and 40 compare the as-cast concentration profile with the profiles at five and 30 minutes heat treatment. Figure 41 shows the changes in the ratio of chromium to nickel. The important region in these plots is the area near the interface at x = 0. Even

in the austenite, where diffusion is slower, five minutes is enough time to allow the chromium and nickel to travel distances of 2-3 microns. Steeper Cr/Ni gradients are set up in the austenite than in the ferrite. These changes could be responsible for interface movement detectable by light microscopy.

This model constrains the boundary concentrations to approach $(C_1+C_2)/2$. This limitation does not allow any conclusions to be drawn about how the ferrite-austenite boundary may move. It does support the idea that with five minutes, the diffusion distances are large enough to cause detectable changes in the microstructure. The steeper gradients in the austenite may favor the growth of ferrite before the gradients flatten out with time and ferrite dissolution begins.

Other limitations include the exclusion of the role of other alloying elements and the step change in concentration required by the model. A more sophisticated mathematical model combined with experimental chemistry measurements would address this question more thoroughly.

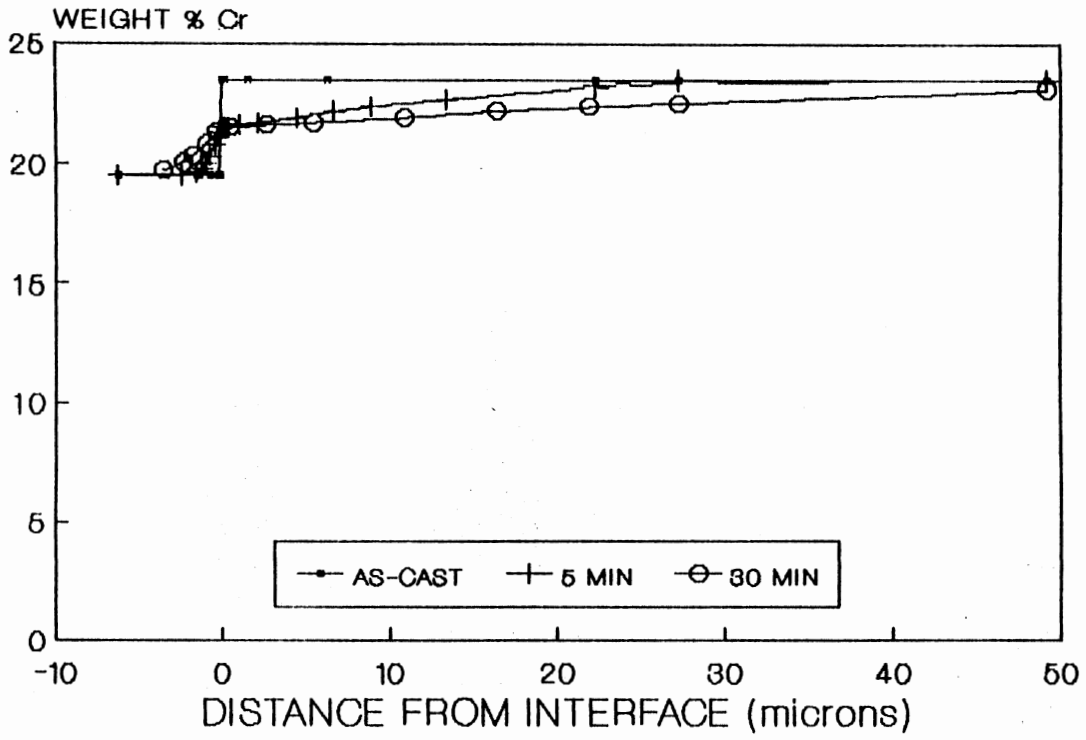

Figure 60. Model of Chromium Diffusion.
Austenite < 0
Ferrite > 0

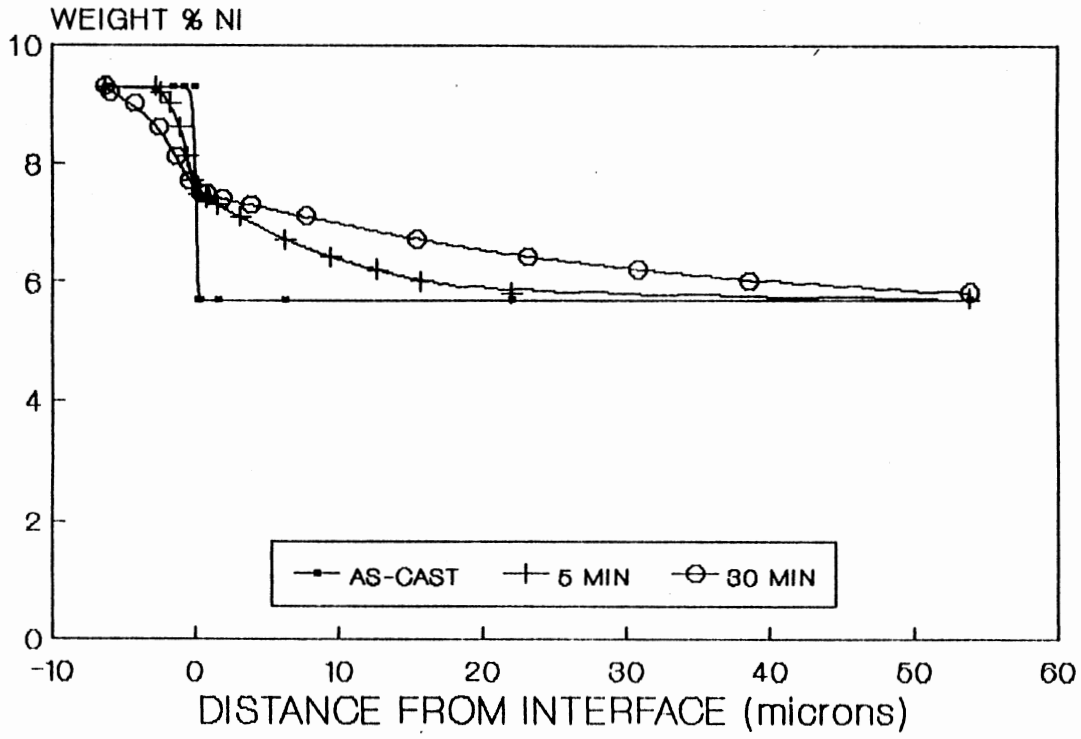

Figure 61. Model of Nickel Diffusion.
Austenite < 0
Ferrite > 0

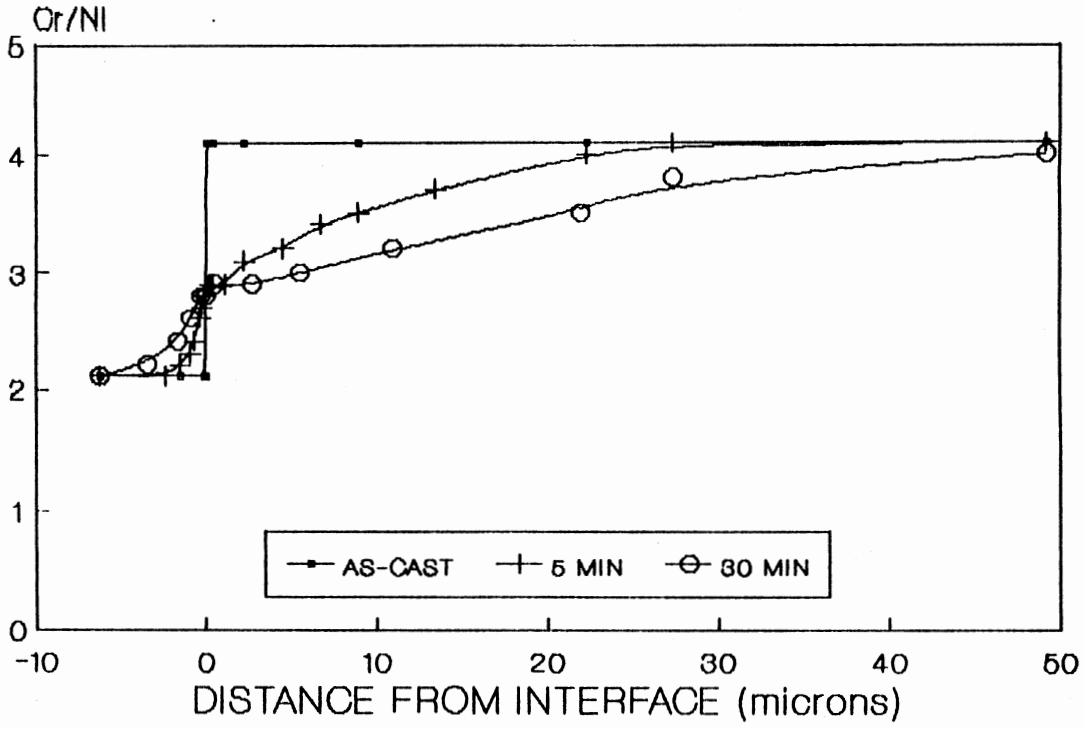

Figure 62. Chromium-nickel Ratio.
Austenite < 0
Ferrite > 0

VITA

Rachael Esther Cohen

Candidate for the Degree of

Doctor of Philosophy

Thesis: THE EFFECTS OF SOLIDIFICATION RATE AND HEAT TREATMENT ON THE MICROSTRUCTURE AND MECHANICAL PROPERTIES OF CERAMIC SHELL INVESTMENT CAST CF3M

Major Field: Mechanical Engineering

Biographical:

Personal Data: Born in Norwich, Connecticut, June 8, 1954, the daughter of Lawrence and Pauline Cohen.

Education: Graduated from Norwich Free Academy, Norwich, Connecticut, in June 1972; received Bachelor of Science degree in Animal Science from University of Connecticut in May 1976; received Master of Science degree in Exercise Science from University of Massachusetts in September 1982; received Master of Science degree in Mechanical Engineering from University of Vermont in May 1986; completed requirements for the Doctor of Philosophy degree at Oklahoma State University in December 1990.

Professional Experience: Research Assistant II, Department of Pathobiology, University of Connecticut, 1976-1978; Assistant in Research, Departments of Cardiothoracic Surgery and Pharmacology, Yale University School of Medicine, 1978-1979; Graduate Assistantship, Health Services, University of Massachusetts, 1979-1980; Laboratory Technician II, Department of Physiology and Biophysics, University of Vermont Medical School, 1982-1983; Graduate and Research Assistantships, School of Mechanical and Aerospace Engineering, Oklahoma State University, 1985-1988; Lecturer, School of Mechanical and Aerospace Engineering, Oklahoma State University, 1989; Metallurgist, Metal Laboratory, Mercury Marine Division of Brunswick Corporation, 1989-1990.